Summer 2019

The benefit of precise chemical shift and concentration referencing in NMR applications

Ming Huang

Department: Chemistry

THE BENEFIT OF PRECISE CHEMICAL SHIFT AND CONCENTRATION REFERENCING IN NMR APPLICATIONS

by

MING HUANG

A DISSERTATION

Presented to the Faculty of the Graduate School of the

MISSOURI UNIVERSITY OF SCIENCE AND TECHNOLOGY

In Partial Fulfillment of the Requirements for the Degree

DOCTOR OF PHILOSOPHY

IN

CHEMISTRY

2019

Approved by:

Klaus Woelk, Advisor
Vadym Mochalin
Paul Ki-souk Nam
Jeffery G. Winiarz
Richard K. Brow

ABSTRACT

In Nuclear Magnetic Resonance (NMR) spectroscopy, the chemical shift and intensity of NMR signals provide critical information about a sample's molecular structure, reaction conditions, and material properties. For the precise determination of structures and properties, it is critical to know sample or reaction conditions such as temperature, pH, concentration, or absolute amount of material. Chemical-shift and signal-intensity calibrations play a key role for extracting the maximum amount of information from NMR experiments. In this dissertation, internal and external reference standards are used to calibrate NMR spectra with respect to chemical shift and signal intensity. Sealed capillary tubes filled with specific solutions (e.g., chloroform, trifluoroacetic acid, hydrochloric acid, ethylene glycol, methanol, aqueous solutions with small amounts of $CuSO_4$) were utilized as external references for chemical-shift and signal-intensity calibrations in liquid-state and solid-state NMR applications. Absolute concentration calibrations are an essential part for quantitative NMR investigations. For concentration calibrations, a number of parameters must be optimized prior to conducting quantitative NMR experiments. Several calibration techniques are presented such as using capillary-tube inserts or CapPack devices as external references. In addition to concentration calibrations, CapPack devices are also used to determine sample temperatures or pH values in liquid-state and solid-state NMR. Applications presented here include (a) determination of residual water in ionic-liquid rocket monopropellants, (b) determination of chemical shifts, relaxation times, and intermolecular transfer of signal saturation for the analysis of interactions between polymer micelles and small molecules in solution, and (c) innovative studies of the release kinetics of small molecules from loaded porous-wall hollow glass microspheres

ACKNOWLEDGMENTS

I would like to express my deepest gratitude to Dr. Klaus Woelk for his caring, guidance, and wisdom. Dr. Woelk' s commitment to high academic standards serves as a constant source of motivation, and the environment provided to his group members could not be more conducive to excellent research. I would also like to recognize Dr. Vadym Mochalin, Dr. Paul Ki-souk Nam, Dr. Jeffery G. Winiarz, Dr. Richard K. Brow for their counsel as members of my graduate committee. This work would also not have been possible without the support of the Missouri S&T Chemistry Department and in-kind donations from Brewer Science Inc. of Rolla, Missouri.

I would like to express special thanks to Dr. Rex E. Gerald II for his continued mentorship and friendship, for his frequent assistance in the completion of experiments, and his unfaltering positive attitude no matter what difficulty I faced in the lab. His strength has carried me through the most difficult stages of this work. I would also like to thank Dr. Michael R. Van De Mark for providing his polymer materials and help me understand related knowledge from his area. I would like to thank Matthew Parker and Ashish Zore for their assistance with research that is reported in this dissertation.

I would also like to thank my mother, Jinxia Wang, my late father, Haiyu Huang, and the family of my brother, Jie Huang, for their endless love, support, and encouragement while I worked towards the completion of my dissertation. Their example has motivated me to follow a path of lifelong education, and for this (and so much more) I am forever grateful. To my other family members and friends: I would have never made it through some challenging times without your best wishes and support.

TABLE OF CONTENTS

LIST OF ILLUSTRATIONS

Page

LIST OF TABLES

Page

1. INTRODUCTION

1.1. THE IMPORTANCE OF CHEMICAL-SHIFT REFERENCING IN NMR SPECTROSCOPY

Nuclear magnetic resonance (NMR) spectroscopy is a keen analytical technique for the elucidation of molecular structures, reaction mechanisms, and materials properties. The response to radiofrequency pulses in NMR spectroscopy is inherently quantitative, which means that an NMR response is directly proportional to the number of nuclei excited by the NMR experiment, and that NMR signal intensities are a measure of molecular concentrations. Moreover, variations in NMR chemical shifts and *J*-coupling constants can provide quantitative information about intra- and intermolecular interactions [1]. The chemical shift (δ) of a signal in an NMR spectrum is the variation of the resonance frequency caused by a variation in the electronic environment around the interrogated nucleus. Numerical values for chemical shifts are typically reported as relative numbers with respect to a prominent resonance frequency of an NMR standard. A reference sample typically consists of a pure substance or a well-defined solution of a molecule with a stable electronic environment that is barely distorted by the electron distribution of the lattice around the molecule [2, 3]. The lattice can be any environment to which the molecule is exposed, such as a pure solvent or a solute dissolved in the solvent. In this context, other molecules can mean the same kind as the referencing molecule or other types of molecules. Differences in the electronic environment can cause an interrogated nucleus to experience a slightly different magnetic field than the external magnetic field applied by the NMR magnet. The electronic environment around a nucleus thereby can have a shielding or de-shielding effect, leading to a slightly lower or a slightly higher magnetic field at the site of

the nucleus, respectively. In turn, the lower or higher magnetic field causes a slightly lower or higher resonance frequency of the nucleus, respectively. It is noted, however, that NMR frequencies, and thus chemical shifts, are not absolute values, but relative measures with respect to the external field of the NMR magnet.

The application of NMR spectroscopy (particularly ^{1}H and ^{13}C spectroscopy) has become an important and widespread analytical technique such that NMR spectra have been obtained and reported from basically every conceivable organic molecule found in nature or synthesized in a lab. NMR spectroscopy in chemistry is so heavily used for structural analysis or molecular identity verification that the American Chemical Society (ACS) requires hands-on access to at least one NMR spectrometer for all undergraduate students of ACS-certified Bachelor of Science degree programs [4].

To calibrate the chemical-shift axis of NMR spectra, it is necessary to define a reference point to which all other NMR resonances are compared. For example, in ^{1}H, ^{13}C, and ^{29}Si NMR spectroscopy, tetramethylsilane (TMS) is used as such a reference, defining the origin (δ = 0 ppm) of the chemical-shift axis. TMS was first chosen as reliable internal chemical-shift reference by Tiers et al. in 1958 [5], but it suffers from a low boiling point (26.5 °C) and easily evaporates at room temperature. Moreover, TMS is only very slightly soluble in water, which makes it hard to add TMS as a reference standard to aqueous solutions. Alternatively, 4,4-dimethyl-4-silapentane-1-sulfonic acid (DSS) has been suggested as reference standard for aqueous solutions [2]. DSS, however, is barely known by NMR spectroscopists and not in frequent use as a reference. Other suggested chemical-shift references for ^{1}H NMR spectroscopy are tetramethylammonium (TMA), methanol, or HOD [2, 5, 6].The HOD molecule, where one of the ^{1}H isotopes in H_2O is substituted by

a ^2H isotope (D = deuterium), is normally found as a trace compound in the deuterated NMR solvent D_2O. The disadvantages of adding reference materials as internal standard to the sample under investigation is that the chemical shift of the reference material may still depend on sample conditions such as concentration, temperature, or pH, and that the reference peaks may overlap with peaks of the sample under investigation.

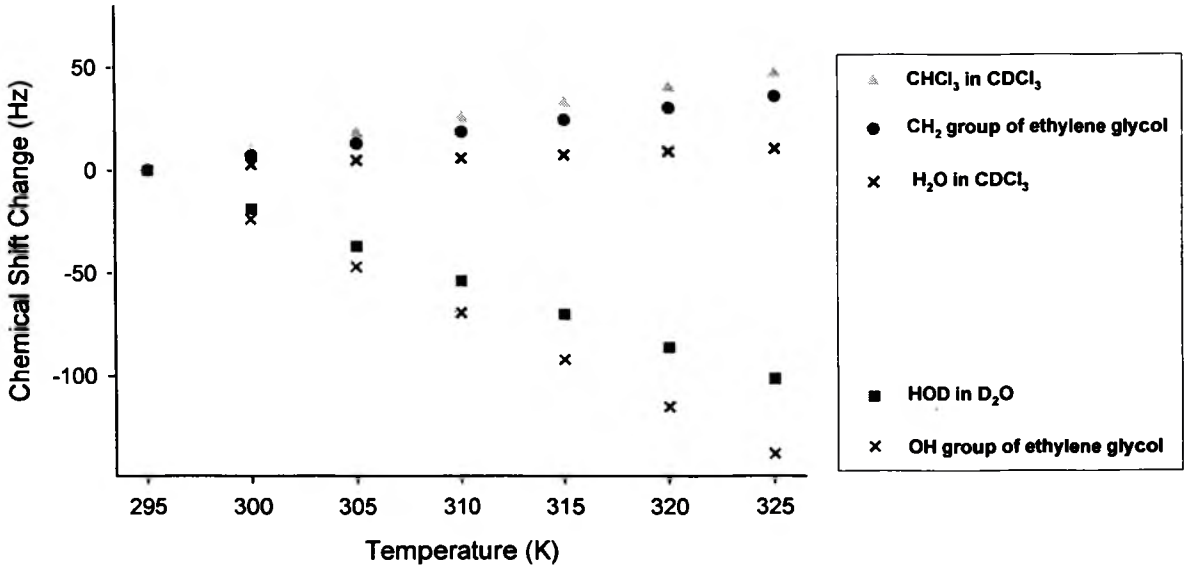

Figure 1.1. Temperature dependence of ^1H chemical shifts for small amounts of HOD dissolved in deuterated water (D_2O) as well as for ethylene glycol, H_2O, and $CHCl_3$ dissolved in deuterated chloroform ($CDCl_3$). The chemical-shift difference ($\Delta\delta$) between the signal for the CH_2-group of ethylene glycol and the signal for the OH-group of ethylene glycol is sometimes used to determine the temperature of a sample.

Figure 1.1 shows examples of ^1H chemical-shift changes as a function of sample temperature. For example, the chemical shift of the ethylene glycol CH_2 signal is less dependent on temperature ($\Delta\delta = 2.997 \times 10^{-3}$ ppm/K) than the ethylene glycol OH signal

($\Delta\delta = -4.667 \times 10^{-3}$ ppm/K) and opposite in sign. In another comparison it is noted that the chemical-shift change for H_2O in $CDCl_3$ is pretty small ($\Delta\delta = 0.875 \times 10^{-3}$ ppm/K) while HOD dissolved in D_2O exhibits a sizeable chemical-shift change in the opposite direction. Because the change of the H_2O chemical shift with temperature is very small, H_2O could be used as a preferred chemical-shift reference for NMR measurements in $CDCl_3$. However, it would be less suitable as a calibration standard for aqueous solutions, where H_2O and D_2O are in fast exchange leading to the formation of mostly HOD. Likewise, a pH-sensitive NMR molecule, i.e., a molecule that changes chemical shift with the pH of a solution, would not provide for a good chemical-shift reference. For example, the chemical shifts of the aromatic protons of 4-hydroxypyridine or cytosine in a mixture of the two compounds change considerably between pH = 9.5 to pH = 13.5 (Figure 1.2) [7].

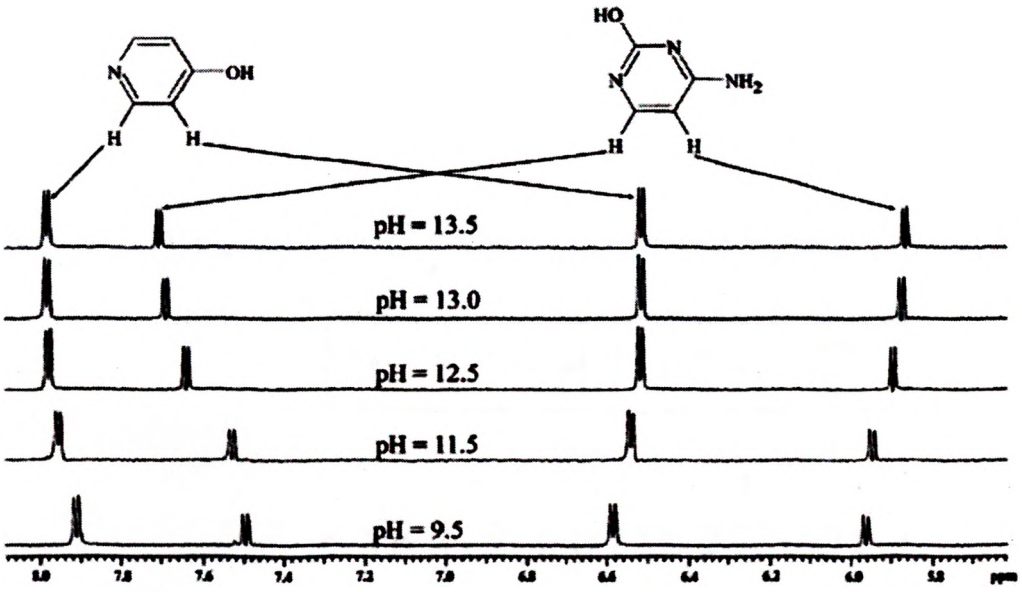

Figure 1.2. Stacked plot of the NMR spectra from the aromatic protons of a mixture of 4-hydroxypyridine and cytosine at different pH values (from ref. [7]).

To avoid a chemical-shift change caused by a changing pH, for example, an external reference should be used, isolating the reference solution completely from the sample solution (Figure 1.3). External references can be composed of the same materials internal standards are, but they are kept isolated from the sample by confining them to coaxial NMR-tube inserts mounted either close to the wall of a standard 5-mm or 10-mm NMR tube (Figure 1.3 a) or positioned concentrically with spacers inside the NMR tube (Figure 1.3 b). While concentrically mounted 1-mm capillary tubes are commercially available (for example: Wilmad-Labglass, WG-1364-1-203M and 529-B), the off-centered version was developed and preliminary studies with capillary tubes mounted to the outside of the NMR tube (exterior capillary tubes, Figure 1.3 c) were conducted as part of this dissertation.

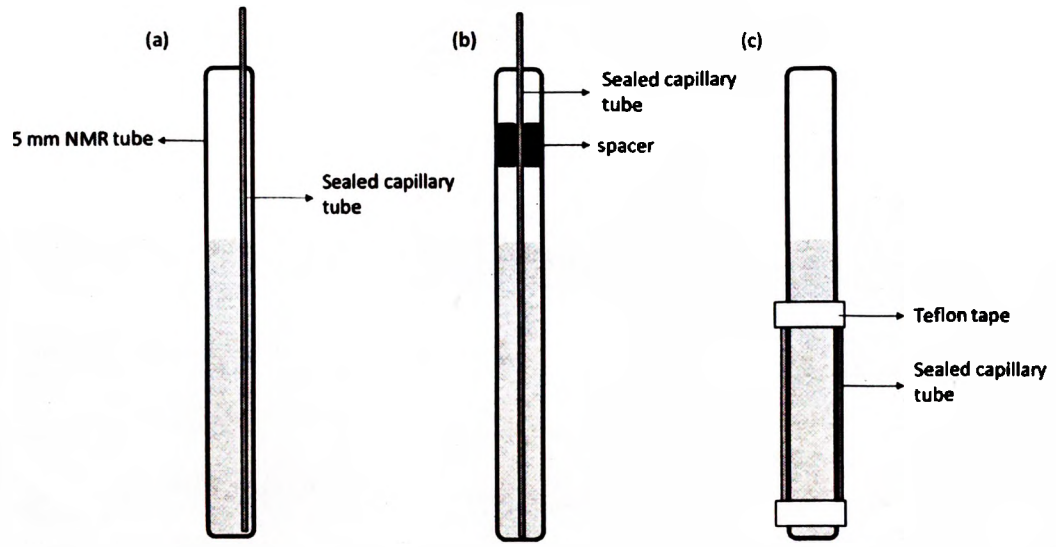

Figure 1.3. NMR-tube assemblies using 360-μm O.D. electrophoresis capillary tubes filled with a reference solution and permanently sealed with the arc of a fusion splicer. (a) Capillary tube mounted to the wall inside a 5-mm or 10-mm NMR tube. (b) Capillary tube positioned concentrically with spacers inside the center of standard 5-mm or 10-mm NMR tubes. (c) Capillary tubes mounted on the outside of a 4-mm NMR tube affixed with standard Teflon tape.

In the experimental work for this dissertation, NMR-tube calibration inserts were manufactured from small-diameter electrophoresis capillary tubes (Figure 1.3). The 360-μm O.D. fused-silica capillary tubes were filled with a reference material or solution, and then sealed by applying the arc of a commercial optical-fiber fusion splicer in a technique called melt-back sealing. Details of this innovative technique for sealing small-diameter, sample-filled capillary tubes are described in ref. [8]. Once sealed, the capillary tubes can be reused multiple times in different experiments with different solvents or different samples. In summary, using external standards is the preferred method for referencing chemical shifts, particularly when samples are used under conditions that may change the chemical shift of the referencing material.

In NMR spectroscopy, deuterated solvents are typically used to minimize large solvent signals that otherwise can obstruct the detection of small sample signals or interfere with their quantification. At the same time, the deuterium resonance frequency of the solvent is used to stabilize the external magnetic field. In a process known as field-frequency lock, the solvent's deuterium frequency is recorded and compared to a frequency that is fixed by the spectrometer. Any deviation from the fixed frequency, for example, due to fluctuations in the external magnetic field, is instantly adjusted by adding field strength to, or subtracting field strength from, the main magnetic field. While the resonances of other nuclei, in principle, may also be utilized to create a field-frequency lock, the deuterium lock system is most convenient and commonly applied because deuterium is often already present in the solvent molecules. A third advantage of the deuterium resonance is that, once it is locked to a fixed frequency, it may as well be used as the chemical-shift calibration reference. Consequently, when a series of samples is recorded

under field-frequency lock with the same deuterated solvent, the chemical-shift axis is automatically calibrated in reference to the deuterium resonance frequency of the solvent. This convenient deuterium referencing is the prime reason why many NMR spectra are currently recorded without the addition of an internal or external reference. However, it was found that the deuterium resonance of a deuterated solvent (especially D_2O) may not be as reliable and steady as commonly expected. In work pertaining to this dissertation, a capillary tube was filled with neat trifluoroacetic acid (TFA), permanently sealed, and used as ^{19}F chemical-shift reference. When the deuterium field-frequency lock was turned on, the ^{19}F signal of TFA appeared to shift to higher chemical-shift values when the pH of a sample solution was reduced (Figure 1.4 a). This change of the ^{19}F chemical shift was observed despite the fact that the TFA was kept completely isolated from the sample in a sealed small-diameter capillary tube. During a subsequent experiment it was found that the ^{19}F TFA signal remained unchanged (Figure 1.4 b) when the deuterium field-frequency lock was turned off. It was therefore concluded that it wasn't the chemical shift of TFA that changed. Instead the NMR spectrometer reacted with a change in external magnetic field to the changing deuterium resonance. This in turn led to a change in the resonance frequencies for both the sample under investigation and the external calibration-standard. Under deuterium-lock conditions, the TFA ^{19}F resonance shifted by as much as 0.16 ppm (31 Hz) when the pH of the solution was changed from alkaline to acidic. In an investigation of the ^{19}F chemical-shift pH dependence of 2-fluoro-3-hydroxymethyl-pyridine (FHMP), a ^{19}F chemical-shift change of 1.44 ppm (270 Hz) was measured under deuterium lock conditions, while only a 1.28 ppm (249 Hz) shift was observed relative to the ^{19}F peak of the independent and isolated TFA resonance.

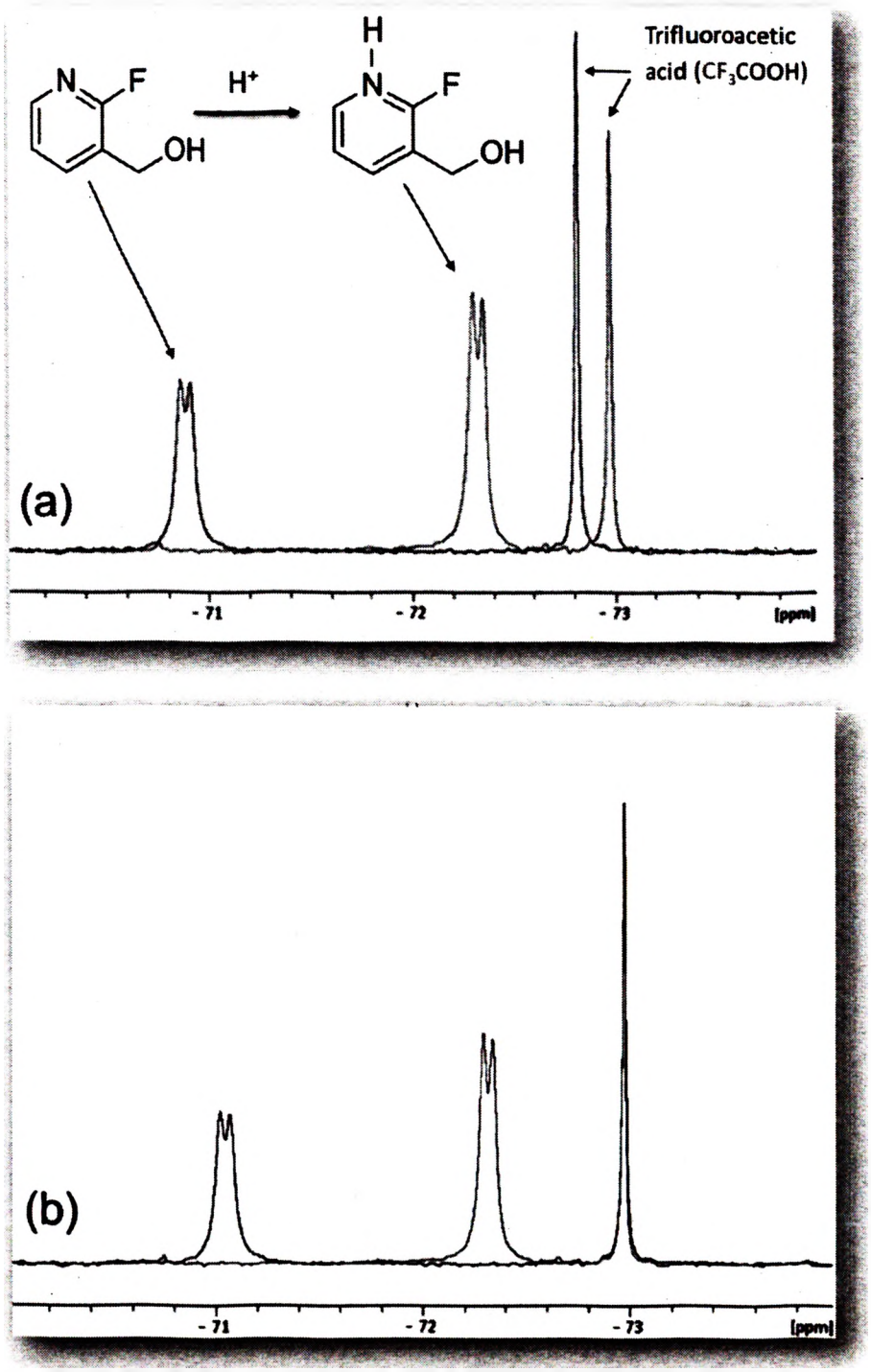

Figure 1.4. ^{19}F NMR spectra recorded from a 5-mm NMR tube filled with 4 μL of 2-fluoro-3-hydroxymethylpyridine (FHMP) dissolved in a 40% mixture of D_2O in H_2O. A sealed capillary tube filled with neat TFA was used as independent ^{19}F chemical-shift reference. The blue spectrum was recorded from the sample solution under alkaline conditions, while the red spectrum was recorded from the same composition under acidic conditions. (a) Using the standard deuterium field-frequency lock, the independent ^{19}F reference signal of TFA appears to be shifted to smaller chemical-shift values. (b) Without deuterium lock, the position of the TFA signal in the blue (basic) and the red (acidic) spectrum remains unchanged.

Another effect that influences the chemical shift of NMR resonances is the addition of paramagnetic substances to a solution (Figure 1.5). Small amounts of paramagnetic impurities are often enough to visibly alter the resonance frequencies of compounds in solution. However, not only the chemical shift is affected by paramagnetic compounds; the NMR relaxation times T_1 (spin-lattice relaxation) and T_2 (spin-spin relaxation) are also considerably shortened by the addition of paramagnetic compounds. This effect is sometimes used to deliberately shorten relaxation times, and with it the time it takes to record a large number of NMR scans. A large number of scans can substantially improve the signal-to-noise ratio in an NMR spectrum, which might be necessary to detect compounds in very dilute systems. The unpaired electrons of paramagnetic cations, such as in Cu^{2+} ions, exhibit large magnetic moments that perturb the local magnetic field seen by the NMR nuclei under investigation [9]. These magnetic field perturbations generally lead to a faster loss of phase coherence (T_2 relaxation) and a faster recovery to thermodynamic equilibrium (T_1 relaxation) than in the absence of paramagnetic ions. In a series of special preliminary examinations, a reference capillary tube was filled with nitromethane and mounted concentrically with spacers inside a standard 5-mm NMR tube. The ^1H NMR signal of nitromethane was used as chemical-shift calibration standard and adjusted to 5.4 ppm (literature value) on the ^1H chemical-shift scale. Distilled water was filled into the remaining space of the 5-mm NMR tube and a spectrum recorded (Figure 1.5 a). Upon the addition of a small crystal of solid $CuSO_4$ another NMR spectrum was recorded. A significant change in the chemical shift of H_2O as well as an increase in spectral linewidth was observed (Figure 1.5 b). Further additions of similar amounts of $CuSO_4$ led to smaller changes in chemical shift and spectral linewidth (Figure 1.5 c and d).

To quantitatively determine the relationship between T_1 and T_2 relaxation times on the one and chemical shift on the other hand, the T_1 CapPack was developed which combines up to seven capillary tubes filled with aqueous solutions of different trace amounts of $CuSO_4$. The trace amounts were adjusted so that seven different signals with different chemical shifts as well as different T_1 and T_2 times can be observed in a single NMR experiment.

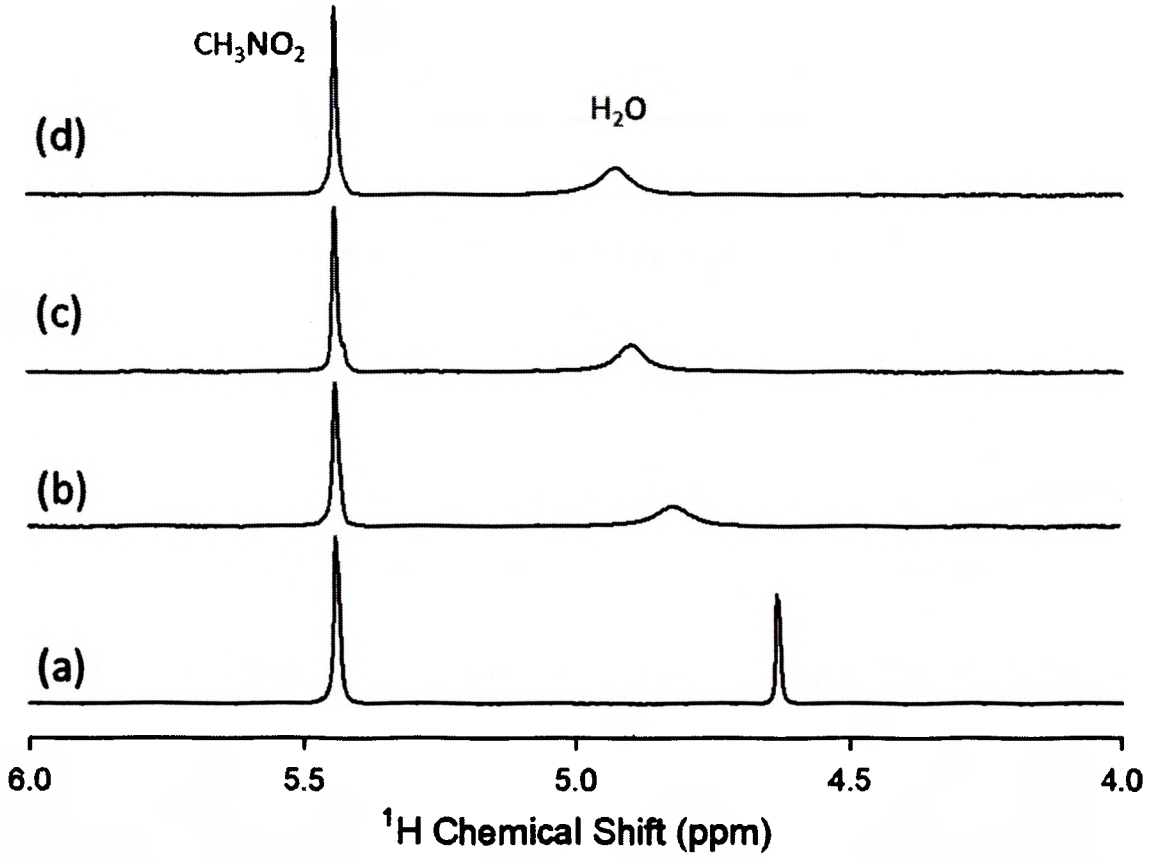

Figure 1.5. ^1H NMR spectra of water doped with different trace amounts of $CuSO_4$. A capillary tube filled with nitromethane was added into the NMR tube as chemical-shift calibration standard (5.4 ppm). A small crystal of solid $CuSO_4$ was added three times to the water. The chemical shift of the H_2O peak originally at 4.7 ppm changes with the addition of $CuSO_4$ while the peak of nitromethane remains at a constant chemical shift.

1.2. THE IMPORTANCE OF CONCENTRATION REFERENCING IN NMR SPECTROSCOPY

The precise determination of a sample concentration is of fundamental interest for many scientific and practical aspects in chemistry and biology. NMR spectroscopy is a powerful tool for this purpose because NMR signal intensities are directly proportional to the number of resonating nuclei. Limitations of quantitative NMR investigations depend only on uncertainties in the experimental conditions and on an accurate calibration of signal intensities to known concentrations. For the highest measurement precision, it is essential that NMR spectra are properly calibrated by a reference standard and that the calibration signal is observed simultaneously with the signals from the analyte solution. Similar to the chemical-shift calibration, a concentration reference can be added as internal standard or as external standard. An internal standard must satisfy several conditions: (1) it must be soluble in the sample solution, (2) any chemical interaction with the sample must be avoided or suppressed, (3) an overlap between sample peaks and reference peaks must be avoided, and (4) the longitudinal relaxation time T_1 must be close to or smaller than the T_1 time of the analyte [10,11]. Because internal standards fill the same volume as the analyte solution, internal standards are generally insensitive to variations in the static magnetic field B_0 or the radiofrequency field B_1. Overall it can be difficult to find a suitable internal standard that satisfies the prerequisites mentioned above. It may also be difficult to determine exactly the concentration of an internal reference compound when it is added to an analyte solution. On the contrary, the sealed capillary-tube concept introduced earlier is a viable choice for external concentration references because the chemical composition of the reference material can be easily controlled and chosen independent of potential interactions with the analyte solution. However, the position of the reference capillary tube

in the NMR tube becomes critical because systematic errors can occur when the analyte is exposed to a different B_0 or B_1 field distribution (B_0 or B_1 inhomogeneities, respectively) than the reference material. When using external reference standards for the quantitative determination of analyte concentrations, it is important to know precisely the volume ratio between the reference and the analyte sample. With the precise knowledge of the volume ratio, the signal-intensity ratio between reference and analyte can be used to determine absolute concentrations. Alternatively, the signal intensity of an external reference can be calibrated by comparison to the signal from an analyte solution with precisely known concentration. The calibrated reference intensity can then be used to determine unknown concentrations of samples filled into the same NMR tube (or, at a minimum, into the same type of NMR tube).

If the NMR signal intensity of a reference sample is used to determine the concentration of an analyte sample, it is also important to confirm that the magnetizations of both the external standard and the analyte are fully relaxed to thermodynamic equilibrium before another NMR scan is recorded. As a rule of thumb for quantitative NMR experiments, the recycle delay between scans should be between five and ten times the longitudinal relaxation time (T_1) depending on the desired precision. Especially when the T_1 relaxation times of reference and analyte are significantly different, an accurate reference-to-analyte signal ratio is measured only after a relaxation delay of five to ten times the longer of the two relaxation times. The experiment in Figure 1.6 shows reference-to-analyte intensity ratios measured for water (T_1 = 2.8 s) as the reference and a solution of trichloroethylene in deuterated chloroform (T_1 > 15 s) as the analyte solution. The intensity ratios are plotted as a function of the relaxation delay (d_1) applied between consecutive

scans in the NMR experiment. When the relaxation delay was set below five times the relaxation time of the analyte (d_1 < 75 s), the reference-to-analyte signal-intensity ratio does not accurately reflect the volume-weighted concentration ratio (number-of-nuclei ratio) between reference and analyte.

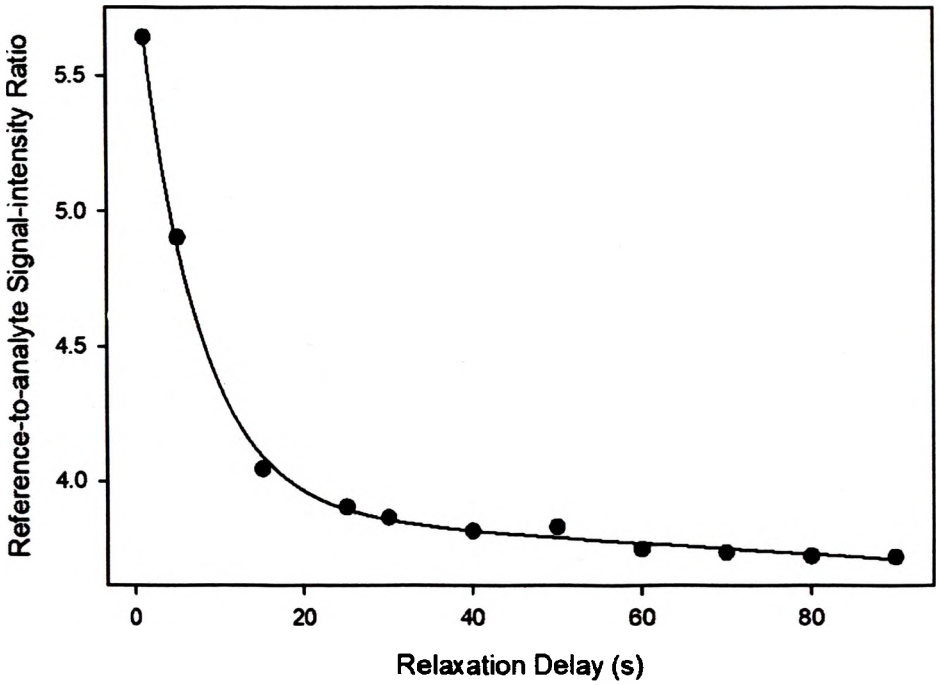

Figure 1.6. Intensity ratio of the ^{1}H NMR signal recorded from a reference capillary tube filled with H_2O to the ^{1}H NMR signal recorded from a 5-mm NMR tube filled with 8.9906 mM trichloroethylene in $CDCl_3$ solution as a function of relaxation delay (d_1) between consecutive scans. The capillary tube was mounted concentrically with spacers inside the 5-mm NMR.

1.3. RESEARCH OBJECTIVES

The main objective of this dissertation is to provide a precise chemical-shift and signal-intensity referencing system using internal and external standards. The internal and external standards are evaluated with respect to specific applications in qualitative and

quantitative solution NMR spectroscopy using different samples as well as different sample conditions. Additionally, small-capillary external standards are used for the first time in magic-angle-spinning solid-state NMR spectroscopy. A small capillary tube is positioned in the center of a magic-angle-spinning rotor and used in situ to determine the temperature inside the rotor while it is spinning.

The specific objectives addressed in this dissertation pertain to developments and applications of chemical-shift and signal-intensity NMR referencing techniques including:

1) The CapPack platform as external chemical-shift calibration devices as well as NMR-temperature measuring devices.
2) External signal-intensity calibrations for quantitative NMR measurements.
3) Gradient and Relaxation CapPack devices for the quality assurance and optimization of NMR spectrometers and NMR pulse sequences.
4) The use of chemical-shift and signal-intensity calibrations in the following NMR applications:
    a. Semi-quantitative determination of the residual water content in ionic-liquid rocket monopropellants.
    b. Determination of chemical shifts, relaxation times, and intermolecular transfer of signal saturation for the analysis of interactions between polymer micelles and small molecules in solution.
    c. Studies of the release kinetics of small molecules from loaded porous-wall hollow glass microspheres.

2. THE CapPack NMR PLATFORM

With the increased sensitivity of modern NMR spectrometers, the minimum amount needed for chemical-shift and signal-intensity calibration of NMR spectra has decreased to a point where a few microliters are sufficient to observe a reference signal. The reduction in the amount of reference material is the basis for the NMR CapPack platform that utilizes small capillary tubes as NMR-tube inserts for external reference standards. The capillary tubes with outer diameters smaller than 400 μm are filled with reference solutions and then permanently sealed by the arc of an optical-fiber fusion splicer. The sealed capillaries are used as external references for chemical-shift and signal-intensity calibrations. Signal-intensity calibrations are particularly important for the emerging field of quantitative NMR spectroscopy. Combining a number of sealed capillaries to form Gradient or Relaxation CapPack devices leads to additional applications for performance evaluations of NMR spectrometers and pulse sequences. A side-by-side Gradient CapPack device is used in combination with transverse magnetic field gradients to monitor and evaluate the excitation profiles of shaped pulses. A Relaxation CapPack device consists of multiple sealed capillary tubes filled with solutions of different T_1 or T_2 relaxation times. If different concentrations of Cu^{2+} ions are used as paramagnetic relaxation agents in aqueous solutions, the T_1 or T_2 relaxation times in the different capillary tubes can cover a relaxation range that extends to more than an order of magnitude. Relaxation CapPack devices are best suited to quantify the effects relaxation has on magnetizations and coherences during the execution of NMR experiments.

Nuclear-spin resonance frequencies are directly proportional to the strength of the external magnetic field, B_0, which varies from one NMR spectrometer to another. Because

of this variability, the frequency axis of NMR spectra is not absolute but must be calibrated by the resonance frequency of a known material [12]. Resonances of known materials may include signals from internal or external standards, solvent signals, signals from previously recorded spectra, or ^{2}H resonances (i.e., D resonances) of deuterated solvents locked in with the spectrometer's field-frequency lock [13]. The most commonly used internal standard is perhaps tetramethylsilane (TMS) which, by convention, defines the zero-point of reference for the chemical-shift ppm axes of ^{1}H, ^{13}C, and ^{29}Si spectra. However, if an analyte material or the sample solvent is suspected to interfere with or alter the resonances of a reference standard, internal standards may not be reliable, and external standards must be used [14]. External standards can be composed of the same materials as internal standards, and they are typically sequestered in commercially available, coaxial NMR-tube inserts (1 mm O.D.) mounted concentrically with spacers inside standard 5-mm or 10-mm NMR tubes [15]. With the increased sensitivity of modern NMR instrumentation, the commercially available inserts may take away too much valuable space that could otherwise be filled with more of the analyte solution. Consequently, smaller capillary tubes with an O.D. less than 400 μm may already be large enough to hold a sufficient amount of reference material. The reduction in the required amount of reference material gives rise to the CapPack platform, where the acronym "CapPack" is used as an abbreviated form of **Cap**illary-tube **Pack**ages. CapPack devices are manufactured from small fused-silica glass capillary tubes with an I.D. as small as 20 μm. They are filled with the desired reference material and permanently sealed with the arc of an optical-fiber fusion splicer [8]. For most NMR applications, CapPack devices provide enough NMR-sensitive materials to calibrate chemical-shift axes for NMR experiments or calibrate NMR signal intensities for the

determination of absolute concentrations or absolute amounts of material in an NMR sample. CapPack devices also allows users to measure the temperature of an NMR sample in situ, to assess the performance of pulse sequences and optimize pulse parameters, to explain artifacts that may occur in spectra, and to reveal spectroscopic results that deviate from theoretical predictions.

2.1. CapPack DEVICES OF SINGLE CAPILLARY TUBES

2.1.1. Chemical-shift CapPack Device. Several different reference standards are currently in use to calibrate the chemical-shift axes of ^{1}H, ^{13}C, ^{15}N, ^{19}F, ^{29}Si, or ^{31}P NMR spectra, as well as the chemical-shift axes of other, less commonly used nuclei [5, 6, 16-27]. For example, tetramethylsilane (TMS), 4,4-dimethyl-4-silapentane-1-sulfonic acid (DSS), trimethylsilyl propionate (TSP), tetramethylammonium (TMA), methanol, or HOD are suggested as reference compounds for ^{1}H NMR [5, 6, 16, 20]. Similar to the variety of reference samples in ^{1}H NMR, several alternative compounds are suggested as reference standards for ^{13}C NMR (e.g., TMS, acetone, DSS, or TSP) [5, 6, 16], ^{15}N NMR (e.g., ammonium, ammonium chloride, ammonium nitrate, or nitromethane) [16, 23, 24], ^{19}F NMR (e.g., difluoromethionine, 5-fluorouracil, fluoroanilines) [18, 19, 21, 22], ^{29}Si NMR (e.g., TMS, silicon oxyfluoride, tetrafluorosilane, or other fluorosilanes) [25, 26], or ^{31}P NMR (e.g., triethylphosphate) [17, 27].

To avoid interferences of the analyte sample with the reference material, an external reference can be used, isolating the reference material completely from the analyte solution. External reference standards can be composed of the same materials as internal standards, but they are kept apart from the sample and confined to an isolated volume

within the NMR sample tube. Single-capillary CapPack devices filled with external calibration standards provide a new, practical, and sustainable option for external standards. A great advantage of using sealed capillary tubes filled with external standards is that they may be re-used multiple times for different experiments with different solvents or different samples without interfering with the samples under investigation. The positioning of the reference capillary tube in an NMR tube, however, can be critical because systematic errors can occur when the analyte is exposed to different B_0 or B_1 inhomogeneities compared with the reference material.

In summary, using external standards is the preferred method for referencing chemical shifts, particularly when analyte solutions are used under sample or reaction conditions that may change the chemical shift of the referencing material. Figure 2.1 shows the ^{1}H NMR spectrum of three single-capillary CapPacks (I.D. of 250 μm each) filled with different reference solutions ($CHCl_3$, CH_3NO_2, DMSO), each mounted at different locations close to the wall of a 5-mm NMR tube. The remaining volume of the NMR tube is filled with D_2O (99.8%). The chemical shifts of the reference signals are compared to the residual HOD signal in D_2O at 4.60 ppm. Table 2.1 summarizes the chemical shifts of the reference materials in the capillary tubes as calibrated relative to the HOD signal at 4.60 ppm. Utilizing different reference materials allows a spectroscopist to select an appropriate chemical-shift reference that is removed from the analyte signals of interest. The recorded chemical-shift values are for pure reference materials (e.g., 100% $CHCl_3$) and can deviate from literature values that may have been recorded under slightly different conditions. Accordingly, for accurate chemical-shift referencing, it is critically important that reference materials are also calibrated first against a common reference standard.

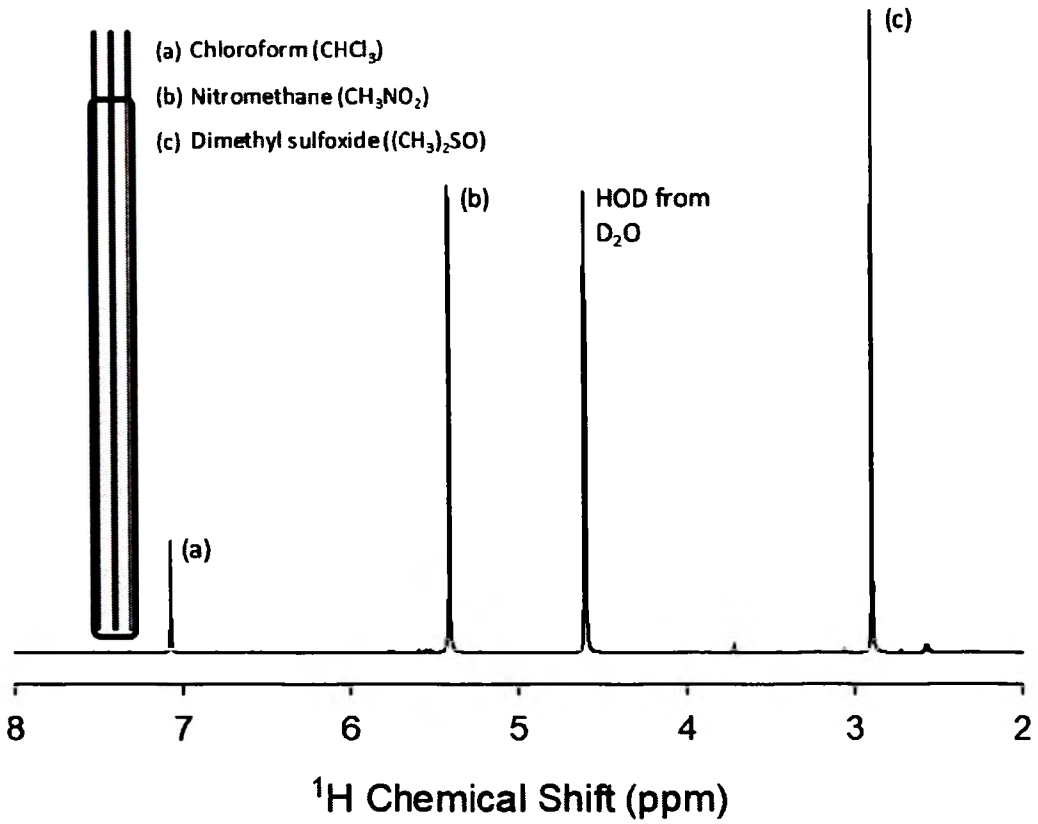

Figure 2.1. ^{1}H NMR spectrum of three single capillary-tube CapPacks (250 μm I.D.) filled with different reference materials. The CapPacks were mounted close to the wall of a 5-mm NMR tube. The signals are assigned as follows: (a) chloroform ($CHCl_3$); (b) nitromethane (CH_3NO_2); (c) dimethyl sulfoxide ($(CH_3)_2SO$). The chemical shift axis was calibrated relative to the HOD signal at 4.6 ppm.

Table 2.1. ^{1}H NMR chemical shift of CapPackd filled with different reference materials. The chemical shifts are assigned relative to the HOD signal at 4.6 ppm and compared to literature values [28, 29].

Chemicals	Measured Chemical Shift (ppm)	Literature Chemical Shift (ppm)	Literature Reference
$CHCl_3$	7.06	7.26	[28]
CH_3NO_2	5.41	4.43 - 5.71*	[28], [29]
$(CH_3)_2SO$	2.89	2.54	[29]

*The chemical-shift range of nitromethane is caused by a changing equilibrium of nitromethane with the aci-anion of nitromethane

2.1.2. Signal-intensity CapPack Device. For the highest precision in quantitative NMR, it is essential that NMR spectra are properly calibrated by a reference standard, and that the calibration signal is observed together or in fast succession with the signals from the analyte solution. Similar to the chemical-shift calibration, a concentration reference can be added as internal or external standard. Sealed single-capillary CapPack devices are a viable choice for external signal-intensity references because the chemical composition can be easily controlled and chosen independent of potential interactions with the analyte solution. Before the signal intensity of an external reference can be used to determine the concentration of an unknown analyte, it must itself be calibrated against a known concentration in the NMR tube. Once calibrated, the reference signal intensity can be used to determine unknown concentrations of samples filled into the same NMR tube (or, at a minimum, into the same type of NMR tube).

2.1.3. CapPack Device for In Situ Temperature Determination. The chemical shift of NMR resonances often change with the sample temperature ranging from slight changes to strong dependencies (see Figure 1.1). While the signals of chemical-shift calibration standards should be as independent of temperature as possible, sample materials that show a strong dependence on temperature can be used to measure the temperature of an NMR sample in situ. To qualify for a temperature-sensing molecule in NMR spectroscopy, it is best if one of the molecule's NMR signals is largely independent of temperature while another signal heavily depends on temperature. Methanol and ethylene glycol are the most commonly used temperature-sensing compounds for ^{1}H NMR spectroscopy [30-32]. The chemical shift of the methanol OH-group, for example, changes substantially with temperature while the CH_3-group signal is almost independent of

temperature. Between 178 K and 330 K, the chemical-shift difference between the OH- and CH_3-group signals of methanol follows the relationship: [32]

$$T = (409.0 - 36.54\,\Delta\delta - 21.85\,(\Delta\delta)^2)\ \mathrm{K} \qquad (1)$$

where T is the absolute sample temperature in Kelvin, and $\Delta\delta$ the chemical-shift difference in ppm between the two functional groups. For ethylene glycol between 273 K and 416 K, the chemical-shift difference between the OH- and CH_2-group signals follows the linear relationship: [32]

$$T = (466.5 - 102.00\,\Delta\delta)\ \mathrm{K} \qquad (2)$$

Both methanol and ethylene glycol have been used as temperature sensing molecules in very different areas of NMR investigations such as biofluid for blood plasma tests [33], temperature-dependent measurements of diffusion coefficients [34], or temperature-dependent adsorption of water on silica surfaces [35].

Similar to chemical-shift and signal-intensity calibrations with single-capillary CapPacks, a temperature-sensing material can be filled into a small capillary tube, permanently sealed with the arc of a fusion splicer, and used as external standard for in situ determination of the temperature of an NMR sample. For example, the temperature-dependent NMR calibration experiments of Figure 1.1 were all conducted using a single-capillary CapPack device for temperature sensing in addition to a single-capillary CapPack device for chemical-shift referencing. The in situ determination of NMR sample temperatures provides a good example for the use of several different single-capillary CapPacks to evaluate different parameters in one experiment (here: chemical shift and temperature).

2.2. CapPack DEVICES OF MULTIPLE CAPILLARY TUBES

2.2.1. Gradient CapPack Devices. A Gradient CapPack device consists of multiple glass-sealed capillary tubes mounted side-by-side and filled with the same NMR-sensitive reference material [8].When a field gradient is applied across the side-by-side coordinate and perpendicular to the long axes of the capillary tubes, the common signal from the capillary tubes will separate into individual signals on the chemical-shift axis depending on the gradient field strength (Figure 2.2 b). Gradient CapPacks are designed to test the performance of frequency-selective pulses or pulse sequences, and to record and document chemical-shift-dependent excitation profiles. For example, a Gradient CapPack device of 10 capillary tubes was used to test the performance of low-power, frequency-selective adiabatic hyperbolic secant pulses (HS1) [36] in the EXCEPT-12 (EXponentially Converging Eradication Pulse Train) solvent-suppression sequence [37]. Figures 2.2 (c) and (d) show gradient spectra after the application of EXCEPT-12 with the HS1 pulse frequency set at the center of the CapPack signals (3.78 ppm). The HS1 pulse width in the EXCEPT sequence was adjusted to 400 ms in the experiment of Figure 2.2 (c) and 300 ms in the experiment of Figure 2.2 (d) leading to suppression bandwidths of 90 Hz and 120 Hz, respectively. Figure 2.2 (c) shows that the signals from the two outer capillary tubes on each side of the Gradient CapPack are undisturbed by the EXCEPT sequence confirming that HS1 pulses affect only resonances within a very limited bandwidth. Within the desired frequency range, signal suppression is asymmetrical and incomplete, which shows that the application of EXCEPT-12 may not lead to the suppression results predicted by the theory. Comparisons between Figures 2.2 (c) and (d) also reveal that the asymmetry in suppression increases with decreasing HS1 bandwidth, i.e., with longer HS1 pulses.

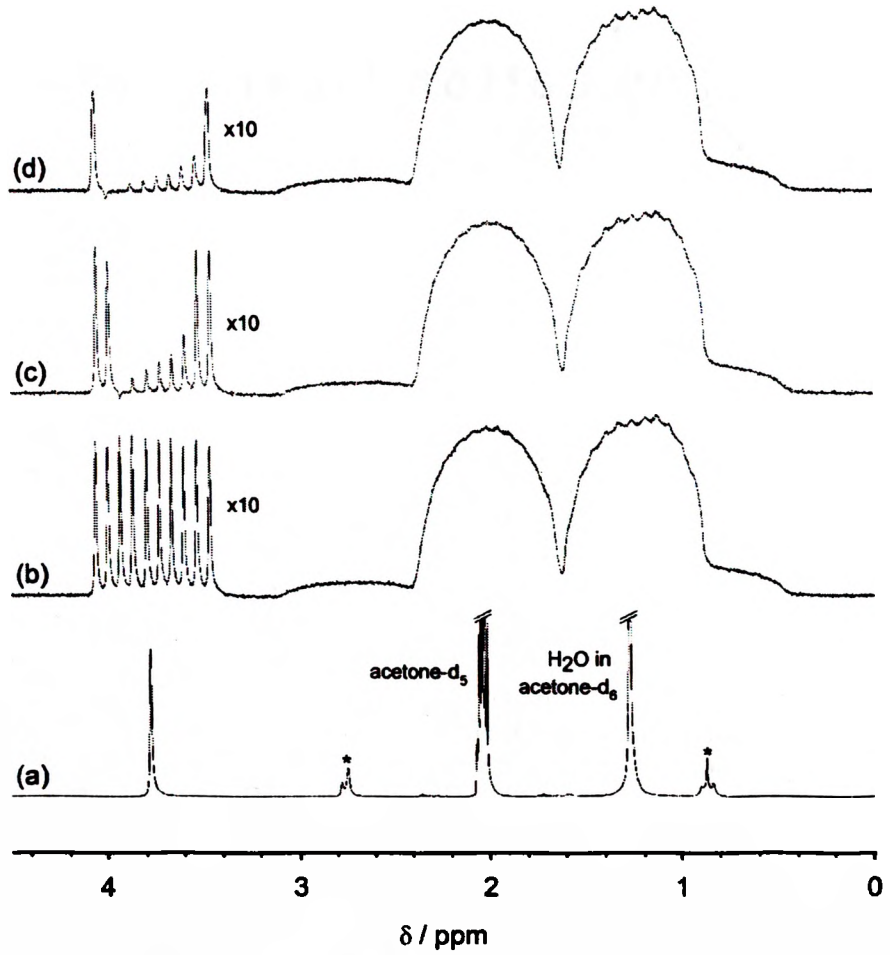

Figure 2.2. ^{1}H NMR spectra recorded from a 10-capillary-tube Gradient CapPack in a 5-mm sample tube using acetone-d_6 (99.8%) as the surrounding solvent: (a) with a standard 90° observe pulse, (b) with a the 90° observe pulse while a 0.81 Gauss cm^{-1} gradient is applied across the 10 side-by-side capillary tubes, (c) with an observe pulse following the application of 400-ms HS1 pulses in an EXCEPT-12 experiment, (d) following the application of 300-ms HS1 pulses in an EXCEPT-12 experiment. The signal-intensity axes of spectra (b), (c), and (d) are amplified by a factor of 10. Upon the application of the gradient, signals from resonances other than the Gradient CapPack are broadened, representing a one-dimensional profile of the NMR tube's circular cross section.

2.2.2. Relaxation CapPack Devices. A Relaxation CapPack device consists of multiple capillary tubes filled with materials of different relaxation times. It is designed to evaluate the effects spin-lattice or spin-spin relaxation can have on magnetizations and coherences during the execution of NMR experiments. If water is used as the reference

material, paramagnetic relaxation agents such as Cu^{2+} ions can be added to adjust the relaxation times of the ^1H resonances in the capillary tubes [38]. At the same time, the addition of Cu^{2+} salts results in a substantial chemical-shift change in the ^1H resonance signal of H_2O. An independent series of NMR experiments was conducted using aqueous solutions with different trace amounts of Cu^{2+} salts at a resonance frequency of 200 MHz (Figure 2.3). A linear relationship between chemical shift change $\Delta\delta$ (in Hz) and relaxation rate T_1^{-1} for the H_2O resonance was established ($\Delta\delta = 4.208\, T_1^{-1}$). Because relaxation rates often depend on the magnetic field strength, it is noted that different linear relationships will result from measurements at different magnetic fields strength.

With increasing amounts of dissolved Cu^{2+} salts, the water resonances not only shift toward higher chemical-shift values but also show substantially broader linewidths caused by shorter spin-spin relaxation times T_2. If the concentration-dependent paramagnetic shift ($\Delta\delta$) is sufficient to separate the signal from one capillary tube on the chemical-shift axis completely from the signals of the other capillary tubes, no external magnetic field gradient is needed to observe the CapPack signals separately. In Figure 2.4, the H_2O resonance signals from a seven-capillary-tube Relaxation CapPack device are shown and labeled with Roman numerals. The Cu^{2+} ion concentrations for the seven capillaries were chosen so that the resonance signals are sufficiently separated from each other, and relaxation times can be evaluated independently and over a wide range of T_1 and T_2.

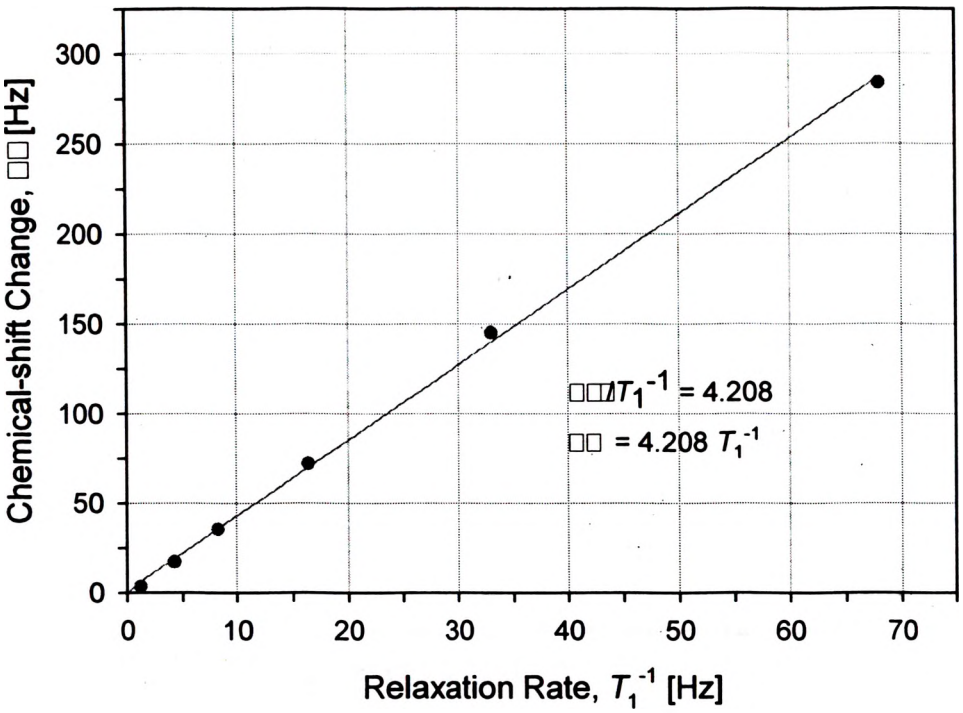

Figure 2.3. ^{1}H spin-lattice relaxation rate T_1^{-1} as a function of chemical shift change $\Delta\delta$ (paramagnetic shift) measured for different trace amounts of $CuSO_4$ dissolved in aqueous solution.

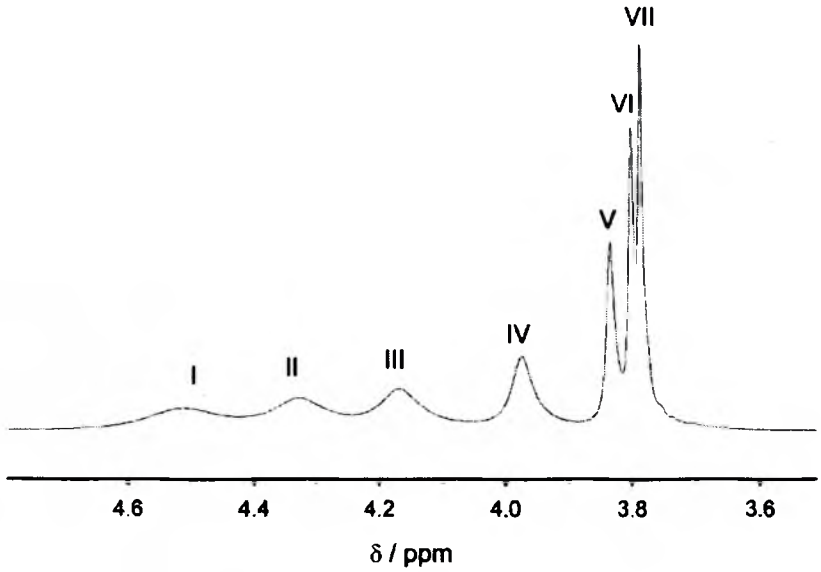

Figure 2.4. ^{1}H NMR spectrum obtained from a seven-capillary-tube relaxation CapPack device containing aqueous solutions with different trace amounts of paramagnetic Cu^{2+} ions. The labels in the spectrum refer to the resonance signals from the seven individual capillaries.

2.2.3. Exterior CapPack Devices. Different from the standard utilization of CapPacks, single-capillary reference tubes can also be mounted on the outside of an NMR tube (Figure 2.5). Utilizing CapPacks on the outside of an NMR tube is termed "Exterior CapPack" for two reasons: (a) to distinguish it from the standard (i.e., interior) use of CapPacks, where the capillary tube is positioned on the inside of an NMR tube, and (b) to distinguish it from "external" reference standards, which do not refer to locations but to reference samples that are completely isolated from the analyte solution. Exterior CapPack devices can be useful as reference standards when the material inside the NMR tube reacts with the polymer or glass surface of the CapPack (e.g., in a polymerization reaction) or

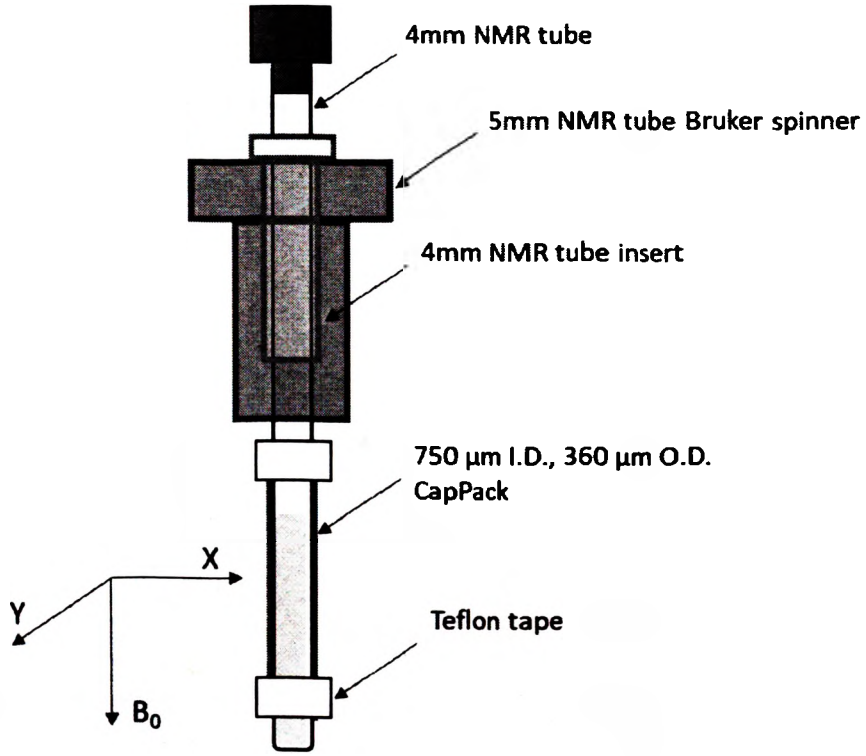

Figure 2.5. Exterior CapPack device. It includes two capillary tubes (75 µm I.D., 360 µm O.D.) filled with the same reference material (e.g., nitromethane) and mounted with Teflon tape on the opposite sides of a 4-mm NMR tube. A sample of 10 µL of ethanol dissolved in 600 µL D_2O is used as the sample inside the 4-mm NMR tube.

when the sample under investigation can cause substantial alkaline glass corrosion. Furthermore, exterior CapPacks may be the best, or even only, choice when a sample inside the NMR tube is air sensitive, light sensitive, or must be kept under inert or pressurized conditions.

Two exterior CapPacks mounted on opposite sides of an NMR tube can assist in homogenizing the main magnetic field across a sample. The homogenization of the main magnetic field by room-temperature coils around the sample area is generally referred to as magnetic-field shimming. Particularly the shimming in the transverse plane (i.e., in the magnetic x and y direction) can be observed directly with a pair of exterior CapPacks. Modern NMR spectrometers are equipped with multiple shim gradient coils that can be used to optimize the line shape for a given sample. Since each sample is different, there is no one ideal shim setting that will give the best results for all samples. The magnetic fields added by NMR shim coils in order to homogenize the main magnetic field are generally based on geometric functionalities (e.g., x, x^2, x^3, y, y^2, y^3) or on superpositions of such functionalities (e.g., xy, xz^2, or even x^2-y^2) [39].

For a combination of two exterior CapPacks filled with the same reference material and mounted on opposite sides of an NMR tube, a single reference peak is only expected when the magnetic field at the two CapPack locations is identical. Poor magnetic field shimming will lead to different magnetic fields at the locations of the exterior CapPacks, resulting in two peaks at different chemical shifts. Basic magnetic field theory predicts that, if the magnetic field on the outside of an NMR tube is optimized, the magnetic field on the inside is also optimized. This applies because there are no active magnetic-field sinks or sources present in the NMR sample. Consequently, superimposing the reference signals

from two oppositely mounted exterior CapPacks automatically optimizes the magnetic field within the NMR sample volume.

The results of a series of exterior CapPack shim experiments are shown in Figure 2.6. Two oppositely mounted exterior CapPacks (as depicted in Figure 2.5) filled

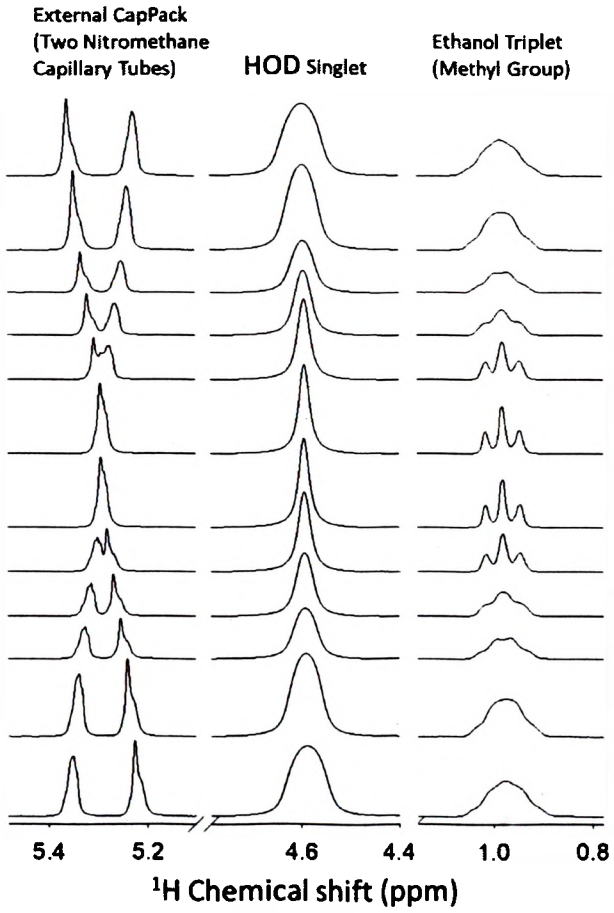

X-Gradient Shim Setting	Splitting (Hz)	Gradient X-axis (mT/mm)
3664	-26.76	-1.443×10^{-4}
4664	-21.59	-1.164×10^{-4}
5664	-16.59	-8.948×10^{-5}
6664	-11.60	-6.252×10^{-5}
7664	-5.89	-3.177×10^{-5}
8664	1.16	$+6.257 \times 10^{-6}$
8664	0.98	$+5.286 \times 10^{-6}$
9664	+3.84	$+2.071 \times 10^{-5}$
10664	+9.10	$+4.908 \times 10^{-5}$
11664	+14.45	$+7.794 \times 10^{-5}$
12664	+19.63	$+1.059 \times 10^{-4}$
13664	+24.80	$+1.338 \times 10^{-4}$

Figure 2.6. ^{1}H NMR spectra of nitromethane in two exterior CapPacks, the remaining HOD peak of the solvent D_2O, and the CH_3-group signal of dissolved ethanol. The most homogeneous field occurs at the *x*-gradient shim setting of 8664. When the *x*-gradient shim setting was increased or decreases in steps of 1000, the nitromethane peaks separated, the HOD peak broadened and the ethanol CH_3 peak loses the triplet resolution. The table to the right of the spectra depicts the separation of the oppositely mounted nitromethane peaks as a function of the *x*-gradient shim setting. The *x*-gradient field strength is calculated from the nitromethane peak separation $\Delta\omega$ (in Hz), the gyromagnetic ratio of protons ($\gamma_H = 42.58$ kHz/mT) and the distance d (in mm) between the exterior CapPacks according to $1000 \times \Delta\omega / (\gamma_H \times d)$.

with nitromethane were positioned along the gradient field of the *x*-direction shim coil. A solution of 10 μL of ethanol dissolved in D_2O was used as the sample inside the 4-mm NMR tube. Several single-pulse ^1H NMR experiments were conducted with a stepwise change in the current applied to the *x*-direction shim coil. The spectra of Figure 2.6 reveal that the magnetic field is optimized at the *x*-gradient shim coil setting with the numerical value of 8664. At this setting, which is specific for the NMR spectrometer in use, the two nitromethane peaks of the exterior CapPacks completely overlap, and the peaks of the sample solution (HOD peak, ethanol triplet) show the smallest linewidth. At this linewidth, the triplet of the ethanol CH_3 group is well resolved, which is an additional indication of a well-shimmed magnetic field. Figure 2.6 also shows that, when the *x*-gradient shim setting is increased or decreases, the nitromethane peaks separate, the HOD peak broadens, and the ethanol CH_3 peak loses its triplet resolution. The table to the right of Figure 2.6 depicts the separation of the oppositely mounted nitromethane peaks related to each of the *x*-gradient shim setting. The strength of the *x*-gradient field ($\Delta B_0(x)$ in mT/mm) is calculated from the nitromethane peak separation ($\Delta\omega$ in Hz), the gyromagnetic ratio of protons (γ_H = 42.58 kHz/mT) and the distance (x in mm) between the exterior CapPacks according to:

$$\Delta B_0(x) = \frac{\Delta\omega}{1000\,\gamma_H\,x} \tag{3}$$

Figure 2.7 shows the optimized ^1H NMR spectrum with the exterior nitromethane CapPacks. In this spectrum, six peaks are resolved. They are assigned from left to right: (a) CH_3 peak of nitromethane (singlet at 5.30 ppm), (b) residual HOD peak of the sample solvent D_2O (singlet at 4.60 ppm), (c) CH_2 group of dissolved ethanol (quartet at 3.46 ppm),

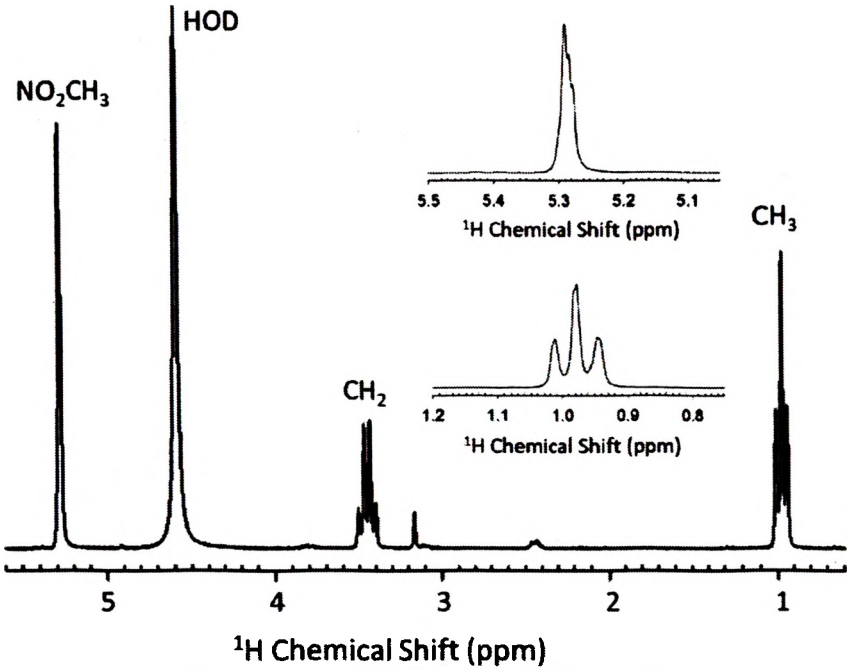

Figure 2.7. ^{1}H NMR spectrum recorded from the 4-mm NMR tube filled with 10 µL ethanol dissolved in 600 µL D_2O. Two exterior CapPack devices were mounted on opposite sides of the NMR tube as depicted in Figure 2.5. The nitromethane peak at 5.30 ppm arises from the exterior CapPacks. The almost completely overlapping nitromethane peaks (inset a) indicate optimum shim setting in the direction of the oppositely mounted CapPacks. At this setting, the triplet of the ethanol CH_3 group is well resolved (inset b), which also indicates a superior magnetic field homogeneity.

(d) unidentified impurity (singlet at 3.17 ppm), (e) unidentified impurity (doublet at 2.46 ppm), (f) CH_3 group of dissolved ethanol (triplet at 0.98 ppm). The insets show enlargements of the triplet resolution of the ethanol CH_3 group at 0.98 ppm and the nitromethane peak at 5.30 ppm. The superior resolution of the CH_3 group is an additional indication that the magnetic field within the sample will be equally shimmed or better than the field at the locations of the exterior CapPacks.

The experimental data of the exterior CapPack shimming procedure show results that correlate with theoretical predictions. Poor shim settings, which typically result in the broadening of NMR peaks, appear as separation of signals for exterior CapPacks. It is

easier to overlap well-resolved, individual signals than it is to minimize the linewidth of a broadened signal from the inside of an NMR tube. Hence the exterior CapPack shim procedure can assist in finding the optimum shim setting, especially for samples with multiple signals in the same chemical-shift region, or for samples with intrinsically broad or asymmetric sample signals (e.g., signals from polymers with large or asymmetric molecular-mass distributions). In the current example, the CH_3 group of nitromethane was used as the reference signal inside the exterior CapPacks because their NMR peak is far removed from, and thus does not overlap with, the HOD or ethanol sample signals. The nitromethane signal will always be in the peripheral view of the spectroscopist, making it less distracting but simple to find and navigate to. The degree to which the nitromethane signals need to overlap is up to the demands of the NMR project. True relevance comes into play when using high-resolution NMR spectroscopy and when publication-grade, narrow, and most symmetric peaks are desired. Regular maintenance and reference experiments with exterior NMR CapPack devices, consisting of a 4-mm NMR tube with two oppositely mounted exterior CapPacks, may also serve as a quick check for optimum spectrometer operation and spectrometer performance documentation.

2.3. SUMMARY OF CapPack UTILIZATIONS

CapPack devices are unique NMR tools for the evaluation, calibration, and optimization of NMR parameters, pulse sequences, and NMR spectrometer hardware. They are fabricated from permanently sealed small fused-silica capillary tubes that have been filled with specific NMR-sensitive reference materials. The sealed capillary tubes are inserted into NMR sample tubes as external reference standards without reacting or

chemically interfering with the samples under investigation. They are used instead of standard, concentric NMR reference inserts that occupy a substantial portion of the available sample volume. The small capillaries of CapPack devices are mounted either concentrically or attached to the wall of standard NMR tubes and can be used for precise chemical-shift and signal-intensity calibration. Filled with temperature-sensing NMR compounds, they are also used for the in situ determination of sample temperatures.

CapPack devices of multiple capillary tubes are used to generate unique NMR signals or profiles that allow the user to assess pulse sequences, optimize pulse parameters, identify artifacts, and investigate spectroscopic results that deviate from theoretical predictions. Gradient CapPack devices are particularly useful to evaluate the performance of frequency-selective pulses or pulse sequences, showing the excitation bandwidth profiles across CapPack signals that have been spread out over a wide range of chemical shifts by a gradient that is applied through one of the transverse room-temperature shim coils. A Relaxation CapPack consists of multiple capillaries each filled with a sample of different relaxation time. When paramagnetic ions such as Cu^{2+} ions are used to shorten the relaxation times of aqueous solutions, a paramagnetic shift caused by the Cu^{2+} ions is sufficient to separate the individual capillary signals from each other. Hence, relaxation studies with signals of substantially different relaxation times can be performed without the application of an external magnetic field gradient.

A special application of CapPacks is the exterior CapPack device, where single capillary tubes are mounted to the outside of an NMR tube. The advantage of exterior CapPack devices is that they don't need to be brought in contact with the sample under investigation. This advantage is particularly useful when a sample is air or light sensitive,

or the sample is suspected to react with the surface of the CapPack. When two exterior CapPacks are mounted on the opposite side of an NMR tube, they can be used to assist in shimming transverse magnetic field gradients in order to homogenize the main magnetic field. This is particularly useful when the NMR spectrum of the sample under investigation has multiple overlapping signals, or when the signals are inherently broad or asymmetric. In general, performance metrics measured with CapPack devices are determined with a minimal amount of experimental time, and the desired information is typically gathered in a single experiment.

3. NMR STUDIES TO DETERMINE THE REMAINING WATER CONTENT INIONIC LIQUID MONOPROPELLANT FOR MULTI-MODE PROPULSION

3.1. BACKGROUND

Ionic liquids are ionic compounds (salts) found in the liquid state at temperatures below 100 °C [40]. Research about ionic liquids has been published in several areas, such as chemical synthesis, electrochemistry, and chemical industry applications [40-45]. Although NMR spectroscopy has provided information about structure and dynamics of ionic liquids, it is a widespread believe that NMR spectroscopy with ionic liquids is particularly difficult [46].

Research conducted in collaboration with Dr. Joshua Rovey (Department of Mechanical and Aerospace Engineering, Missouri S&T) showed that NMR spectroscopy, when appropriately referenced for chemical shift and signal intensity, can provide critical information about the water content in ionic-liquid monopropellant for multi-mode propulsion and electrospray mode applications. The goal of this collaboration was to determine whether differently prepared mixtures of the ionic liquid 1-ethyl-3-methylimidazolium ethyl sulfate ([Emim][$EtSO_4$]) and the propulsion boosting ingredient hydroxylammonium nitrate (HAN) are obtained water-free for optimum combustion performance. The following mixtures were provided by the collaborators:

Table 3.1. Mass percent analysis of investigated propellant mixtures.

Sample	[Emim][$EtSO_4$]	HAN [%]	Water [%]
HAN-A	38.9	56.5	3.0
HAN-B	41.3	58.7	unknown
HAN-C	41.4	58.6	unknown

3.2. NMR SPECTROSCOPY

Standard ^{1}H NMR spectroscopy was performed on neat [Emim][$EtSO_4$], and on the three [Emim][$EtSO_4$] – HAN propellant mixtures described in Table 3.1. [Emim][$EtSO_4$] in aqueous solution was tested to verify the NMR results agreed with the manufacturer's analysis data. The three [Emim][$EtSO_4$] – HAN propellant mixtures were tested to study the water content of the propellant samples using HAN prepared according to three different synthesis techniques. The water content in the [Emim][$EtSO_4$] – HAN propellants is a concern because water is a volatile impurity. Its presence will not only decrease performance (because it reduces combustion temperatures) and impact electrospray modes (because it boils off), but it can also be detrimental for achieving stable electrospray operation. Therefore, a propellant with no water content or as little as possible water is desirable.

NMR measurements in aqueous solutions are a standard and information-rich analysis technique in chemistry and related disciplines. ^{1}H NMR chemical shifts reflect the electronic environment of hydrogen nuclei in chemical compounds and thus can be associated with chemical functional groups. The exact chemical-shift position of hydrogen atoms, however, depends not only on the intramolecular electronic environment, but may also be affected by the surrounding solvent and, in case of water as the solvent, by the pH of the solution. It is well known that hydration and hydrogen bonding plays a significant role in the condensed phases of water [47], and that the chemical shift of a solute will be influenced by these two effects. Furthermore, rapid exchange of hydrogen ions (H^+ ions, i.e., protons) or hydroxide ions (OH^- ions) from the solvent with those at dissolved substrate molecules can lead to a collapse of solvent and solute NMR signals into a single,

often broadened, NMR signal at a weighted-average chemical-shift position. Hence, the amount of water and the intensity of hydrogen bonding will influence chemical shift and lineshape of solvent and solute NMR signals in a particular sample. While this is typically seen as a disadvantage in NMR spectroscopy because of the loss of specificity and the loss of the ability to quantify substrates, the relative position and lineshape of averaged, exchangeable hydrogen atoms can still provide useful information when comparing samples with different amounts of residual water.

Samples of neat [Emim][$EtSO_4$] and the three [Emim][$EtSO_4$]-HAN mixtures were placed into standard 5-mm NMR tubes and investigated with a Bruker AVANCE DRX 200 MHz liquid-state NMR spectrometer. No deuterated solvents (such as D_2O) were added, and the samples were investigated without the deuterium field-frequency lock that is typically used to stabilize the magnetic field of NMR spectrometers. ^1H NMR spectra were recorded at room temperature using a 16-scan single-pulse excitation. The pulse angle was set to about P1 = 85° with a relaxation delay of D1 = 5 s between consecutive scans. Standard sample spinning was employed to enhance spectral resolution. Because no field-frequency lock could be used to homogenize the magnetic field, a specially developed magnetic-field shimming procedure was applied to each sample optimizing the free induction decay (FID) performance before conducting NMR experiments. A conventional Fast Fourier Transform (FFT) routine was used to convert FID data to NMR spectra.

Figure 3.1 shows the 200-MHz ^1H NMR spectrum of a neat [Emim][$EtSO_4$] sample (Sigma Aldrich Co. LLC.) and the assignment of resonance frequencies (NMR signals) to the chemical structure. Six signals are observed for the [Emim] cation (a to f in Figure 3.1) and two for the [$EtSO_4$] anion (A and B in Figure 3.1). Small amounts of residual water

are identified by a signal at 4.0 ppm in the shoulder of the [Emim] ethyl CH_2-group signal (3.1 ppm). A quantitative signal analysis after deconvolution of the two overlapping signals confirms the manufacturer's claim of about 0.1% by mol residual water in the commercially available product. There are also some unidentified minor impurities (< 0.3% ^1H by mol) observed in the sample (NMR signals at 1.0, 2.0, 2.7, 3.7-3.9, 6.9-7.8, and 8.8 ppm).

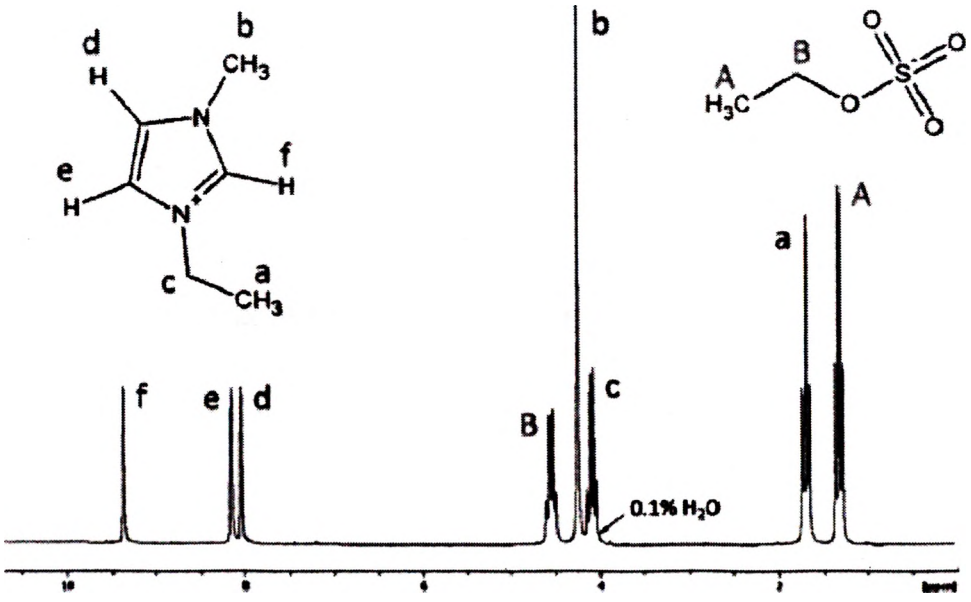

Figure 3.1. ^1H NMR spectrum of neat [Emim][$EtSO_4$] (sigma Aldrich Co. LLC.).

Figure 3.2 shows a stacked plot of NMR spectra of the different mixtures of [Emim][$EtSO_4$]-HAN using HAN prepared by different techniques. Each of these samples (HAN-A, HAN-B, HAN-C) contain different amounts of residual water due to the HAN preparation process. It is expected that the water content decreases from HAN-A to HAN-B

to HAN-C, and indeed this is confirmed by the NMR spectra. Because no deuterated solvent, and thus no field-frequency lock, was used in this series of experiments, the triplet NMR signal of the [$EtSO_4$] CH_3-group was used as internal chemical-shift reference (dashed vertical line in Figure 3.2). While the chemical shifts of the eight [Emim][$EtSO_4$] signals are fairly constant, the HAN and water NMR signals have collapsed into one that moves significantly toward higher ppm values (5.56 ppm, 9.98 ppm and 10.01 ppm in a, b, and c, respectively) with decreasing amounts of residual water. The linewidth of the collapsed HAN/H_2O signal also depends on the water content; the signal becomes significantly sharper (more narrow) as the water content decreases (57.6 Hz, 11.5 Hz, and 5.7 Hz in a, b, and c, respectively). From this analysis, it follows with great certainty that the amount of residual water in the sample prepared according to HAN-C (c) contains less water than the sample prepared according to HAN-B (b).

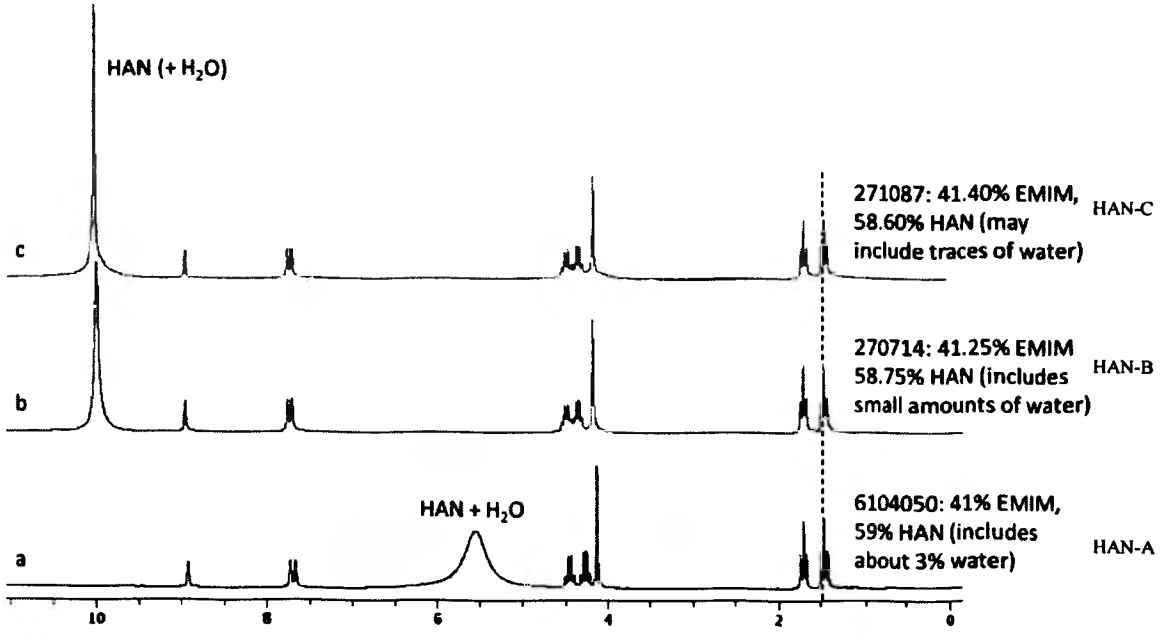

Figure 3.2. Stacked plot of NMR spectra of HAN-[Emim][$EtSO_4$] prepared with the samples of Table 3.1.

3.3. SUMMARY

Three chemical mixtures proposed for application as multi-mode propellants and electrospray modes were experimentally characterized for their remaining water contents. The propellants used hydroxylammonium nitrate (HAN) as oxidizer and propulsion boosting ingredient and the ionic liquid 1-ethyl-3-methylimidazolium ethyl sulfate ([Emim][$EtSO_4$]) as a novel propulsion fuel. By choosing an appropriate internal reference that did not change chemical shift with the amount of remaining water, the residual relative amount of water in the multi-mode propellant mixture was determined by accurately discerning very small chemical-shift differences in the signal of the propulsion boosting ingredient HAN. Even very small amounts of water caused a noticeable change in the chemical shift as well as the linewidth of the HAN signal due to the strong interactions between the polar HAN molecules and water molecules. The choice of internal reference was critical for the reliable determination of the residual water content.

4. STUDY THE ADSORPTION BEHAVIOR OF SMALL MOLECULES WITH COLLOIDAL UNIMOLECULAR POLYMERS (CUPS) USING SATURATED TRANSFER DIFFERENCE NMR

4.1. BACKGROUND

Polymer nanoparticles are becoming increasingly important as carriers in the field of drug delivery and sensing. Depending on the chemical structure of the material present on the surface of the nanoparticle, it can interact with a variety of molecules including biological ones present in our body. These interactions can alter or inhibit the functioning of the nanoparticle itself or the biological molecule interacting with it. This can lead to nanoparticle toxicity [48-51]. It is therefore crucial to study the extent of these small molecule-nanoparticle interaction to determine the toxic potential of the nanoparticles. Colloidal unimolecular polymers (CUP) [52] particles developed by VanDeMark et. al. are true nanoscale materials with size ranging from 3-9 nm in diameter. They are formed when the individual polymer chains collapsing into a sphere due to hydrophobic/hydrophilic interactions of the polymer with a change in solvent composition. The bulk of the sphere consist of the hydrophobic units of the polymer chain whereas the hydrophilic group stick out on the surface. The positive [53] or negatively [52] charged hydrophilic group present on the surface provide the stability to the suspension and prevents aggregation. CUPs are formed by a single polymer chains collapsing into a particle which makes it easy to fine tune its size by changing the molecular weight [54]. The procedure to make these CUP particles is very simple and the suspension is free of any surfactant or additives. This makes the CUP system clean and convenient for studying their fundamental properties and interaction with other molecules.

Solid-state [55-58] as well as liquid-state [59-61] NMR spectroscopy have been used as a tool for determination of structures of molecules covalently adsorbed on the surface of nanoparticles. Liquid-state NMR can also be used if the molecules are non-covalently adsorbed on the surface. NMR techniques like measuring the diffusion coefficients [62], Diffusion ordered spectroscopy (DOSY) [63], Nuclear overhauser effect spectroscopy (NOESY) [64], hydrogen/deuterium exchange, and chemical shift analysis can be used to study the dynamics of the adsorption and desorption of the molecule with the nanoparticle surface. Saturated transfer difference (STD) NMR experiment is another such technique that can be used to study the adsorption equilibrium of a molecule with the nanoparticle surface [65-67].

STD NMR has been used widely used to study the binding affinity of the ligand molecule to a protein receptor. This experiment involves taking a difference of the "on resonance" spectrum and a "off resonance" spectrum to obtain a "difference" spectrum. For the on-resonance experiment, the signal of the protein receptor is saturated by blasting with RF radiation. If the ligand is bound to the receptor, it will receive this saturation from the receptor and its peak intensity will be reduced. For the off-resonance or reference spectrum, the saturation is performed far from the ligand or receptor signals. Ligands that do not bind will not receive any saturation transfer and will have the same peak intensity as the reference. The difference spectrum will show the peaks of the ligand that bind to the receptor. This technique has been used extensively to in drug screening studies [66] and recently Zhang et. al. used this method to study the binding of small molecules to nanoparticle surfaces [68, 69]. They studied the binding of isopropanol and water molecules to the surface of carboxylate-modified polystyrene nanoparticle beads. The

nanoparticles used in their study were large in size and have slow tumbling which leads to short T_2 relaxation times and broad peaks. The peaks for the polystyrene nanoparticles was so broad that it merged into the baseline and disappeared.

CUP particles on the other hand due to their small size can tumble faster thus giving broad but distinct peaks for different groups present in the polymer backbone. It allows us to study the interaction of small molecules with each of the specific groups present in the nanoparticle. We can saturate the region in the NMR spectrum that shows the resonance of the specific group present in the nanoparticle and observe its saturation transfer to the small molecule. In this experiment, we will be studying the binding of small molecules to carboxylate-based CUP particles made from poly (methyl methacrylate-co-methacrylic acid). The CUP particles show two distinct broad peaks that due to the resonance of two different groups present in the polymer chain. These groups can act as specific sites present on the nanoparticle surface and we will study the adsorption behavior of the small molecule with each of those sites.

4.2. EXPERIMENTAL

Methyl methacrylate (MMA), methacrylic acid, 2,2-azobis (2-methylpropionitrile) (AIBN), 1-dodecanethiol and benzyl alcohol were purchased from Aldrich. Tetrahydrofuran (THF) was purified by distillation. Methyl methacrylate was passed through basic alumina column to remove the inhibitors and then distilled in presence of copper bromide. Methacrylic acid was distilled prior to use. AIBN was recrystallized from methanol and 1-dodecanethiol was used as received. Deionized water was used throughout the experiment. Deuterium oxide (99.9 % atom D) was purchased from Aldrich.

Poly (methyl methacrylate-co-methacrylic acid) was prepared by free radical polymerization using MMA and MAA in molar ratio 9:1 with AIBN as the initiator and 1-dodecanthiol as the chain transfer agent. The mixture was refluxed in THF for 24 h with a continuous flow of Argon through the assembly. The reaction mixture was precipitated into cold DI water with a high shear mixing to remove the water soluble MAA. The polymer was then dried in a vacuum oven at 50 C to remove the solvent and MMA. The absolute molecular weight of the polymer was measured using a Viscotek model 305 gel permeation chromatography instrument equipped with refractive index detector, low and right-angle light scattering detector, and intrinsic viscosity detector. The instrument is manufactured by Malvern Corp. The measurement was made in THF at flow rate of 0.5 ml/min and injection volume was 100 µl. The acid number of the dry polymer was measured using standard ASTM method. The solvent used was THF and aqueous potassium hydroxide solution was used as base for titration.

The polymer chain is collapsed into CUP particles using a process called water reduction. The polymer is first dissolved in THF to make a 10 % w/w solution and stirred overnight. Then, 1N sodium hydroxide solution prepared DI water is added to neutralize the acid groups according to its acid number. To this solution equal amount of pH modified water (pH= 8.5-9) is added slowly using a peristaltic pump at a rate of 1.24 g/min. The pH of the solution should be maintained between 8.5 and 9 throughout the water addition process. THF is then stripped off using vacuum and the solution is filtered through a 0.45 µm Millipore membrane to get rid of any foreign materials. The solution can be concentrated further by stripping the water or it can be diluted using pH modified water (pH = 8.5-9). The size of the CUP particles can be measured by dynamic light scattering

using a Microtrac Nanotrac 250 instrument. Solution viscosity was used instead of water.

Sample for NMR experiment were prepared by drying the CUP solution to remove all the water using vacuum at room temperature. The dried CUPs were dissolved in Deuterium oxide to make a 5% w/w solution. Different concentration of benzyl alcohol in CUPs solution were prepared by weighing them directly in the NMR tube and shaking. The solutions were allowed to equilibrate for 24 h before making measurements.

All NMR experiments were conducted with a Bruker 5-mm broadband probe inside a Bruker AVANCE DRX spectrometer operating at a proton frequency of 200 MHz. For standard one-dimensional ^{1}H NMR experiments, the Bruker single-pulse excitation ZG was used with 16 scans, 2 s relaxation delay and 32 k data-point acquisition. A capillary tube filled with concentrated HCl solution was used as chemical-shift reference. For the STD experiments, the Bruker pulse sequence STDDIFF, originally designed to acquire data in a two-dimensional data matrix, was modified to become a one-dimensional experiments. Solvent suppression was not employed. The selective saturation sequence was executed with 6890-μs and 8000-μs sinc pulses (bandwidth of 290 Hz and 250 Hz, respectively) with the power adjusted by the Bruker SELZG pulse program (60 db and 66 db, respectively). The 90° high-power observe pulse was calibrated by finding the maximum in a nutation plot of signal intensities as a function of pulse width. The relaxation delay was set to 5 × T_1 of the small molecule benzyl alcohol. Relaxation times of the benzyl-alcohol signals were determined by inversion-recovery NMR experiments. The total saturation time ranged from 0.05 to 5 s. For reference experiments, the saturation pulse was executed off-resonance at 19 kHz (95 ppm) from the standard transmitter and receiver frequency with the power level set to a minimum (120 db). For the STD

experiments, the saturation sequence was applied to the resonances at either R1 or R3 (Figure 4.1) depending on the intended resonance for saturation. A relaxation delay of 10 s, acquisition time of 2 s, and spectral width of 10 ppm were used, while 8 scans (following 2 dummy scans) were averaged in each experiment. All NMR experiments were carried out at a temperature of 299.2 ± 0.2 K. Recorded FIDs were processed using Bruker Topspin 1.3 software and signal intensities determined by Topspin integration routines with automatic baseline and phase corrections.

4.3. RESULTS AND DISCUSSION

Table 4.1. Properties of polymer and CUPs.

Properties	Molecular weight, M_w	Acid Number[1]	ρ^2	Measured particle size[3] (nm)	Calculated Particle size[4] (nm)
Poly (MMA-co-MAA)	60,000	56.1	1.2274	5.5	5.4

1- Measured in mg of KOH per gram of sample.

2- Density of Dry polymer, g/cc

3- Particle size measured with DLS instrument.

4- Particle size calculated from molecular weight $R = \frac{3 \times M_w}{4\pi\rho N_A}$

Table 4.1 show the properties of the polymer and size of the CUP particles. The NMR spectrum of the polymer dissolved in chloroform-d (spectrum A) and CUP solution

in water (spectrum B) at same concentration (5% w/w) are shown in Figure 4.1. The resonances R1, R2 and R3 in both the spectrum are from the methyl (CH_3), methylene (CH_2) and methoxy group of the polymer. The resonances become broad when the polymer collapses into CUPs which is expected because the chain mobility is drastically reduced, and the T_2 relaxation times become very small. However, unlike the polystyrene nanoparticles, where the resonances are so broad that they merge into the baseline, CUPs have enough molecular tumbling to show some intensity and less broad signal. The molecular tumbling can be attributed to the small size of the CUP particles (3-9 nm) as compared to the large size polystyrene nanoparticles (20 nm or larger). This renders CUP nanoparticles uniquely interesting for performing saturation-transfer experiments on a specific group of the nanoparticle now that we can see a clean resonance from that group. The resonances R1 and R3 can be clearly seen in the spectrum from CUP solution while the resonance R2 seems to have merged into R1 and seen as a hump to the R1 peak.

Figure 4.2 shows the chemical shift for five different concentrations of benzyl alcohol prepared in 5% CUP solution and one concentration of benzyl alcohol in D_2O. Adding more benzyl alcohol causes the resonance of the aromatic and methylene group from benzyl alcohol to move upfield. The shape of the aromatic resonance also changes with increasing concentration of benzyl alcohol. At low concentration, the aromatic resonance shows two peaks that are overlapped which at higher concentration can be seen as two separate peaks with additional splitting in the peaks.

In this saturation transfer experiment, individual resonances (R1 and R3) from the CUP are saturated and the interaction of the solvent molecule with that specific group in

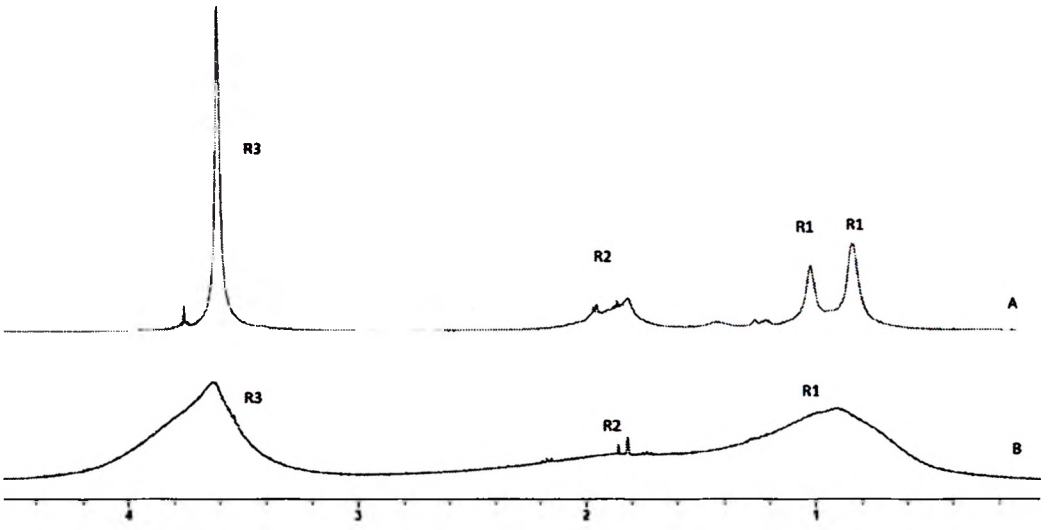

Figure 4.1. NMR spectrum of 5% w/w concentration of polymer in chloroform-d (A) and 5% CUP solution in D_2O. The R1, R2 and R3 are the resonances from the methyl, methylene and the methoxy group in the polymers. The resonances become broad when the polymer is in collapsed state as in CUP solution which indicates restricted mobility of the groups.

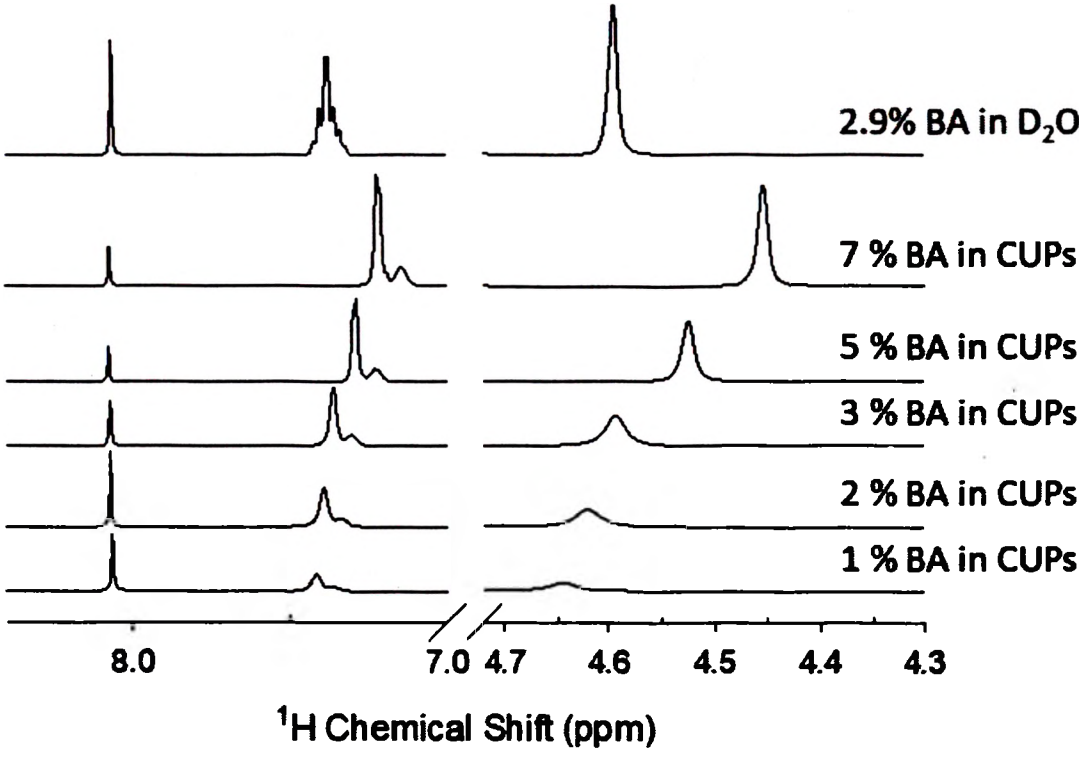

Figure 4.2. Chemical shift and peak shape of Aromatic and methylene groups of 1%, 2%, 3%, 5% and 7% benzyl alcohol in CUP solution and 2.9% in D_2O without CUPs. The peaks move upfield as the concentration is increased.

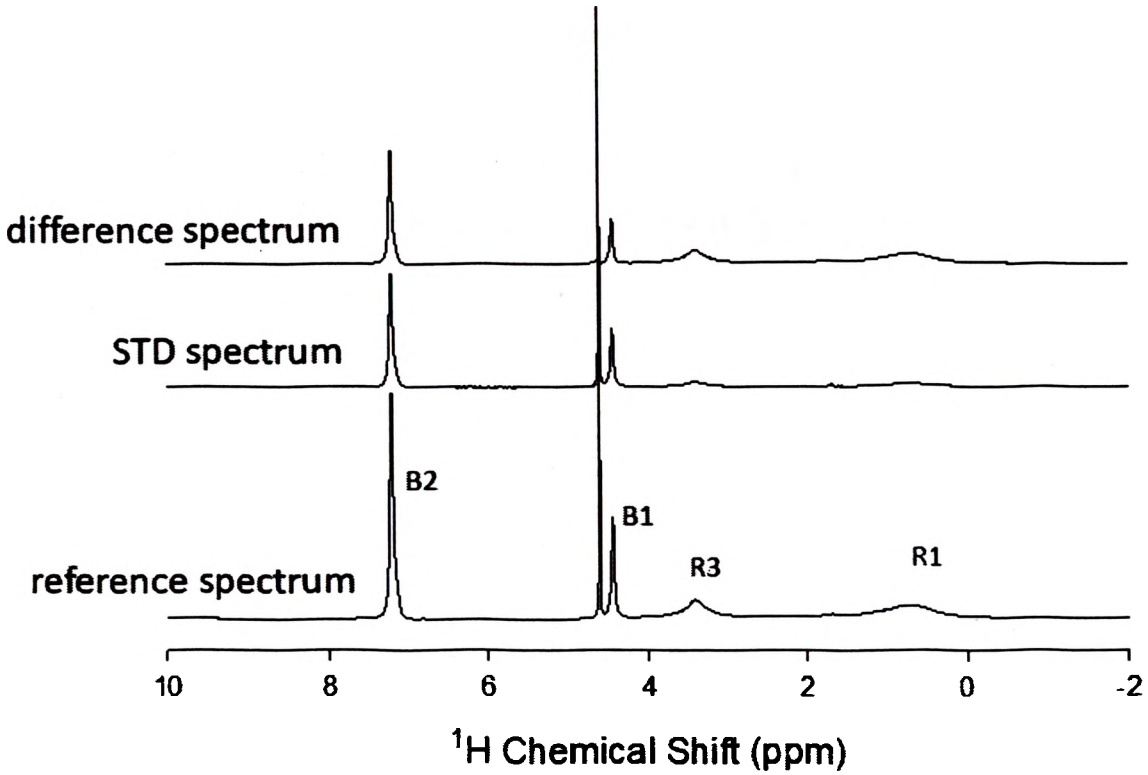

Figure 4.3. ^{1}H saturation transfer difference (STD-NMR) results for 1% benzyl alcohol in 5% CUP solution. The benzyl alcohol peaks can be seen in the difference spectrum which indicates that it is binding to the CUP particles.

the polymer chain is observed. Figure 4.3 shows the reference, saturation and the difference spectrum for 1% benzyl alcohol in 5% CUP solution while saturating the resonance R1. The STD difference spectrum shows the interaction of the Aromatic ring (B2) and the methylene group (B1) of the benzyl alcohol molecule with methyl (R1) group of the polymer chain. As a control, another difference spectrum was acquired in the absence of CUP which did not show any peaks form the benzyl alcohol molecule. This indicates that the STD effect observed in Figure 4.3 is due to the saturation transfer from the methyl group to the benzyl alcohol molecule and not due to direct saturation of the molecule in any way.

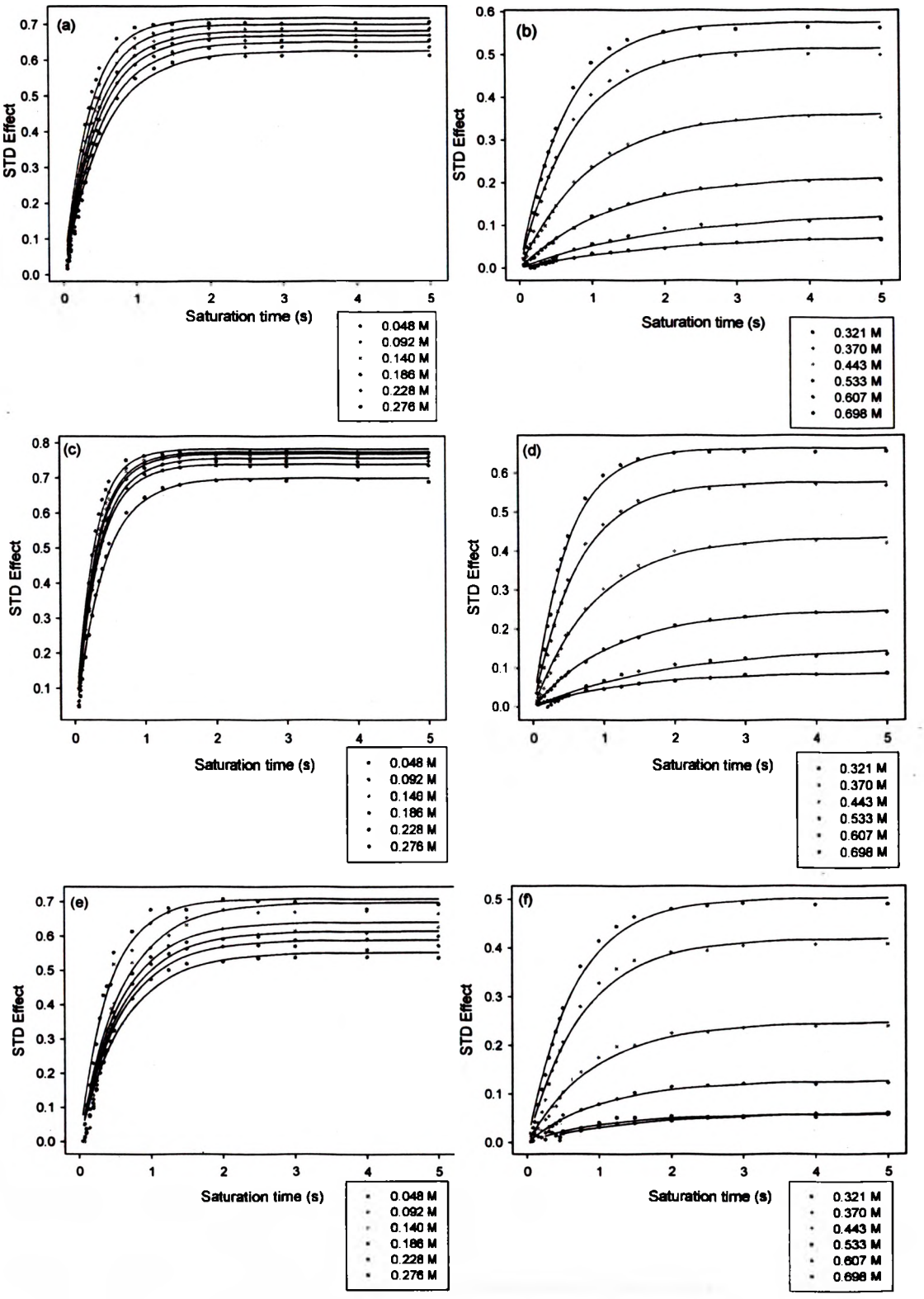

Figure 4.4. STD effect build up with increasing saturation time for various concentration (shown in legend) of benzyl alcohol in presence of 5% CUPs. (a-b) for Aromatic group of benzyl alcohol while saturation of R1 peak of CUPs, (c-d) for Aromatic group of benzyl alcohol while saturation of R2 peak of CUPs and (e-f) for methylene group of benzyl alcohol while saturation of R1 peak of CUPs.

$$STD\ Effect = \frac{I_{Ref} - I_{Sat}}{I_{ref}} = \frac{I_{STD}}{I_{ref}} \quad (4)$$

The STD effect is defined as the ratio of integral of difference peak to that of the integral of the reference peak. I_{Ref} is the integral of peak in reference spectrum, I_{Sat} is the integral of peak in saturation spectrum and I_{STD} is the integral of peak in difference.

Figure 4.4 shows the plot of STD effect as function of saturation time for the different concentration of benzyl alcohol prepared in 5% CUP solution. Figure 4.4a and 4.4b, show the STD effect for the aromatic ring and methylene group of benzyl alcohol while saturating the methyl peak (R1). Figure 4.4c shows the STD effect for the aromatic ring while saturating the methoxy peak (R3). The STD effect of the methylene group of benzyl alcohol when saturating the methoxy peak could not be analyzed due to issue with proper phasing. The methylene peak of benzyl alcohol overlaps with the water peak for concentrations 0.048 M to 0.276 M. Hence, peak deconvolution was done using the Origin software to get the integral value for calculating the STD effect. At higher concentrations, due to the upfield shift of the resonance, the methylene peak become separate from the water peak. The STD effect increases with saturation time and reaches a maximum value at long saturation times. The maximum STD effect can be seen decreasing as we increase the concentration of benzyl alcohol. The STD effect for methylene group at 0.607 M and 0.698 M concentration show poor fit and were not used for further calculations. Knowing the concentration of the benzyl alcohol ([BA] mols/l) and the concentration of CUPs ([CUP] mols/l), we can calculate the STD Amplification factor (STD-AF):

$$STD - AF = \frac{I_{STD}}{I_{Ref}} \frac{[BA]}{[CUP]} \quad (5)$$

[CUP] should ideally be the concentration of the Binding sites on the CUPs but at present we have no information on the number of sites present per CUP particle.

Concentration of CUPs is same as the concentration of polymer assuming that each polymer chain collapses in to one particle.

By fitting the STD-AF results to a binding isotherm we can get the dissociation constant K_D, of the non-specific adsorption that occurs between the benzyl alcohol molecule and the group in the polymer that is being saturated. Angulo et. al. [70] has shown that direct fitting of STD-AF can lead to overestimation of the KD value especially at higher concentration and longer saturation times due to ligand rebinding. To avoid this, we have used the initial slopes of the STD-AF curve,

STD-AF(0) to get the binding isotherm. The initial slope can be calculated by taking the derivative at time zero of the exponential fit of the STD-AF buildup curve.

$$STD - AF\ (t) = STD - AF(max.)[1 - \exp(-kt)] \quad (6)$$

$$STD - AF(0) = STD - AF(max.)[k] \quad (7)$$

Where t is the saturation time and k is the buildup constant. Figure 4.5 show the plot of STD-AF(0) against the concentration of benzyl alcohol. As seen from the plot, the STD-AF(0) increases as we increase the concentration of benzyl alcohol but after reaching a maximum at a certain concentration it starts to decrease. So far, this trend has not been observed in any other studies done in proteins or Nanoparticles using STD NMR method. Studies done on proteins have shown a fit to Langmuir isotherm where the value increase with concentration and eventually reaches a plateau indicating the saturation of binding sites of the protein. Similar, results are observed in the study of isopropanol adsorbing on polystyrene nanoparticles in the concentration range that was being studied. The curve up

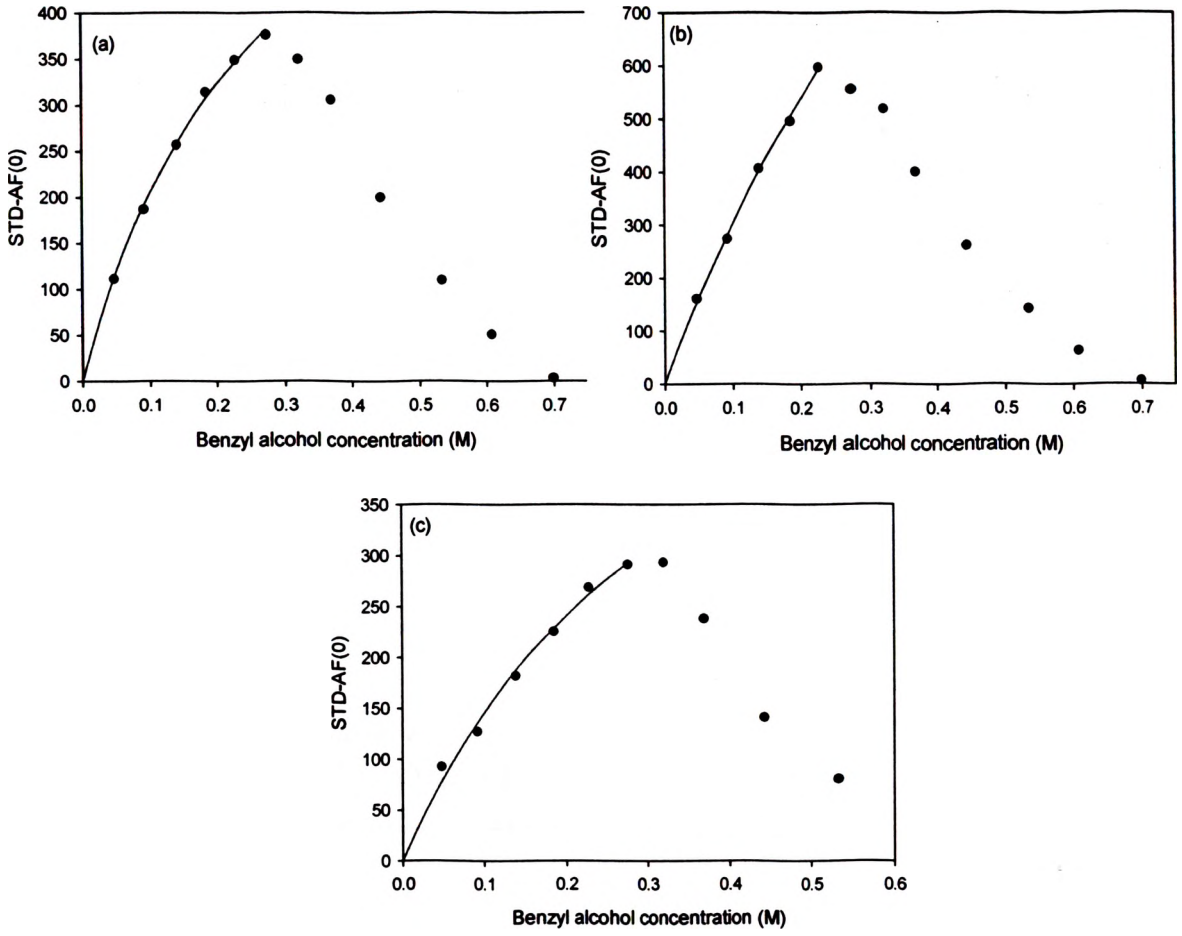

Figure 4.5. Plot of STD-AF(0) calculated from eq. 7 against benzyl alcohol concentration. The points represent the experimental data and the line represent the curve fit to Langmuir isotherm shown in eq. 8. (a) for Aromatic group of benzyl alcohol while saturation of R1 peak of CUPs, (b) for Aromatic group of benzyl alcohol while saturation of R2 peak of CUPs and (c) for methylene group of benzyl alcohol while saturation of R1 peak of CUPs.

to the maximum STD-AF(0) value could however be fitted to a Langmuir isotherm.

$$STD - AF\ (0) = \frac{STD - AF(0)_{max}[L]}{K_D + [L]} \tag{8}$$

Where STD-AF(0)$_{max}$ is the maximum number of binding sites (B_{max}) and K_D is the dissociation constant. Table 4.2 shows the B_{max} and the K_D values for the Aromatic (B2) and methylene (B1) group when peaks R1 and R3 are saturated.

Table 4.2. Maximum number of sites (B_{max}) and dissociation constant (K_D).

Polymer group saturated	Benzyl alcohol peak observed	B_{max}	K_D
R1 – methyl	Aromatic	759.79	0.24
R1 – methyl	Methylene	674	0.36
R3 – methoxy	Aromatic	2385	0.69

The dissociation constant gives the indication of the binding affinity of the molecule with the CUPs. Smaller the dissociation constant, stronger is the binding affinity. The interaction of Aromatic group of benzyl alcohol with the methyl group (R1) is stronger than with the methoxy group (R3). This could be due to the hydrophobic nature of the aromatic ring and polarity of the oxygen in methoxy group. The interaction Aromatic group with R1 is slightly stronger than methylene group. This is also evident from the maximum value of the STD effect. The maximum STD effect for the aromatic is greater than the methylene which indicates stronger interaction with the R1 group in the CUPs. The presence of the polar hydroxyl group next to the methylene could be the cause of weaker interaction. There is not much difference between number of binding sites (B_{max}) for the Aromatic and the methylene group with the R1 group on the CUP particle. The methoxy group (R2), however, show more binding sites as compared to the methyl group (R1) for Aromatic ring. The benzyl alcohol molecule could be bound to the methoxy group by hydrogen bonds with oxygen. Each methoxy group can possibly hydrogen bond to more than one benzyl alcohol molecule which will give higher number of binding sites. The binding of the benzyl alcohol molecule through hydrogen bonding keeps the aromatic group ring away from the methoxy group which results in weaker interaction as seen from the K_D values. The decrease in the STD-AF(0) at higher concentration can be due to

increase in mobility of the benzyl alcohol in the CUPS as it reaches the glass transition due to plasticization. As the exchange becomes faster, the efficiency of the saturation transfer drops and eventually approaches zero as the exchange becomes extremely fast. Different groups in the polymer can have different glass transition depending on the mobility of that group. For Poly (MMA-co-MAA) the methoxy group has higher mobility as compared to methyl and therefore it reaches the glass transition at lower concentration of benzyl alcohol. This can be seen in Figure 4.5 (a) and (b) where the STD-AF(0) drops at a higher concentration for the methyl group as compared to the methoxy group.

4.4. SUMMARY

In this work, we observed the binding behavior of small molecules like benzyl alcohol with CUP particles. The STD-NMR experiment shows that the molecule binds to the CUP particles and receives the saturation transfer. The CUPs NMR spectrum can show resonance from the different groups present in the polymer backbone. This makes it a unique nanoparticle system where we can study the interaction of the small molecules with a specific group present in the CUP particle. This study shows that the benzyl alcohol molecule, through its aromatic ring, interacts stronger with the methyl group in the CUPs as compared to the methoxy group. CUP particle have a potential for use as a drug delivery system. Knowing how these particles interact through the different groups present in them, can allow us to modify them so as to promote or avoid interaction with a specific biological molecule present in human bodies.

5. CHEMICAL-SHIFT AND LINESHAPE STUDIES WITH MATERIALS LOADED INTO POROUS-WALL HOLLOW GLASS MICROSPHERES

5.1. BACKGROUND

Glass biomaterials are playing a pivotal role in biomedical research [71]. Since the first generation of such glass materials was developed in the 1960s, they have been widely used in dental [72] and tissue engineering applications [73-75]. Biocompatible glass microspheres are spherical particles with diameters in the micrometer range. Recently, porous-wall hollow glass microspheres (PWHGMs) have attracted the interest of researchers due to their specifically engineered hollow-cavity SiO_2 structure that consists of 1-μm thick porous walls [76]. The center of the hollow cavity can be filled with different materials for various applications. PWHGMs were originally fabricated for use by the Department of Energy (DOE) for national security and energy applications [77], as well as waste management and environmental remediation projects [76, 78]. Because of their unique properties such as high and controllable permeability, low density, the storage cavity, and a large surface area, PWHGMs have been used in storage batteries [79], material adsorption [80], gas sensors [81], hydrogen storage [82], security technology [83] and other applications [84, 85]. The porous walls and the hollow cavities of PWHGMs render them suitable micro-containers for biomedical applications, such as for drug delivery [86] and cancer therapies [86, 87].

PWHGMs were characterized largely by optical microscopy, scanning electron microscopy (SEM) [88], transmission electron microscopy (TEM) [89], confocal laser scanning microscopy (CLSM) [90], and dynamic light scattering [90]. However, these techniques only provided the characterization of the surface, shell thickness, and pore

dimple sizes of PWHGMs. To obtain information about what has been loaded inside the cavities of PWHGMs for targeted biomarker and drug delivery, an analytical technique such as NMR spectroscopy is needed that can provide real-time specific information about the loaded materials and their potential releasing mechanisms. NMR spectroscopy is one of the most powerful analytical tools used in pharmaceutical [91], biomedical [92], and chemical investigations in industry and academia. Unequivocal analytical evidence can be discerned from NMR spectra such as chemical structures, dynamics, and conformational information [93]. NMR techniques are inherently quantitative, as signal intensities directly relate to the number of nuclei, and hence the number of molecules under investigation. Unlike other commonly used analytical techniques, sample preparation for NMR spectroscopy is simple, and no sample separation such as in high-performance liquid chromatography (HPLC) or gas chromatography (GC) is required. Moreover, NMR is a non-destructive technique and thus most suitable for the study of reaction kinetics [94]. NMR spectroscopic techniques have been widely used in drug discovery, where detailed insights into interactions between molecules and a surrounding matrix are desired [95]. However, no NMR studies on PWHGMs and their potential use in targeted drug delivery are known. With the fundamental advantages of NMR and its versatility, valuable information can be acquired from NMR spectra to evaluate the applicability of PWHGMs in targeted biomedical applications.

This work is the first report of utilizing NMR spectroscopy to characterize materials loaded into PWHGMs and their release kinetics from the PWHGMs. The results are expected to provide fundamental and practical insight for future applications of PWHGMs in drug delivery. A vacuum-based loading system was developed to load target materials

into PWHGMs. A follow-up washing procedure was included to remove excess amounts of materials from the outside of the PWHGMs. Two binary systems, $CHCl_3/D_2O$ and n-dodecane/D_2O, were evaluated to obtain NMR evidence that materials were loaded into the PWHGMs. The esterification reaction of isopropanol with acetic acid and the reverse reaction, the hydrolysis of isopropyl acetate, were followed by ^1H NMR spectroscopy to provide experimental evidence for the exchange of materials between the inside of the PWHGMs and the surrounding solution. PWHGMs loaded with water (H_2O) were submerged into D_2O to study the kinetics of H_2O release from PWHGMs. NMR spectroscopy provided time-dependent data that could be fitted to a double-exponential raise to maximum curve, which was interpreted as the release of H_2O from two types of PWHGMs, those with and those without large openings in the porous walls.

5.2. MATERIAL AND METHODS

5.2.1. Porous-wall Hollow Glass Microspheres (PWHGMs). PWHGMs were provided by Mo-Sci Corporation (Rolla, MO). The size distribution of the PWHGMs ranged from 20 μm to 75 μm with a 1 μm shell thickness. The surfaces of the porous glass walls contain pore dimples with diameters that range in size from 10 to 300 nm. The porous glass walls consist of interconnected channels that range in size from 1 to 100 nm. However, large openings (> 1 μm) in the PWHGM walls constitute a recurring feature of the PWHGM sample used in this study, and were characterized by field emission scanning electron microscopy (FESEM) (Hitachi 4700, Tokyo, Japan).

5.2.2. Loading Substances and Washing PWHGMs. The loading procedure was performed by using a typical laboratory vacuum pump system (Figure 5.1). A desired

amount of PWHGMs was placed into a glass vial, which was then connected to a standard laboratory vacuum pump (Welch 1400 B) using a tightly-fitting flexible rubber hose. The rubber hose provided an air-tight seal to the vial and could be pierced with a syringe needle. The vacuum pump was turned on for about one hour to remove all air from the vial and the PWHGMs. The airflow was controlled to be reasonably low to avoid breaking the delicate PWHGMs shell walls and to prevent the PWHGMs from being aspirated out of the glass vial. After the desired vacuum is reached, a valve in the vacuum supply line between the vial and the vacuum pump is closed. The liquid materials or solution to be loaded into the PWHGMs is slowly injected through the rubber hose into the evacuated glass vial with a syringe. Before and after the loading procedure, the PWHGMs were inspected with an inverted microscope (Olympus IX51, Olympus, Center Valley, PA, USA). Afterwards, the PWHGMs were washed by centrifugation with a solvent that was immiscible with the solution loaded inside the PWHGMs. The washing procedure was typically repeated three times. The PWHGMs were transferred into a 5-mm NMR tube after washing with several

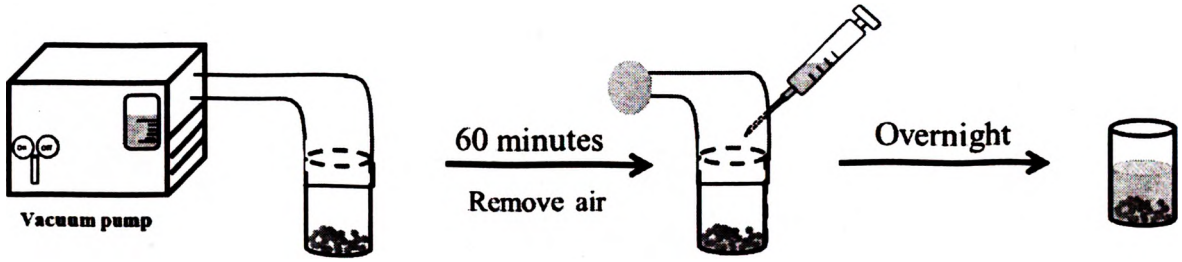

Figure 5.1. Schematic diagram of a vacuum system used to load PWHGM with liquid materials or solutions. The integrated system consists of a vacuum pump, a glass vial, a rubber tube, and a syringe. The fully-loaded PWHGMs are shown at the bottom of the vial.

small portions of the appropriate NMR lock solvent. The supernatants collected during the washing procedures were examined separately by ^{1}H NMR spectroscopy.

5.2.3. NMR Evidence of Materials Loaded in PWHGMs. A series of ^{1}H NMR control experiments were conducted on a system composed of the two immiscible liquids $CHCl_3$ and D_2O (Sigma-Aldrich, St Louis, MO) to quantify the ^{1}H chemical shifts and integrals of the $CHCl_3$ peaks. Different quantities of $CHCl_3$ (1 μL, 2 μL, 5 μL, 7 μL, 10 μL, 15 μL, and 20 μL) were added sequentially to 750 μL of D_2O contained in a 5-mm NMR tube to map the limited solubility of $CHCl_3$ in D_2O. ^{1}H NMR spectra were recorded for every mixture. PWHGMs were then loaded with $CHCl_3$ according to the vacuum-based loading system and washed three times with D_2O according to the washing procedure. The final suspension in D_2O of PWHGMs loaded with $CHCl_3$ was transferred into a 5-mm NMR tube, and the sample was gently shaken before NMR analysis to ensure that the PWHGMs were homogeneously distributed in the NMR active volume. NMR spectra of the PWHGMs loaded with $CHCl_3$ and suspended in D_2O were recorded, and integrated signal intensities of the $CHCl_3$ peak were used to evaluate the loaded PWHGMs. The same experimental procedures were employed in the second series of control experiments using a system composed of the two immiscible liquids n-dodecane ($C_{12}H_{26}$) and D_2O to quantify the ^{1}H chemical shifts and integrals of the $C_{12}H_{26}$ peaks.

5.2.4. Materials Exchange from the Interior of PWHGMs to the Surrounding Solution. The acid-catalyzed hydrolysis reaction control experiments employing isopropyl acetate were carried out by initially adding 20 μL of isopropyl acetate to a 5-mm NMR tube containing 750 μL D_2O. After an initial ^{1}H NMR spectrum was recorded, 5 μL of concentrated H_2SO_4 was added to the solution, and then another ^{1}H NMR spectrum was

immediately recorded. Additional ^{1}H NMR spectra were recorded 10 and 20 minutes following the initiation of the reaction. PWHGMs were subsequently loaded with isopropyl acetate according to the vacuum-based loading protocol and washed according to the washing procedure. The loaded PWHGMs were transferred into a 5-mm NMR tube, and an initial ^{1}H NMR spectrum was recorded immediately following the addition of 5 μL of concentrated H_2SO_4. A second ^{1}H NMR spectrum was recorded after 10 minutes.

5.2.5. Kinetic Studies of Materials Released from PWHGMs. Kinetic studies of materials released from PWHGMs were performed with PWHGMs loaded with H_2O and suspended in D_2O. The H_2O-loaded PWHGMs were washed with $CHCl_3$ before their use. An external ^{1}H NMR chemical-shift and concentration reference was used in the kinetics studies, consisting of a flame-sealed 1-mm CapPack capillary tube filled with $CHCl_3$ that was inserted vertically into and along the long axis of a 5-mm NMR tube. The H_2O-loaded PWHGMs were carefully transferred into the bottom of the 5-mm NMR tube such that the sample height remained just below the NMR active volume of the NMR tube. D_2O was slowly and carefully added into the 5-mm NMR tube to avoid disturbing the PWHGMs. A series of ^{1}H NMR spectra was subsequently recorded at regular intervals for approximately 8 hours, resulting in a total of 185 ^{1}H NMR spectra.

5.2.6. Acquisition of ^{1}H NMR Spectra, Processing, and Peak Assignments. All ^{1}H NMR spectra were obtained using a Bruker 5-mm BBFO probe in a 400 MHz Bruker AVANCE III HD NMR Spectrometer. The data were acquired with the following acquisition parameters: sample temperature 298 K, spectral width 4800 Hz, data points 32k, pulse width 14.3 μs (~ 90° tip angle), recovery delay between scans 2 s, and the number of scans 16. After the acquisition of the free induction decay data and a Fourier

transform calculation, the ^1H NMR spectra were phase- and baseline-corrected with automated routines from the spectrometer's TOPSPIN® 3.1 software. The peak assignments are listed in the table below.

Table 5.1. ^1H NMR chemical shifts assignment for materials used in PWHGMs experiments.

Chemicals	Chemical shift (ppm)	Chemicals	Chemical shift (ppm)
H_2O	4.63	$CHCl_3/D_2O$ emulsion	7.20
HOD	4.63	CH_3COOH	1.84
$CH_3(CH_2)_{10}CH_3/D_2O$ emulsion	0.77	$(CH_3)_2CHOH$	0.96
phase-separated $CH_3(CH_2)_{10}CH_3/D_2O$	0.81	$(CH3)_2CHOH$	3.81
$CH_3(CH_2)_{10}CH_3/D_2O$ emulsion	1.17	$(CH_3)_2CHOOCCH_3$	1.04
phase-separated $CH_3(CH_2)_{10}CH_3/D_2O$	1.20	$(CH3)_2CHOOCCH_3$	4.77
$CHCl_3$ dissolved in D_2O	7.55	$(CH3)_2CHOOCCH_3$	1.86

5.3. RESULTS AND DISCUSSIONS

5.3.1. Characterization of Empty PWHGMs. Figure 5.2 shows electron micrographs of PWHGMs, their spherical hollow cavity, and different size pore dimples and holes in the walls. The FESEM images confirm that the PWHGMs are indeed spherical with a smooth outer surface (Figure 5.2a). In some cases, there are pieces of broken

PWHGMs attached to the surfaces of the intact PWHGMs. The diameters of the PWHGMs range from 20 μm to 70 μm. A broken PWHGM shell was also imaged by FESEM to show the central hollow cavity (Figure 5.2b). Higher magnification of the PWHGM shell showed many indentions on the surface, which are identified as pore dimples in the outer walls (Figures. 5.2c & 5.2d). The pore dimples are visible as circular indentations because the conformal coating by gold sputtering, which was used to prepare the PWHGMs for FESEM imaging, covered the interiors of the pore dimples. There are two distinct size ranges of the pore dimples: (a) a great number of small pore dimples with sizes between 10 nm and 20 nm, as shown in Figure 5.2c, and (b) a small number of relatively large pore dimples with diameters between 50 nm and 75 nm, as shown in Figure 5.2d. The substantial difference between the average diameter and depth of the pore dimples (large and small) and the much

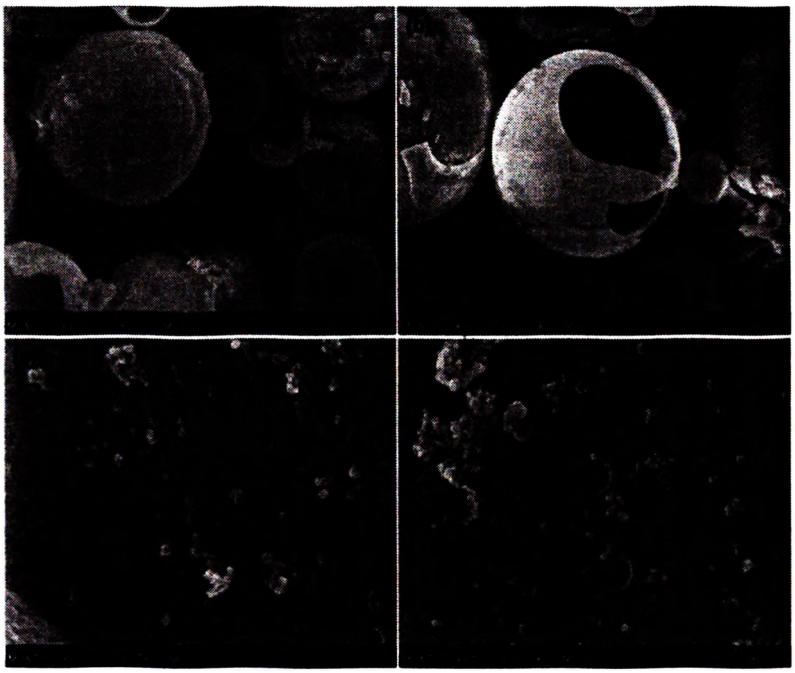

Figure 5.2. SEM images of PWHGM surfaces. (a): the surface of PWHGMs; (b): the central hollow cavity and through-hole; (c) depiction of 10-20 nm pore dimples; (d) depiction of 50-70 nm pore dimples on the walls of PWHGMs. A 50 μm scale bar is indicated for (a) and (b), and a 500 nm scale bar is indicated for (c) and (d).

larger through-holes in the walls of the PWHGMs has a major impact on the rates of release of materials from the PWHGMs as shown later in the kinetic study. Overall, the pore dimples, through-holes, and the spherical hollow cavities are characteristic of PWHGMs, making them distinguishable from other microspheres.

Figure 5.3 contains detailed images of the channels that provide pathways for molecules to pass through the PWHGM shell wall. The thickness of the PWHGM shell wall is confirmed to be 1 μm (Figure 5.3c). The magnified picture (Figure 5.3d) shows the tortuous channels in the PWHGM shell wall. This critical feature helps explain the release of materials in the kinetics study described below.

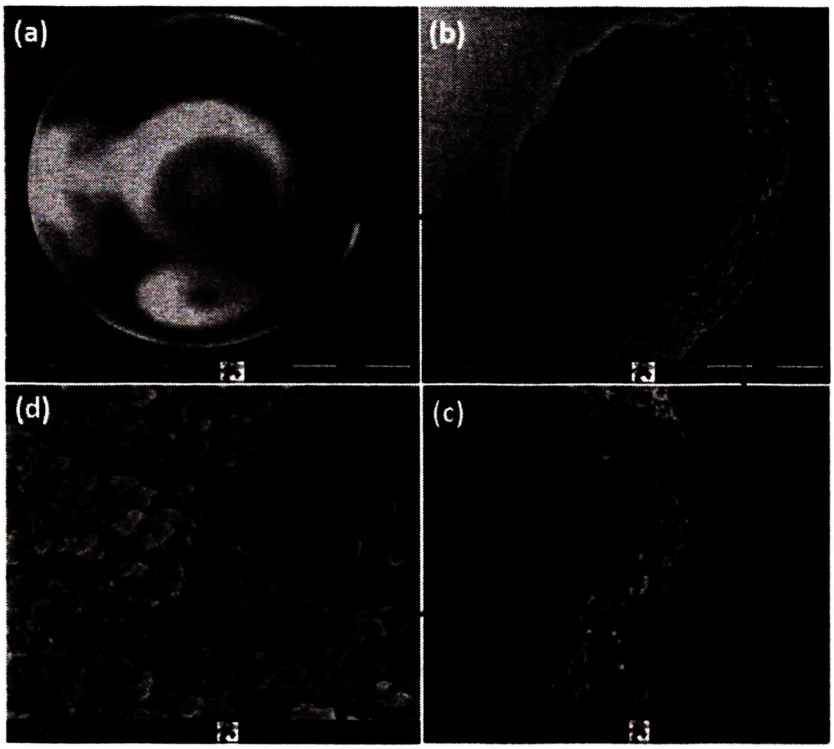

Figure 5.3. SEM images of microspheres surfaces. (a): the surface of microspheres; (b): the central hollow cavity and through-hole; (c) depiction of 1 μm-thick shell wall; (d) the tortuous channels in the PWHGM shell wall. Scale bars of 30 μm, 3 μm, 1 μm, and 500 nm are indicated for (a), (b), (c), and (d), respectively.

5.3.2. Characterization of $CHCl_3$-loaded PWHGMs. Photographs were taken of PWHGMs with a digital camera before and after the PWHGMs were loaded with liquid materials (Figures 5.4a and 5.4b). Unloaded PWHGMs filled with air float to the top of the liquid (Figure 5.4a), while the loaded PWHGMs sink to the bottom (Figure 5.4b). Even though the SiO_2 of the glass PWHGMs, the main component of the PWHGMs' shells, has a higher density (2.2 g/cm^3 [96]) than most common liquids (e.g. H_2O: 0.9950 g/cm^3 [97]), the air inside the PWHGMs, which has a much lower density (1.225×10^{-3} g/cm^3 [98]), limits the average density of unloaded PWHGMs to values below the density of most common liquids. Therefore, unloaded PWHGMs will float, for example, on top of the water.

On the other hand, PWHGMs loaded with a liquid will sink to the bottom when immersed in the same liquid due to a higher average density (Figure 5.4b). Unloaded and loaded PWHGMs were imaged with inverted optical microscopy as shown in Figure 5.4c and Figure 5.4d, respectively. Because the index of refraction is substantially lower for air compared to common liquids, the images of the unloaded PWHGMs look very different from those of the loaded PWHGMs. The stark appearance of H_2O-loaded PWHGMs with 1-μm thick walls in Figure 5.4c is the result of the difference in refractive index between liquid (H_2O in this case) and air. Note that the subtle spherical contours of the PWHGMs are visible under the microscope even after the PWHGMs were filled with liquid because the indexes of refraction for water and glass are distinct. Figures 5.4c and 5.4d demonstrate that the PWHGMs keep their structural integrity throughout the loading process, which confirms that the exerted pressure differences during the loading process do not destroy the PWHGMs.

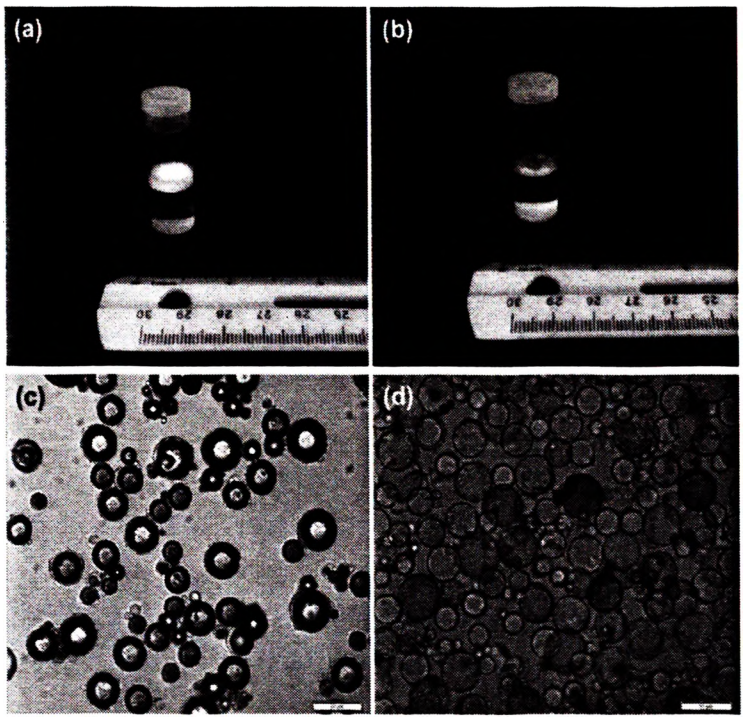

Figure 5.4. Images of PWHGMs in H_2O before and after loading with H_2O. (a) Unloaded PWHGMs suspended above H_2O; (b) H_2O-loaded PWHGMs submerged in H_2O; (c) inverted microscopic image of unloaded PWHGMs under white light; (d) inverted microscopic image of H_2O-loaded PWHGMs under white light. Scale bars in (c) and (d) are 50 μm each.

The effectiveness of the washing procedure for PWHGMs was evaluated using ^1H NMR spectroscopy on the system of the immiscible liquids $CHCl_3$ and D_2O (Figure 5.5). The ^1H NMR spectrum in Figure 5.5b shows that two distinct peaks for $CHCl_3$ can be observed at 7.55 ppm and 7.20 ppm before the washing procedure, which are assigned to dissolved $CHCl_3$ and a $CHCl_3/D_2O$ emulsion, respectively. The occurrence of a peak at 7.20 ppm for $CHCl_3$ in a $CHCl_3/D_2O$ system indicates that the concentration of $CHCl_3$ in D_2O exceeded the solubility limit. Thus, in the supernatant, there was $CHCl_3$ in greater quantity than the dissolution limit. However, after the third wash, no peak was detected at 7.20 ppm (Figure 5.5b), which indicated that all the $CHCl_3/D_2O$ emulsion was removed

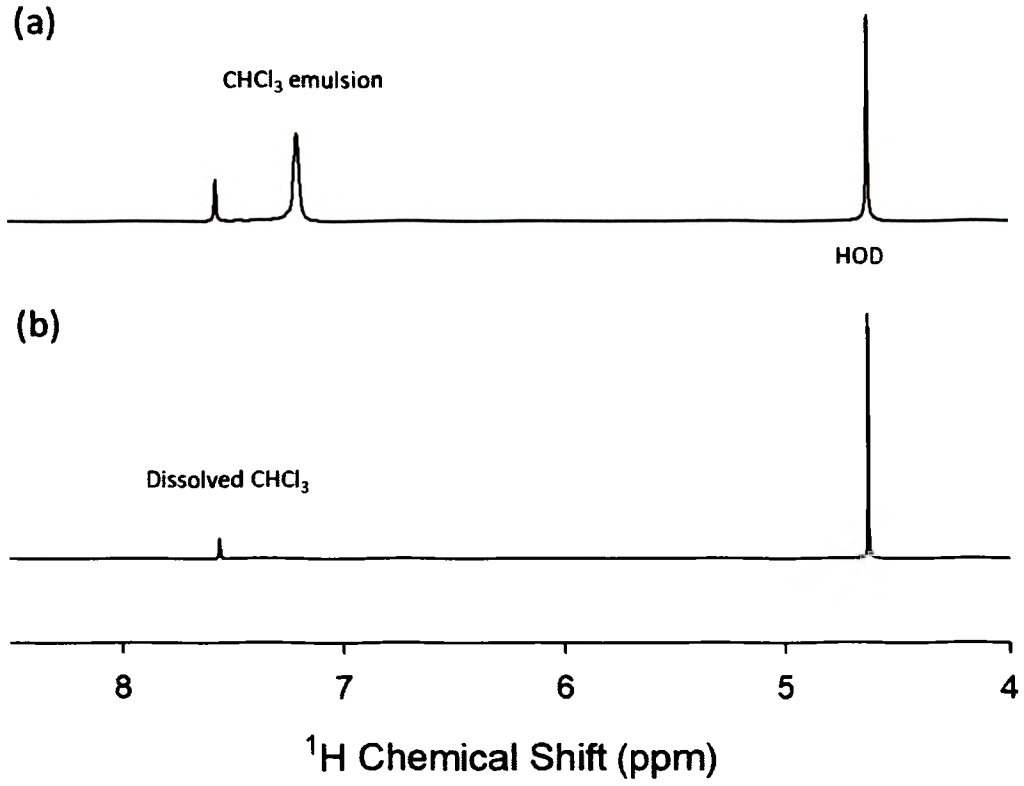

Figure 5.5. ^1H NMR spectra of supernatants collected during the D_2O washing process of $CHCl_3$-loaded PWHGMs. a) ^1H NMR spectrum of supernatant collected from $CHCl_3$-loaded PWHGMs immersed in D_2O. From left to right are the assigned ^1H NMR peaks for $CHCl_3$ dissolved in D_2O, $CHCl_3/D_2O$ emulsion, and HOD. b) ^1H NMR spectrum of supernatant collected after the third D_2O wash of $CHCl_3$-loaded PWHGMs; the $CHCl_3/D_2O$ emulsion peak is no longer detectable.

and that only a small quantity of dissolved $CHCl_3$ remained in the D_2O solvent. This residual quantity of $CHCl_3$ could not be removed completely and may have originated from $CHCl_3$ that leaked out of the PWHGMs during the final D_2O washing step. The comparison of ^1H NMR spectra of D_2O supernatants collected at different stages during the D_2O washing process demonstrates that a centrifugation-based D_2O-washing procedure effectively removes excess $CHCl_3$ used to load the PWHGMs.

5.3.3. Explanation of ^{1}H NMR Spectra of D_2O Supernatants from $CHCl_3$-Loaded PWHGMs. A series of control experiments was conducted to understand the immiscible binary system of $CHCl_3$ in D_2O, which is relevant to the D_2O-washing process of $CHCl_3$-loaded PWHGMs. When 5 μL of $CHCl_3$ is added to 750 μL of D_2O, a narrow singlet peak for dissolved $CHCl_3$ is observed at 7.55 ppm in the ^{1}H NMR spectrum (Figure 5.6a). The solubility of $CHCl_3$ in H_2O at 20 °C is 8.09×10^{-3} g/mL [99]. Equivalently, the maximum solubility of $CHCl_3$ in 750 μL D_2O should be reached by adding 4.08 μL $CHCl_3$. We calculated, using the density of $CHCl_3$ (1.49 g/mL at 25 °C), that there was 9.93×10^3g $CHCl_3$ per mL D_2O when 5 μL of $CHCl_3$ was added to the 750 μL of D_2O. The integral of the $CHCl_3$ singlet peak was 0.1318 relative to the integral of the HOD peak at 4.63 ppm (1.0000) (Figure 5.6a). As more $CHCl_3$ was added, the integral of the peak for the singlet representing dissolved $CHCl_3$ increased. The peak for the dissolved $CHCl_3$ reached saturation with an integral of 0.1437 (~100%) when 7 μL of $CHCl_3$ were added to 750 μL of D_2O. As more $CHCl_3$ was added to D_2O, for example, 10 and 15 μL of $CHCl_3$, a new broader peak appeared at 7.20 ppm (Figure 5.6b). This peak is assigned to microscopic $CHCl_3$ droplets suspended in D_2O as an emulsion. The further addition of $CHCl_3$ (> 15 μL) to 750 μL of D_2O resulted in the reproducible observation of the macroscopic phase separation of the two immiscible liquids.

After a sample of PWHGMs was loaded with $CHCl_3$ and washed with D_2O, the $CHCl_3$-loaded PWHGMs were suspended in 750 μL of D_2O, and a ^{1}H NMR spectrum was recorded (Figure 5.7). The ^{1}H NMR spectrum in Figure 5.7 was included in a series of ^{1}H NMR spectra of control samples composed of $CHCl_3$ in D_2O as shown in Figure 5.8. The

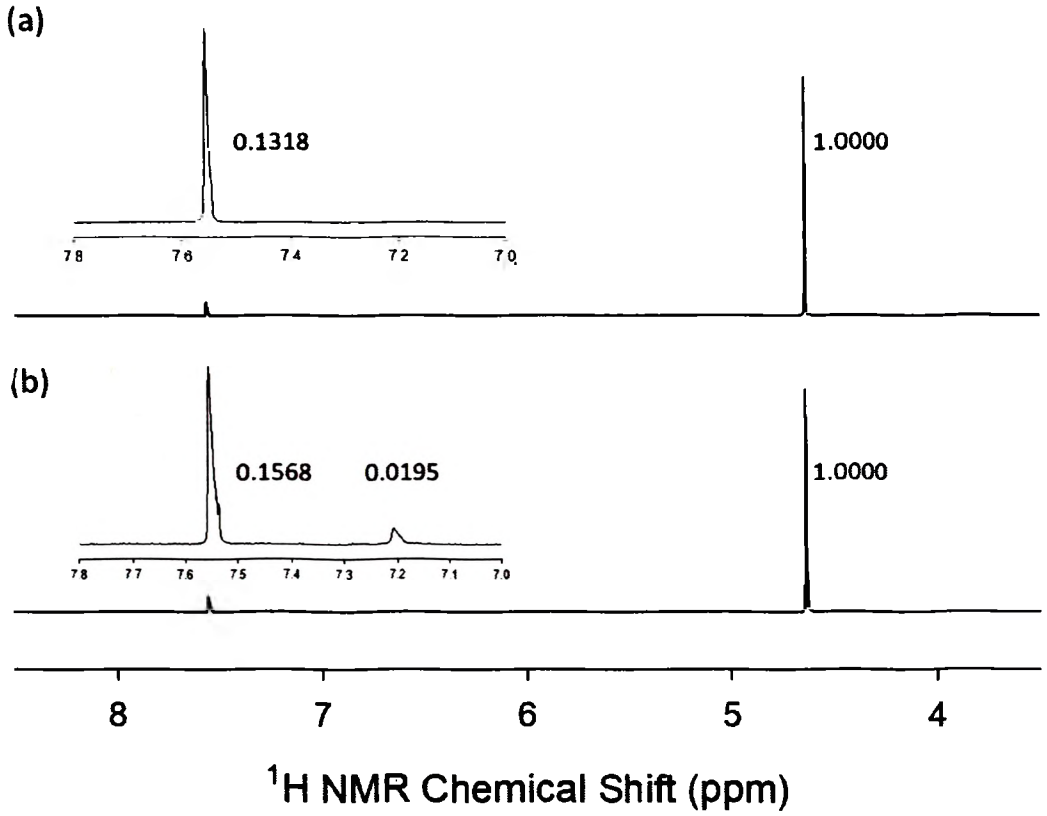

Figure 5.6. Binary immiscible system consisting of $CHCl_3$ and D_2O. (a) 5 μL of $CHCl_3$ in D_2O resulting in a sharp peak at 7.55 ppm representing dissolved $CHCl_3$; (b) 15 μL of $CHCl_3$ in D_2O resulting in a sharp peak at 7.55 ppm representing dissolved $CHCl_3$ and a second $CHCl_3$ peak at 7.20 ppm representing a $CHCl_3/D_2O$ emulsion.

^1H NMR spectrum of the $CHCl_3$-loaded PWHGMs was positioned between the lower spectrum for 2 μL of $CHCl_3$ in 750 μL of D_2O and the upper spectrum for 5 μL of $CHCl_3$ in 750 μL of D_2O because the integral of the peak due to dissolved $CHCl_3$ at 7.55 ppm for the $CHCl_3$-loaded PWHGMs sample was between the integrals for the dissolved $CHCl_3$ peak in the two control spectra. The ^1H NMR spectra for the control samples composed of 1-7 μL of $CHCl_3$ in 750 μL of D_2O do not reveal a peak at 7.20 ppm, which would indicate the presence of a $CHCl_3/D_2O$ emulsion. Therefore, the broad peak observed at 7.20 ppm in ^1H NMR spectrum of the $CHCl_3$-loaded PWHGMs is assigned to $CHCl_3$-loaded

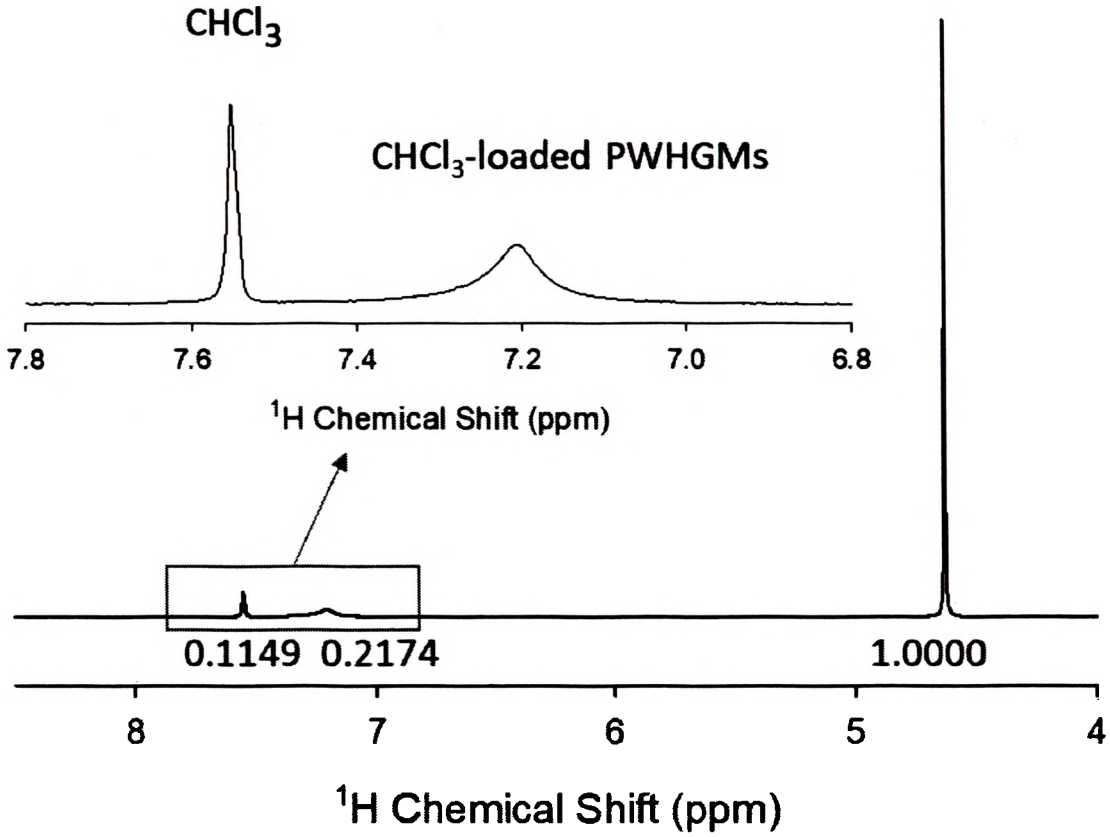

Figure 5.7. ^{1}H NMR spectrum of $CHCl_3$ inside of PWHGMs suspended in D_2O. The peaks from left to right are assigned to dissolved $CHCl_3$ in D_2O (7.55 ppm), $CHCl_3$ inside PWHGMs (7.20 ppm), and HOD (4.63 ppm). See text for a justifications of the $CHCl_3$ peak assignments.

PWHGMs. The $CHCl_3$ inside the PWHGMs has the same chemical shift as the control sample $CHCl_3/D_2O$ emulsion, indicating that the $CHCl_3$ molecules experience the same chemical environment [93]. The PWHGMs filled with $CHCl_3$ can be considered as providing the template for amounts of $CHCl_3$ that exceed the solubility of $CHCl_3$ in D_2O, however not manifesting as $CHCl_3/D_2O$ emulsions but rather as $CHCl_3$ droplets surrounded by the glass shells of PWHGMs.

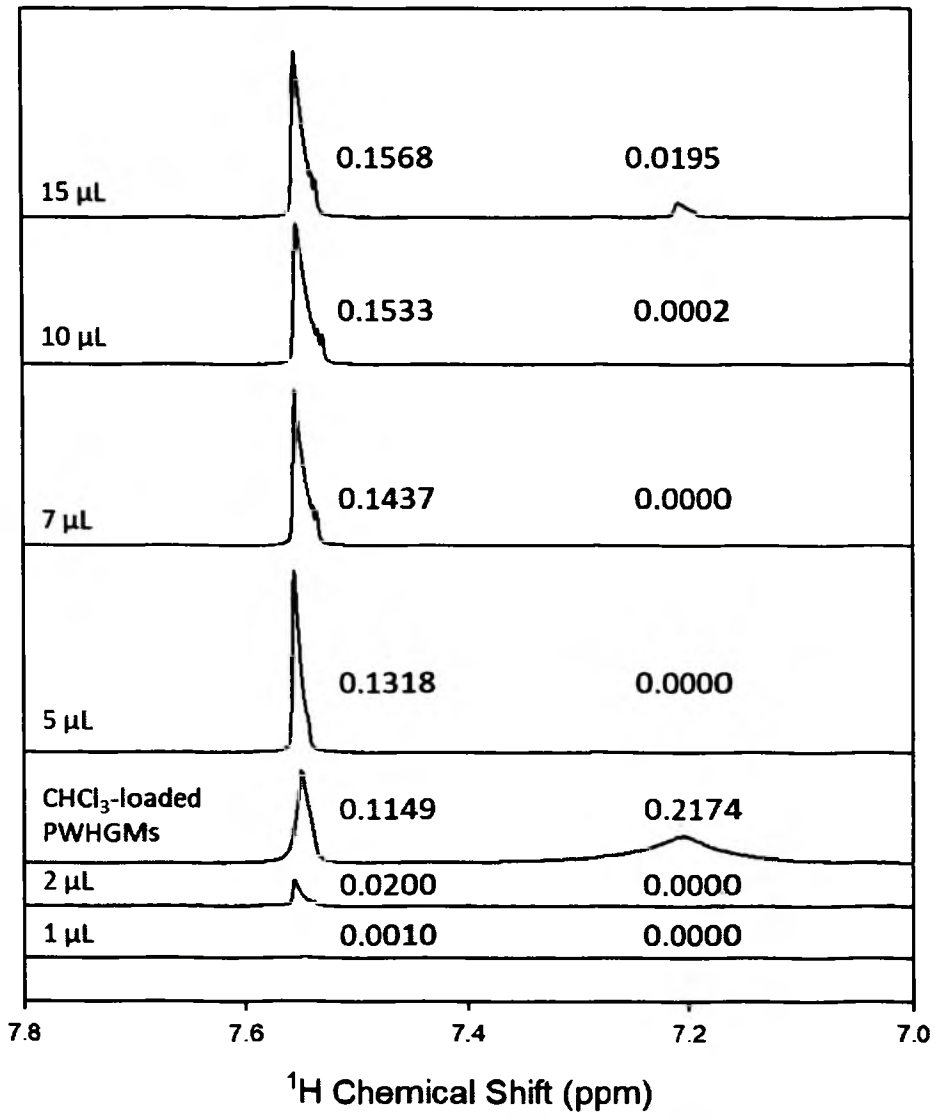

Figure 5.8. ^{1}H NMR spectra of $CHCl_3/D_2O$ emulsions (black) and $CHCl_3$-loaded PWHGMs in D_2O (red). The amounts of $CHCl_3$ in µL added to 750 µL of D_2O are indicated in a column on the left side of the spectra. The integrals reporting the amount of dissolved $CHCl_3$ in the ^{1}H NMR spectra are shown in a center column. The integrals reporting the amount of $CHCl_3$ in $CHCl_3/D_2O$ emulsions and $CHCl_3$-loaded PWHGMs in D_2O in the ^{1}H NMR spectra are shown in a column on the right side of the spectra. The ^{1}H NMR spectrum of $CHCl_3$-loaded PWHGMs in D_2O shows an integral of 0.1149 for dissolved $CHCl_3$, which was used to position the spectrum in between the control spectra for 1 and 5 µL of $CHCl_3$ in 750 µL of D_2O. The broad peak at 7.20 ppm in the ^{1}H NMR spectrum of $CHCl_3$-loaded PWHGMs in D_2O shows an integral value of 0.2174, which is exceedingly larger than the integral values for the corresponding peaks in the ^{1}H NMR spectra of all samples that contain $CHCl_3/D_2O$ emulsions.

5.3.4. Characterization of $C_{12}H_{26}$-loaded PWHGMs. An additional immiscible binary system, consisting of n-dodecane in D_2O, was also studied. Figure 5.9 shows ^1H NMR spectra of 1 μL to 10 μL of $C_{12}H_{26}$ in 750 μL of D_2O. When 1 μL of $C_{12}H_{26}$ was added to 750 μL of D_2O, there were three sets of peaks observed in the ^1H NMR spectrum. The singlet HOD peak at 4.63 ppm is from residual protons in the lock solvent D_2O. The asymmetric peak pattern at 1.17 ppm is assigned to the CH_2 groups of $C_{12}H_{26}$ while the poorly-resolved triplet peak at 0.77 ppm is assigned to the CH_3 groups of $C_{12}H_{26}$. When 1 μL of $C_{12}H_{26}$ was added to 750 μL of D_2O, the mass concentration of $C_{12}H_{26}$ in D_2O was 1×10^{-3} g/mL (5.9 mM), which is much greater than the reported solubility of $C_{12}H_{26}$ in water (3.7×10^{-9}g/mL or 0.022 μM at 25 °C [100]). Presuming that the solubilities of $C_{12}H_{26}$ in H_2O and D_2O are similar, the amount of $C_{12}H_{26}$ dissolved in D_2O is far below the detection limit of conventional ^1H NMR spectroscopy (~1 μM), and only a $C_{12}H_{26}/D_2O$ emulsion contributes to the peaks observed in the spectrum. This observation becomes more pronounced when more $C_{12}H_{26}$ is added to the D_2O solvent of several NMR control samples (e.g., 1-10 μL of $C_{12}H_{26}$ in 750 μL of D_2O) as shown in Figure 5.9. For the control sample composed of 10 μL of $C_{12}H_{26}$ in 750 μL of D_2O, there are four NMR signals present in addition to the HOD/H_2O peak at 4.63 ppm. The broad peaks next to the peaks assigned earlier to the CH_2 and CH_3 groups of $C_{12}H_{26}$ originate from a distribution of larger globules of $C_{12}H_{26}$ in D_2O. The macroscopic phase separation of $C_{12}H_{26}$ in D_2O (large dodecane globules of different shapes) creates a distribution of magnetic environments for the $C_{12}H_{26}$

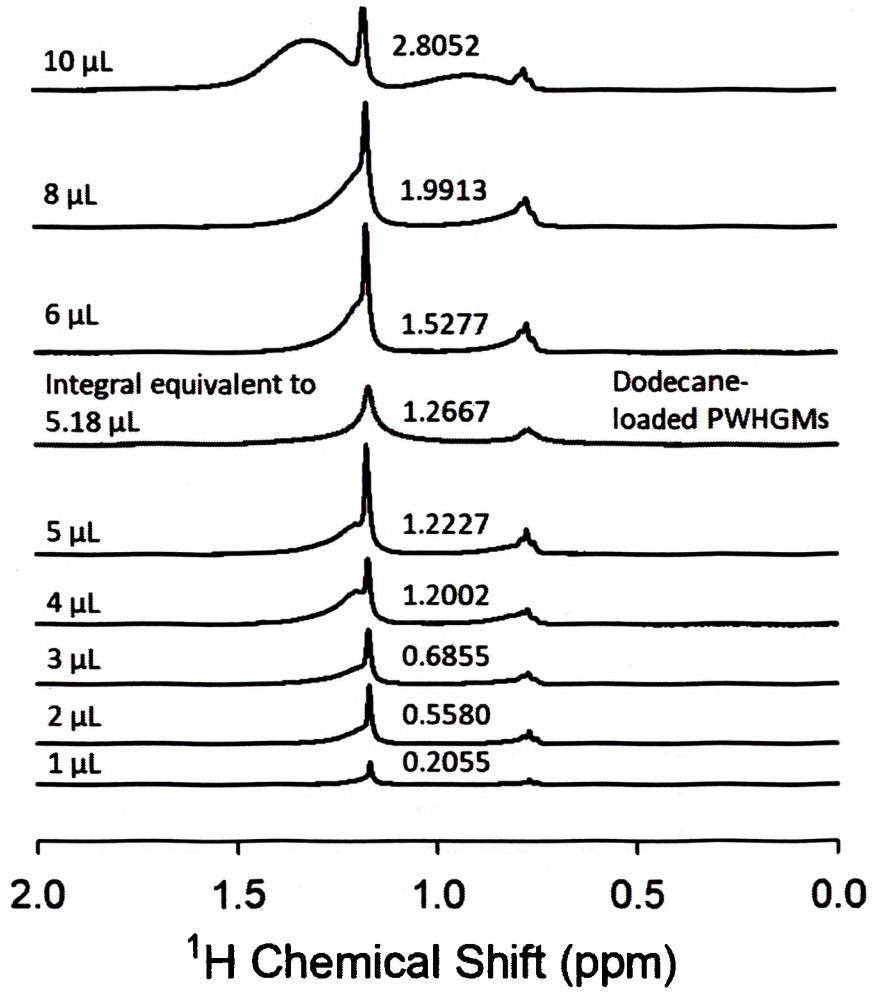

Figure 5.9. ^{1}H NMR spectra of $C_{12}H_{26}$ in D_2O emulsions (black) and $C_{12}H_{26}$-loaded microspheres in D_2O (red). The amounts of $C_{12}H_{26}$ in µL added to 750 µL of D_2O are indicated in a column on the left side of the spectra, and the total integrals of the $C_{12}H_{26}$ peaks are shown in a column in the middle of the spectra. The amount of 5.18 µL of $C_{12}H_{26}$ shown in the ^{1}H NMR spectra of $C_{12}H_{26}$-loaded microspheres in D_2O was determined by analysis of the integrals of the spectra.

molecules, which is revealed by the very broad peaks in the ^{1}H NMR spectra. The ^{1}H NMR spectrum of $C_{12}H_{26}$-loaded PWHGMs suspended in D_2O is also included in Figure 5.9 (red). Importantly, the spectral features of the $C_{12}H_{26}$-loaded PWHGMs suspended in D_2O

are distinctly different from spectral features of the $C_{12}H_{26}/D_2O$ emulsion samples. For example, the broad shoulder peak at 1.20 ppm for the CH_2 groups in the ^1H NMR spectra of the samples composed of 5 and 6 μL of $C_{12}H_{26}$ in 750 μL of D_2O is missing in the ^1H NMR spectrum of $C_{12}H_{26}$-loaded PWHGMs suspended in D_2O. Note that the total integrals of the ^1H NMR peaks for $C_{12}H_{26}$ in all spectra are used to position the ^1H NMR spectrum of $C_{12}H_{26}$-loaded PWHGMs suspended in D_2O in between the ^1H NMR spectra of the two control samples composed of 5 and 6 μL of $C_{12}H_{26}$ in 750 μL of D_2O.

PWHGMs were loaded with $C_{12}H_{26}$ according to the loading procedure described in Section 2.2 above and washed three times with D_2O. Afterward, the PWHGMs were re-suspended in D_2O and transferred to a 5 mm NMR tube. The recorded ^1H NMR spectra of $C_{12}H_{26}$ in D_2O and $C_{12}H_{26}$-loaded microspheres in D_2O are shown in Figure 5.10. There are four ^1H NMR peak features observed in the spectrum of $C_{12}H_{26}$ in D_2O shown in Figure 5.10a: (1) the sharp peak for the CH_2 groups at 1.17 ppm; (2) the broad shoulder peak for the CH_2 groups at 1.20 ppm; (3) the triplet peak for the CH_3 groups at 0.77 ppm; and, (4) the broad shoulder peak for the CH_3 groups at 0.81 ppm. The splitting of the triplet peak for the CH_3 groups is not resolved, and the asymmetric two-peak feature for the CH_2 groups is very broad and appears as a broad peak overlapped with a narrow peak. On the other hand, Figure 5.10b reveals the broadened, symmetric peak shapes observed for a typical sample of $C_{12}H_{26}$-loaded PWHGMs. There are two ^1H NMR peak features observed in the spectrum of $C_{12}H_{26}$-loaded PWHGMs in D_2O shown in Figure 5.10b: (1) the symmetric peak for the CH_2 groups at 1.17 ppm; and, (2) the symmetric peak for the CH_3 groups at

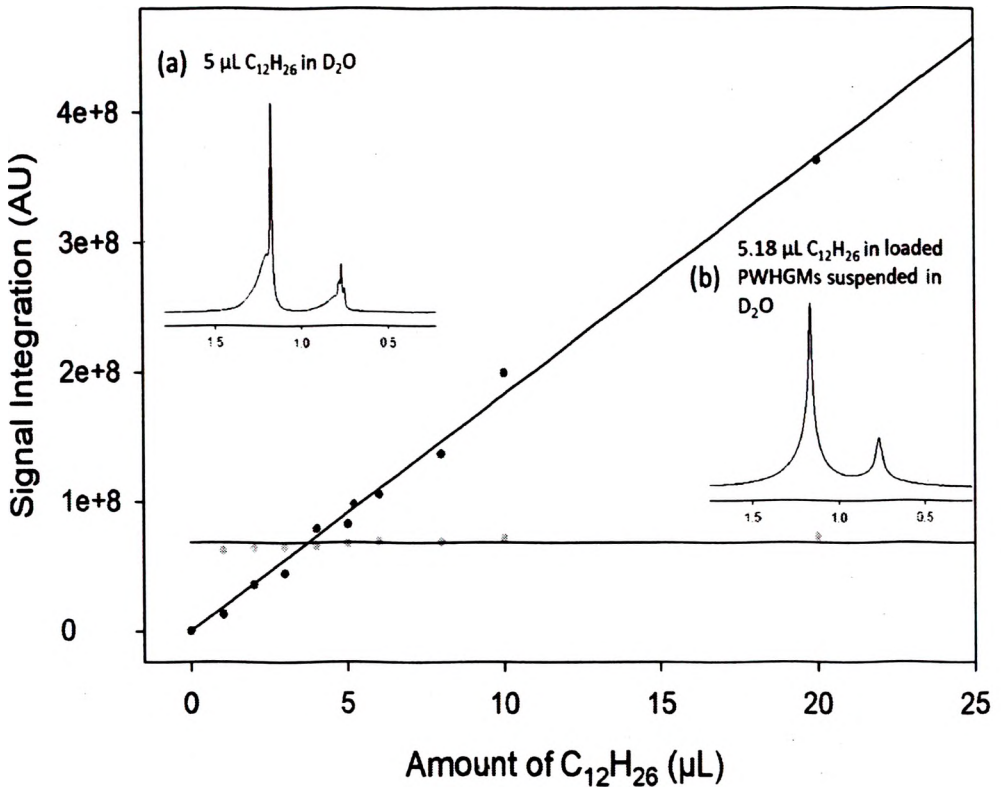

Figure 5.10. A calibration plot of the absolute integrals of the $C_{12}H_{26}$ peaks vs. the corresponding amounts of metered $C_{12}H_{26}$ mixed with D_2O (filled blue circles); the corresponding line is the best linear fit to the data. A calibration plot of the absolute integrals of the HOD peaks from D_2O vs. the corresponding amounts of the metered $C_{12}H_{26}$ mixed with D_2O (filled green circles); the corresponding line represents the mean of the data recorded from the internal reference HOD. The red filled circle is the absolute integral of the $C_{12}H_{26}$ signal for a sample containing $C_{12}H_{26}$-loaded PWHGMs suspended in D_2O. (a) ^1H NMR spectrum of an emulsion sample composed of 5 µL of $C_{12}H_{26}$ mixed with D_2O. (b) ^1H NMR spectrum of $C_{12}H_{26}$-loaded PWHGMs suspended in D_2O, where the amount of $C_{12}H_{26}$, determined by integration, is 5.18 µL.

0.77 ppm. In the control experiments, four sets of peaks were noticed for $C_{12}H_{26}$. As explained previously, the two narrow peaks were assigned to the $C_{12}H_{26}/D_2O$ emulsion while the phase-separated $C_{12}H_{26}$ globules generated the two broad peaks. The ^1H NMR signals from the CH_2 and CH_3 groups of the $C_{12}H_{26}$ loaded in the PWHGMs exhibit similar

chemical shifts to the ^{1}H NMR signals of the $C_{12}H_{26}/D_2O$ emulsion observed in the control experiments. $C_{12}H_{26}$ in the PWHGMs is a template for bulk $C_{12}H_{26}$ fluid in the form of microdroplets, and thus it has the same chemical environment as the $C_{12}H_{26}/D_2O$ emulsion, leading to similar chemical shifts. This interpretation is consistent with the binary system of $CHCl_3$ and D_2O. When the $C_{12}H_{26}$ molecules are confined in the PWHGMs, there is no phase separation, and therefore, the ^{1}H NMR signals that have the same chemical shift as the $C_{12}H_{26}/D_2O$ emulsion must originate from inside of the PWHGMs.

5.3.5. Materials Release from the Interior of PWHGMs to the Surroundings. The hydrolysis of isopropyl acetate was evaluated with ^{1}H NMR spectroscopy as a useful system for studies of PWHGM release kinetics. ^{1}H NMR experiments focused on the formation of acetic acid and isopropanol, where the latter exhibits a septet peak for the CH group that is not only separated from the septet peak for the CH group of the isopropyl acetate but also from the singlet peak for HOD. The ^{1}H NMR spectra shown in Figure 5.11 focus on the septet peak of isopropanol recorded before the addition of acid (catalyst), directly after the addition of acid, 10 minutes after the addition of acid, and 120 minutes after the addition of acid. Before the addition of the acid catalyst, the ^{1}H NMR spectrum showed only baseline noise around 3.81 ppm, indicating that isopropanol was not present. Next, the acid-catalyzed hydrolysis reaction was initiated by adding 5 μL of concentrated H_2SO_4. A septet peak is barely observed at 3.81 ppm and assigned to the CH group of newly formed isopropanol. ^{1}H NMR spectra recorded at the reaction times of 10 minutes and 120 minutes reveal that the intensity of the septet peak increased as the reaction proceeded, leading to higher S/N ratios. This result demonstrates that it took some time to reach equilibrium for the reversible hydrolysis reaction, and that the reversible reaction is

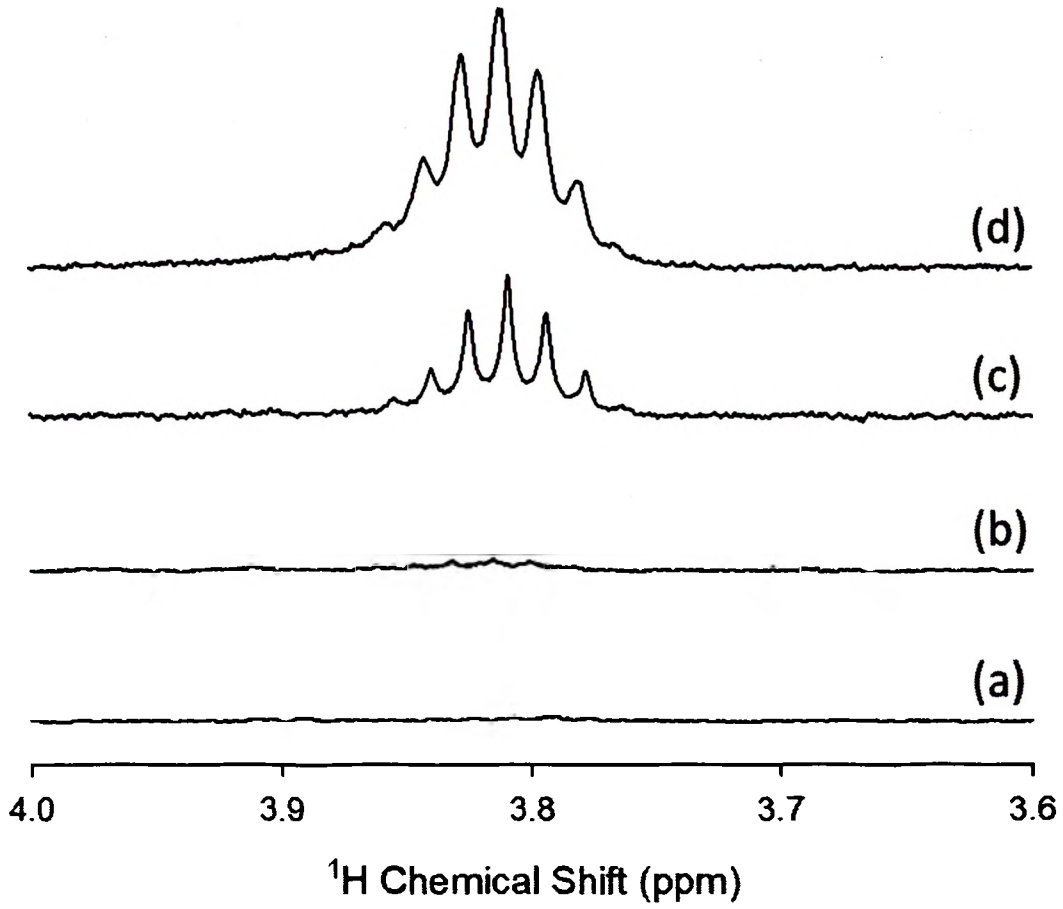

Figure 5.11. An empty section of the ^{1}H NMR spectra of a sample of isopropyl acetate-loaded PWHGMs recorded in D_2O solvent where the septet peak for isopropanol is expected to appear (bottom spectrum). Three additional spectra show the formation of isopropanol during the acid-catalyzed hydrolysis of isopropyl acetate molecules that were initially contained in the PWHGMs. The spectra were recorded (a) before the addition of concentrated sulfuric acid, (b) directly after the addition of acid, (c) 10 minutes after the addition of acid, and (d) 120 minutes after the addition of acid catalyst.

suitable for the evaluation of the exchange of materials between the inside and outside of the PWHGMs. Therefore, both the presence and increase of the isopropanol septet peak can be used as evidence for chemical exchange between the inside of the PWHGMs and the surrounding solution. Details of the exchange process remain to be elucidated. The observation that the isopropanol septet is well resolved provides evidence that the

isopropanol is in the D_2O solvent surrounding the isopropyl acetate-loaded PWHGMs. Furthermore, the isopropyl acetate initially contained within the PWHGMs was the only source for the isopropanol that was metered by ^1H NMR on account of the corresponding hydrolysis reaction. Additional investigations are required to explain the general location of the hydrolysis reaction, whether inside the PWHGMs or in the surrounding solution or both.

In a repeated experiment, PWHGMs were again loaded with isopropyl acetate and washed with D_2O. ^1H NMR spectra were recorded after the PWHGMs were initially suspended in 750 μL of D_2O in the presence of concentrated H_2SO_4 and 10 minutes later (Figure 5.12). A broad ^1H NMR peak for the CH group of isopropyl acetate was observed at 4.78 ppm, with the septet peak somewhat resolved (Figure 5.12a). Another broad ^1H NMR peak observed at 3.81 ppm is assigned to the isopropanol CH group, which demonstrates the formation of isopropanol. However, the septet is only somewhat resolved, which indicates that the isopropanol is preferentially formed inside the PWHGMs. Isopropanol formed outside of the PWHGMs should exhibit a well resolved ^1H NMR septet. The formation of isopropanol inside the PWHGMs indicates that H^+ propagates into the PWHGMs and initiates the hydrolysis reaction within the PWHGMs. Nevertheless, a second ^1H NMR spectrum (Figure 5.12b) recorded 10 minutes after the addition of concentrated H_2SO_4 shows the highly resolved septet peak from the CH group from isopropyl acetate at 4.77 ppm as well as the peaks from the CH_3 and CH groups from isopropanol at 0.96, 3.81 ppm, respectively, indicating the presence of isopropyl acetate and isopropanol outside the PWHGMs. Another indication that material exchanged

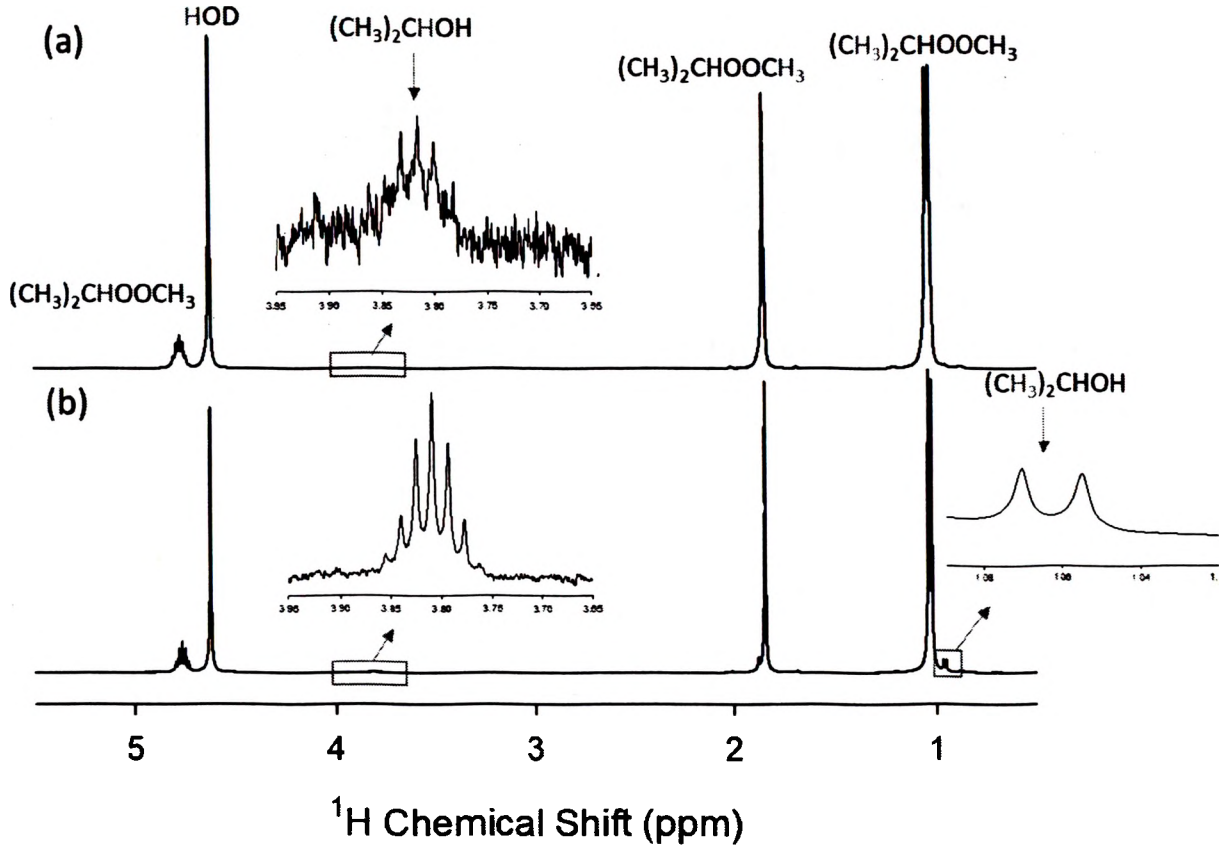

Figure 5.12. ^{1}H NMR spectrum of PWHGMs loaded with isopropyl acetate and suspended in D_2O. (a) with 5 μL of concentrated H_2SO_4 added; (b) after 10 minutes reaction time. The highly resolved isopropanol septet at 3.81 ppm in (b) indicates that the isopropanol is in the solution surrounding the PWHGMs.

between the cavities of the PWHGMs and the surrounding solution is that most of the PWHGMs slowly floated to the top of the NMR tube because of the lower density of isopropyl acetate (0.87 g/mL) inside the PWHGMs compared with D_2O in the surrounding solution. By floating to the top, the PWHGMs left the NMR-sensitive volume (RF coil) whereas the ^{1}H NMR signals for the dissolved isopropanol and the isopropyl acetate could still be observed in the ^{1}H NMR spectra. Hence the observed signals must be from isopropyl acetate and isopropanol dissolved in D_2O. The increasing ^{1}H NMR peak intensity

of the isopropanol CH group indicates that the reaction was still proceeding, and material was still leaching out of the PWHGMs. This demonstrated that a significant exchange of H^+ and isopropyl acetate occurred between the inside of the PWHGMs and the surrounding solution.

5.3.6. Kinetic Studies of PWHGMs Releasing Materials. ^{1}H NMR is an intrinsically quantitative technique in which the integrated signal intensity is directly proportional to the number of protons in the NMR-active volume of the sample. In this exemplary release study of H_2O-loaded PWHGMs in D_2O, the changing intensity of the H_2O peak relative to the peak intensity of the external reference peak ($CHCl_3$) is plotted as a function of time. The data plotted in Figure 5.13 appeared to represent a double-exponential rise to a maximum and thus were evaluated by a numerical fitting procedure using a 5-parameter double-exponential curve described by the following equation:

$$I = 6.35 + 78\%\,(1 - \exp(-0.0481\,t)) + 22\%\,(1 - \exp(-0.0063\,t)) \qquad (9)$$

The best fit to the experimental data (black dots) is included in Figure 5.13 as a solid line curve. The fit has a correlation coefficient of $R^2 = 0.9977$ and a standard error of approximately 1%. The uncertainty in the starting point of the H_2O release relative to the initial ^{1}H NMR spectrum (± 1 min) adds another 1% to the standard error. The individual parameters are interpreted below.

The curve has a constant intercept, which means that it does not start at zero intensity (y_0 intercept = 6.35). The intercept represents the 0.2% HOD residue already present in the surrounding solvent (D_2O). The curve fit exhibits the combination of two exponential curves, where one applies to 78% (± 2%) of the released H_2O and the other to the remaining 22% (± 2%). The 78% signal portion shows a faster release, with a time

constant of approximately 18 - 20 minutes, while the 22% signal portion shows a much slower release time constant of approximately 160 minutes. The two different release rates may result from PWHGMs only with 10-100 nm dimples (Figure 5.2) and PWHGMs with dimples and ~1 μm through-holes (Figure 5.3), respectively. Because the largest dimension of an H_2O molecule is only 0.275 nm, the sizes of the dimple diameters in the PWHGM walls, as well as the sizes of the channel dimensions in the glass walls, largely exceed the size of an H_2O molecule. Thus, H_2O is believed to traverse the thinner glass wall under the dimples but still through the significantly restricted tortuous channels of the glass walls. The effect a dimple has on the effective thickness of the porous glass wall under the dimple is minimal (< 5%), as illustrated in Figure 5.14. Dimples of diameters 10-100 nm reduce the thickness of the porous glass wall below the dimple to approximately 900-990 nm, whereas larger through-holes pierce the porous glass wall completely (Figure 5.14a). The materials inside PWHGMs with dimples only are released much slower via the tortuous pathways compared to the PWHGMs with large through-holes that pierce the walls (Figure 5.14b) and, thus, do not obstruct the release of materials from the inside of the PWHGMs. Hence, about 78% of the materials inside the PWHGMs is released relatively fast from PWHGMs with through-holes, while about 22% is released from PWHGMs with only dimples. Repeating this release experiment showed very similar results, where the optimized curve-fit parameters (percentages and release rates) fell within the standard errors reported above.

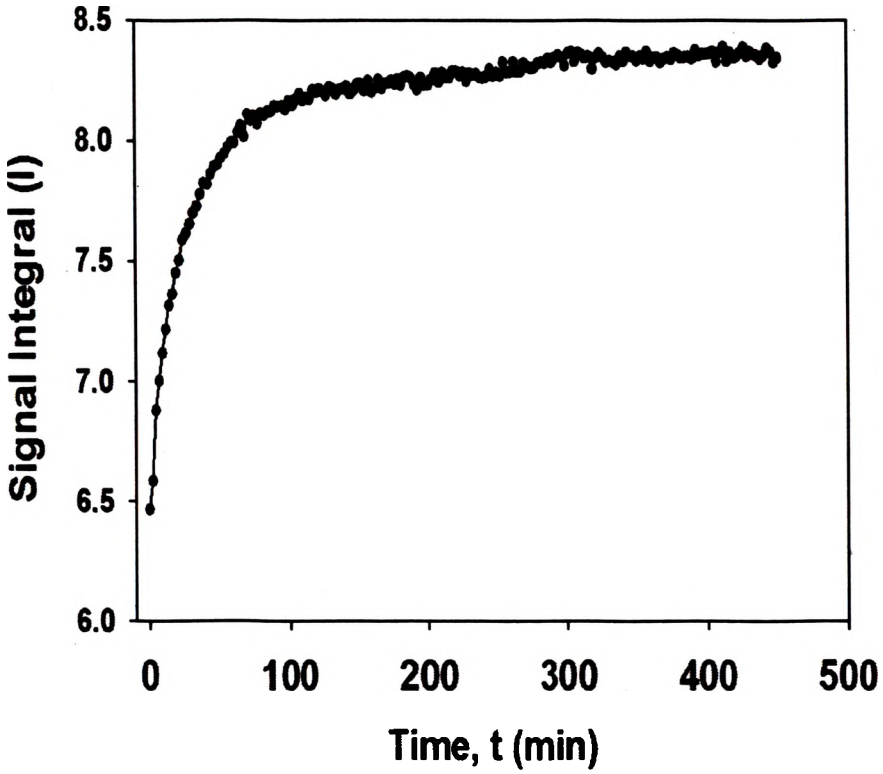

Figure 5.13. ^{1}H NMR signal intensity of HOD/H_2O in D_2O as a function of time fitted with a 5-parameter bi-exponential curve. The faster releasing portion accounts for 78%, while slow releasing portion accounts for 22%.

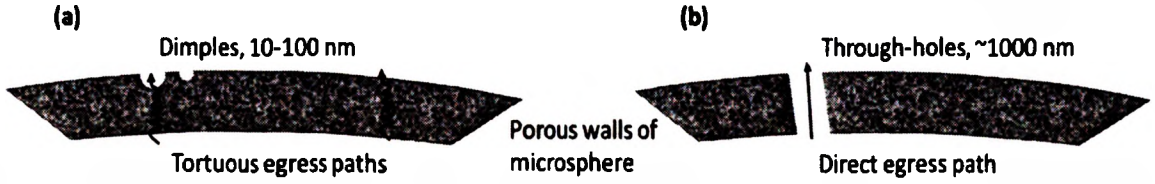

Figure 5.14. Schematic of the effect of dimples and their diameters on the residual thickness of the porous glass wall of a PWHGM at the site of a dimple. (a) PWHGMs with 10-100 nm-diameter dimples that provide tortuous egress pathways that are slightly shorter through the porous glass walls for materials to exit slowly; (b) PWHGMs with ~1000 nm-diameter through-holes that provide direct egress pathways in the porous glass walls for the materials to exit quickly.

5.4. SUMMARY OF PWHGM STUDIES

In this study, a vacuum-based system and an effective washing procedure were successfully developed for loading materials into PWHGMs. The loading system was employed to fill PWHGMs with liquid materials. Digital photographs revealed the success of the material loading process for several PWHGM samples.

^{1}H NMR evidence for $CHCl_3$-loaded PWHGMs was obtained using an immiscible binary system composed of $CHCl_3$ and D_2O. The broad ^{1}H NMR peak at 7.20 ppm was identified as the $CHCl_3$ inside the PWHGMs, which has the same chemical shift as the ^{1}H NMR peak for a $CHCl_3/D_2O$ emulsion. Integrals of the dissolved $CHCl_3$ peak at 7.55 ppm in control experiments of 1-15 μL of $CHCl_3$ in D_2O and PWHGMs experiment of $CHCl_3$-loaded PWHGMs were used to compare the ^{1}H NMR peaks for $CHCl_3/D_2O$ emulsions to the peak for $CHCl_3$-loaded PWHGMs. The comparisons of the spectral peak characteristics (shape and relative integral) provided *prima facie* evidence for the first observations of a compound contained in PWHGMs. Additional and distinct *prima facie* evidence for guest-loaded PWHGMs was provided by comparing ^{1}H NMR spectra of $C_{12}H_{26}$-loaded PWHGMs and $C_{12}H_{26}/D_2O$ emulsions. Symmetric ^{1}H NMR peaks at 1.17 and 0.77 ppm were identified as the CH_2 and CH_3 groups, respectively, of $C_{12}H_{26}$-loaded PWHGMs. Broad ^{1}H NMR shoulder peaks at 1.20 and 0.81 ppm were identified as the CH_2 and CH_3 groups, respectively, of phase-separated $C_{12}H_{26}$ globules in $C_{12}H_{26}/D_2O$ emulsion samples, which always appear in addition to the ^{1}H NMR peaks at 1.17 and 0.77 ppm for the CH_2 and CH_3 groups, respectively, of the $C_{12}H_{26}/D_2O$ emulsions. Importantly, the broad ^{1}H NMR shoulder peaks at 1.20 and 0.81 ppm for $C_{12}H_{26}$ globules are never present in the ^{1}H NMR spectra of $C_{12}H_{26}$-loaded PWHGMs.

The formation of isopropanol was the indicator of the reaction of isopropyl acetate in the PWHGMs with concentrated H_2SO_4 in the surrounding solution. The release kinetics of H_2O from H_2O-loaded PWHGMs into a surrounding solution of D_2O provided further evidence of material exchange between PWHGMs and a surrounding solution. A 5-parameter double-exponential curve fit of the ^1H NMR signal intensity for H_2O as a function of time indicated two release rates with distinct time constants. The fast release rate was attributed to the release of materials contained in PWHGMs with large diameter (~1 μm) through-holes in the porous glass walls. The slow release rate was attributed to the release of materials contained in PWHGMs without through-holes. The release rate study indicates that only 22% of the as-received PWHGM sample is composed of microspheres with intact porous glass walls that are not breached by large through-holes.

For the first time to our knowledge, the ^1H NMR results described in this work provide both static and dynamic direct information about loaded materials in PWHGMs. The results of this study are expected to benefit the design of PWHGMs as drug carriers in applications for targeted delivery systems used for medical and diagnostic applications in human health care.

6. CapPack DEVICES FOR IN SITU TEMPERATURE MONITORING IN SOLID-STATE MAGIC-ANGLE-SPINNING (MAS) NMR INVESTIGATIONS

6.1. BACKGROUND

For many NMR investigations, it is important to know the temperature of the sample under investigation, particularly when changes in temperature can cause changes in chemical structures, chemical dynamics, or reactivity [101,102]. Especially in dynamic processes, where different compounds are at equilibrium or where conformational changes occur within the investigated molecule, the sample temperature is an important factor that can influence concentrations and lifetimes, respectively, of the participating compounds. Furthermore, for the stability of biomolecules, it is critical to keep the temperature fairly constant without much room for deviations. Accordingly, temperature control and temperature monitoring is most important in liquid-state NMR investigations of biomolecules, pharmaceuticals, or sensitive organometallic compounds [103,104]. The single-capillary CapPack device introduced in Section 2.1.3 offers a solution, which allows the NMR spectroscopist to determine the sample temperature with a high precision (± 0.1 K) directly from signals in the NMR spectrum.

More recently, solid-state magic-angle-spinning (MAS) NMR spectroscopy has become popular for investigations of temperature-sensitive materials such as different types of tissues [105, 106], or solid biomaterials and pharmaceuticals [107]. However, the fast rotation of the solid samples (currently up to 14 kHz) that is required for recording high-resolution solid-state NMR spectra can cause significant sample heating, which is not captured by the conventional methods of monitoring and controlling the temperature of an MAS sample.

A small single-capillary CapPack device for NMR temperature monitoring in MAS NMR investigations was developed that fits into standard, commercially available MAS rotors.

6.2. SOLID-STATE IN SITU NMR THERMOMETER DEVICE

Figure 6.1 shows a single-capillary CapPack temperature sensing device for in situ temperature measuring in solid state MAS NMR spectroscopy. A standard electrophoresis capillary tube (360 μm O.D., 75 μm I.D.) was filled with the temperature-sensing NMR compound ethylene glycol and permanently sealed with the arc of a fusion splicer. A particular challenge was to adjust the length of the capillary tube to exactly 10 mm without

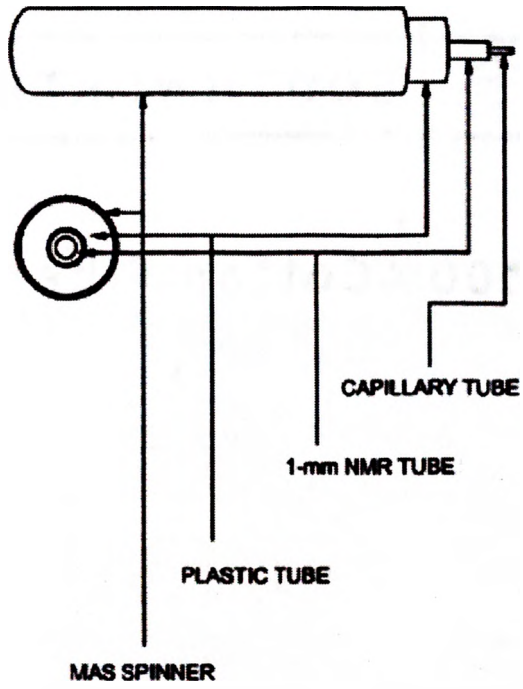

Figure 6.1. In situ NMR thermometer device for solid-state magic angle spinning (MAS) NMR spectroscopy. A capillary tube filled with temperature-sensing material is positioned inside of a 1-mm NMR tube. The 1-mm NMR tube is then positioned inside of a plastic tube that is used to center the capillary tube within the MAS rotor.

losing too much of the ethylene glycol material in the fusion process. The length of 10 mm is determined by the maximum sample height inside the MAS rotor. The small temperature CapPack with the ethylene glycol reference material is centrally placed in the sample (e.g., a compressed powder) that is contained in the MAS rotor. In an initial investigation, the capillary tube was positioned inside of a cut portion of a 1-mm NMR tube, which was then positioned inside of a plastic tube. The assembly of capillary tube, 1-mm NMR tube, and plastic tube were positioned inside of the MAS rotor (see Figure 6.1). The plastic tube was used to center the 1-mm NMR tube and the small temperature CapPack tube in the MAS rotor. A plastic tube is not required when a powdered sample material can be tightly packed inside the MAS rotor. Further, a drill bit or similar device can be used in a lathe to drill a concentric hole in the packed powdered sample material inside of the MAS rotor. The sealed capillary tube with the reference material is then placed in the drilled center hole and the powder around the inserted capillary tube compacted again. A special tool was manufactured from an aluminum rod that tightly fits the inside of the MAS rotor but leaves a central hole so that the inserted CapPack is not damaged.

The capillary tube used for the MAS CapPack device can also be filled with other reference material, which then can be used for in situ NMR chemical-shift or signal-intensity calibrations. It is further noted, that the reference material for MAS CapPacks may not only be a liquid but can also be a solid. Because the CapPack inside the MAS rotor will be spun at the same velocity as the MAS sample, high-resolution spectra are obtained not only from the sample but also from the reference material. Solid glycine, lead nitrate, or different cobalt complexes, for example, are well-known solid-state NMR reference materials [108-110].

6.3. FEASIBILITY TEST OF IN SITU TEMPERATURE MONITORING OF A SOLID-STATE NMR SAMPLE

A capillary tube for the MAS CapPack device was filled with 100% ethylene glycol and permanently sealed with the arc fusion splicer. The MAS CapPack was positioned inside the MAS rotor as described above (Figure 6.1), using a plastic tube to keep the capillary centered along the axis of rotation. The polymer material of the plastic tube did not produce a signal in the solid-state ^{1}H NMR spectrum. A rotor cap was placed on the MAS rotor to seal in the MAS CapPack as well as the plastic tube. The rotor was then placed in the MAS probe. The air jets of the high-speed rotation system were used to spin the rotor at different pre-set spinning rates (0.5 kHz, 6 kHz, 8 kHz, 10 kHz, and 14 kHz). After a pre-set spinning rate was achieved, the temperature was allowed to equilibrate for 5 min; thereafter, a single-pulse ^{1}H MAS NMR experiment was conducted. Figure 6.2 shows a set of stacked NMR spectra from the CH_2 and OH groups of ethylene glycol. A shift of the CH_2 peak of ethylene glycol with increasing spinning speed is clearly visible. The chemical-shift differences between the CH_2 group signal of ethylene glycol and the OH group signal of ethylene glycol was measured in ppm. From the measured chemical-shift differences, the sample temperature inside the MAS rotor was determined according to Equation (2) in Section 2.1.3. While the temperature measured by the spectrometer's thermocouple device, which is placed close to, but outside of, the MAS rotor, indicated a temperature increase less than 10 K when the spinning speed was increased from 0.5 to 14 kHz, the chemical-shift difference between the CH_2 and the OH group of ethylene glycol indicated a significant increase in temperature (33 K) with increasing spinning speed (from 292.7 K at 0.5 kHz to 325.8 K at 14 kHz). The temperatures determined in situ from the difference between the ethylene glycol signals are depicted in Figure 6.2 to the right of

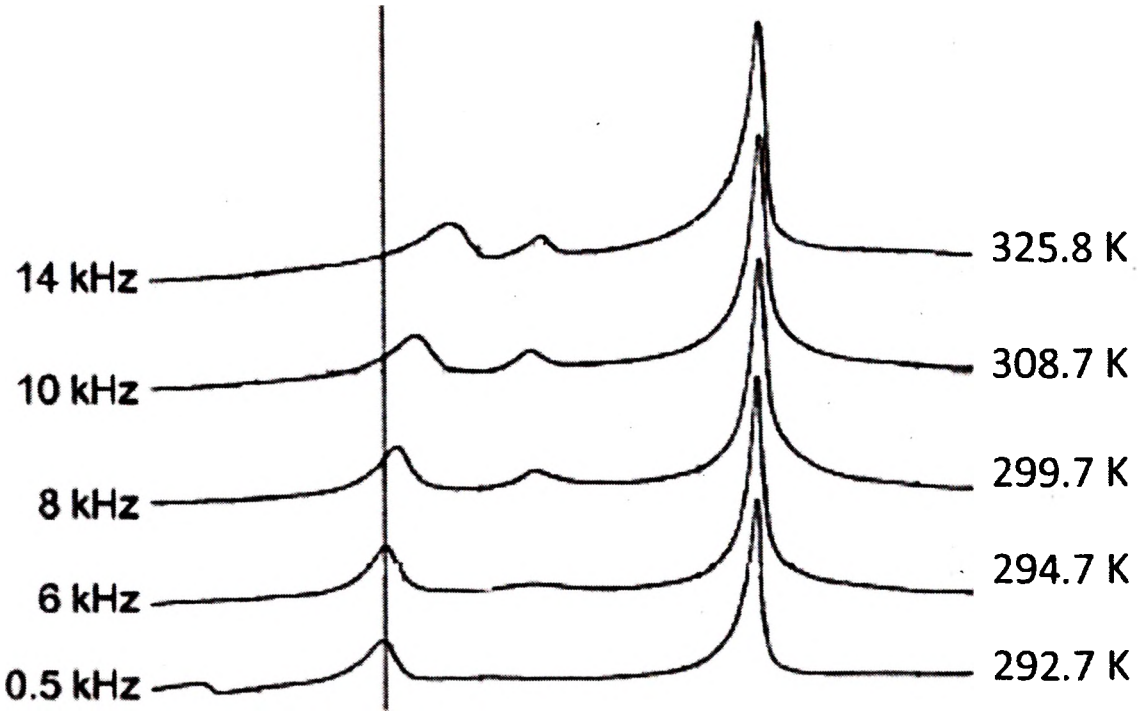

Figure 6.2. NMR spectra recorded from a MAS CapPack device in a MAS rotor as a function of spinning speed. The capillary tube of the CapPack device contained ethylene glycol as the temperature sensing NMR material. Numbers to the left reveal the pre-set spinning speeds of the MAS rotor, while the numbers on the right indicate the sample temperature as measured by the spectrometer's thermocouple device.

each spectrum. To better visualize the signal shift in the NMR spectra, a vertical line in Figure 6.2 shows the position of the CH_2 group NMR signal at 292.7 K. Figure 6.3 shows the temperatures determined from the ethylene glycol NMR spectra as a function of the spinning speed, as well as a table that summarizes the experimental results.

6.4. SUMMARY

The in situ NMR temperature measuring technique, using a single-capillary tube CapPack device with ethylene glycol as the temperature sensing material, has been expanded to include in situ temperature measurements in solid-state NMR spectroscopy.

A small capillary tube (360 μm O.D., 75 μm I.D., length of 10 mm) filled with ethylene glycol was permanently sealed and inserted concentrically into an MAS rotor. The temperature determined in situ from the chemical shift difference between the CH_2-group signal and the OH-group signal of ethylene glycol increased substantially with the spinning speed of the MAS rotor. This measurement was in contrast to the temperature indicated by

Spinning Speed (kHz)	Chemical Shift Difference (ppm)	Temperature (k)
14	1.39	325.8
10	1.56	308.7
6	1.65	299.7
2	1.7	294.7
0.5	1.72	292.7

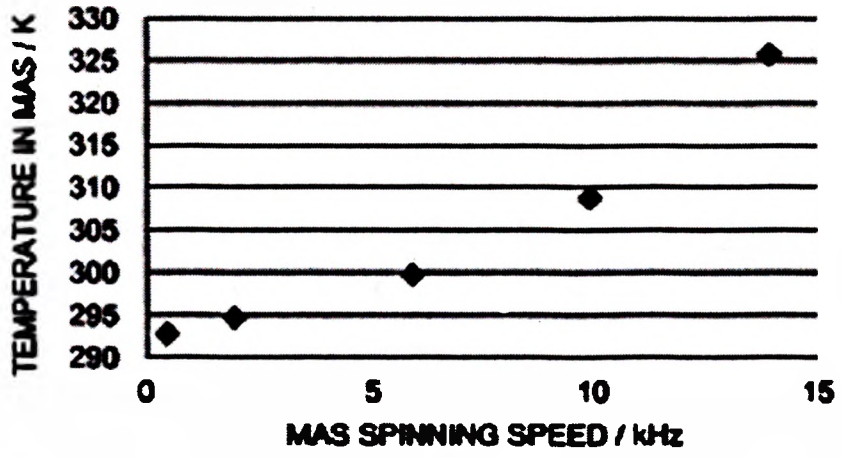

Figure 6.3. MAS sample temperature as a function of MAS rotor spinning speed. The temperatures were determined by the chemical shift difference between the NMR peaks of the CH_2 group and the OH group of the temperature-sensing material ethylene glycol. Despite a fairly constant temperature indicated by the spectrometer's thermocouple measuring device, which is placed close to, but outside of, the MAS rotor, the in situ determination of the sample temperature shows a significant increase in temperature with the rotor's spinning speed.

the thermocouple device of the NMR spectrometer, which determines the temperature at the outside of the MAS rotor. As a result, the spectrometer may provide a false sense of temperature that can, at higher spinning speeds, lead to the destruction of sensitive materials, or to the wrong determination of thermodynamic and kinetic constants, for example, when investigating conformational changes in biomolecules. At the maximum spinning speed (14 kHz), the temperature measured in situ was more than 25 K higher than indicated by the spectrometer's temperature measuring device.

7. CONCLUSION

Nuclear Magnetic Resonance (NMR) spectroscopy is an instrumental analysis technique that has far-reaching applications in the physical sciences and related industries. Most chemists use NMR for the structural elucidation of small to macromolecular molecules. For the precise determination of molecular structures and materials properties, it is critical to know sample or reaction conditions such as temperature, pH, concentration, or absolute amount of material. Because any of the conditions mentioned above can have a non-negligible influence on the chemical shifts of the signals in an NMR spectrum, it is important to calibrate the chemical-shift axis of NMR spectra and know the conditions under which a spectrum is recorded. Internal and external standards were used in each of the presented applications to calibrate the chemical-shift axis or assign concentrations to the observed signal intensities.

The use of commercially available electrophoresis capillary tubes that are filled with a reference material and then permanently sealed with the arc of an optical-fiber fusion splicer is introduced as a superior external reference. The presented external capillary-tube reference standards are high-quality devices for the precise determination of concentrations as well as parameters of analyte solutions and their reaction conditions. External chemical-shift references were used, for example, to determine the temperature of solutions under investigation. In addition, concentration calibrations were used for quantitative NMR spectroscopy. The concept of capillary-tube devices was then extended to investigations with reference capillaries mounted to the outside of standard NMR tubes. The so-called exterior CapPack devices were also used to assist in homogenizing (shimming) the transverse components of the main magnetic field of the spectrometer.

Internal references were used in Sections 3. and 5. of this dissertation in order to quantify the amount of analytes present in solution. In Section 3, the amount of residual water was determined for differently prepared mixtures of hydroxylammonium nitrate (HAN) and the ionic liquid 1-Ethyl-3-methylimidazolium ethyl sulfate ([Emim][$EtSO_4$]). The triplet NMR signal of the [$EtSO_4$] CH_3-group was used as chemical-shift reference because it is independent of the water content as long as water is not a major component of the mixture. While the chemical shifts of the sample signals are fairly constant, the HAN and water resonances collapse into one signal that moves significantly toward higher ppm values with decreasing amounts of residual water. In addition, the linewidth of the collapsed HAN/H_2O signal depends on the water content; the signal becomes significantly sharper (more narrow) as the water content decreases. In Section 5, a new technique was introduced to load porous-wall hollow glass microspheres (PWHGMs) with chemicals of small molecules ($CHCl_3$, dodecane, H_2O). The calibrated signal intensities of the small molecules played an important role in quantifying the kinetic constants of releasing the chemicals from the microspheres. The residual HOD NMR signal of the solvent D_2O served as an internal quantification and chemical-shift reference.

Section 4 exemplifies the use of a different material, concentrated hydrochloric acid (HCl), as chemical-shift and concentration reference. Concentrated hydrochloric acid was chosen because its NMR signal (8.11 ppm) is far removed from all other signals in the analysis. The section describes the reliable use of external calibration standards in the more involved saturation-transfer difference NMR spectroscopy, leading to the analysis of interactions between benzyl alcohol and different moieties in polymer micelles.

In Section 6, the application of temperature-sensing materials in CapPacks is extended to solid-state NMR spectroscopy. A small single-capillary tube of only 10 mm in length is inserted concentrically into an MAS rotor for solid-state NMR measurements. The temperature determined from the difference in chemical shift between the CH_2-group signal of the temperature sensing ethylene glycol and its OH-group signal indicates that the sample temperature increases significantly with the spinning speed of the MAS rotor (up to 33 K at a spinning speed of 14 kHz). This temperature increase was not revealed by the NMR spectrometer's thermocouple device that is placed close to, but outside of, the MAS rotor. The spectrometer's thermocouple device indicated a temperature increase of less than 10 K at the maximum spinning speed of 14 kHz.

APPENDIX

ACCOMPLISHMENTS

PUBLICATIONS (7)

1. Ming Huang, Sisi Chen, Rex E. Gerald II, Jie Huang, Klaus Woelk, **Pioneering NMR Studies of Materials Loaded Porous Wall Hollow Glass Microspheres**, submitted to *Materials Science and Engineering C: Material for Biological Applications*.

2. Ming Huang, Lingyu Chi, Jie Huang, Annalise R. Pfaff, Rex E. Gerald II, Klaus Woelk, ***In Situ* NMR Monitoring System and Methods for Measuring pH and Temperature**, full-utility U.S. patent has been accepted by the USPTO for examination, a first office action was received, a second office action is pending.

3. Ming Huang, Klaus Woelk, Rex E. Gerald II, **CapPack Devices and Related Methods for Quality Assurance and Optimization of NMR Spectrometers**, invited contribution to *Encyclopedia of Magnetic Resonance*.

4. Lingyu Chi, Ming Huang, Annalise R. Pfaff, Jie Huang, Rex E. Gerald II*, Klaus Woelk*, **Capillary-tube Package Devices for the Quantitative Performance Evaluation of Nuclear Magnetic Resonance Spectrometers and Pulse Sequences**, *Review of Scientific Instruments*, Vol 89, Issue 12, 123115, Dec 28, 2018.

5. Lingyu Chi, Ming Huang, Rex E. Gerald II, and Klaus Woelk, **Solid State NMR Spectroscopy/Imaging in situ Measuring Devices and Methods for Calibration and Determining one or more Quantitative Properties of a Target Sample**, U.S. Patent 10,067,079 B2 (issued Sep, 4th, 2018).

6. Yingxin He, Arun K. Itta, Abdo-alslam Alwakwak, Ming Huang, Fateme Rezaei, Ali A. Rownaghi, **Aminosilane-grafted SiO_2-ZrO_2 Polymer Hollow Fibers as Bifunctional Microfluidic Reactor for Tandem Reaction of Glucose and Fructose to 5-Hydroxymethylfurfural,** *ACS Sustainable Chem. Eng.* Vol 6, Issue 12 (17211-17219), Oct 29, 2018.

7. Alex J. Mundahl, Steven P. Berg, Joshua Rovey, Ming Huang, Klaus Woelk, Durgesh Vinod Wagle, Gary A Baker, **Characterization of a Novel Ionic Liquid Monopropellant for Multi-Mode Propulsion,** *Proc. 53rd AIAA/SAE/ASEE Joint Propulsion Conference*, DOI: 10.2514/6.2017-4756.

ORAL PRESENTATIONS (4)

1. Ming Huang, Sisi Chen, Rex E. Gerald II, and Klaus Woelk, **NMR Studies of Porous Wall Hollow Glass Microspheres (PWHGM),** project from MO-Sci company at Missouri S&T, February, 4th, 2016, Rolla, MO, USA

2. Ming Huang, Rex E. Gerald II, and Klaus Woelk, **Methods for qNMR: Spin Counting in NMR Coil: Using High Resolution ^{1}H NMR Spectrum,** Midwest Regional of the American Chemical Society meeting, October 21-24, 2015, St. Joseph, MO, USA

3. Ming Huang, Sisi Chen, Rex E. Gerald II, and Klaus Woelk, **Methods for qNMR: Spin Counting in NMR Coil Using Doty Apparatus,** 3rd Branson NMR Meeting, October 16-17, 2015, Branson, MO, USA

4. Ming Huang, Sisi Chen, Rex E. Gerald II, and Klaus Woelk, **NMR/MRI of Therapeutic Microspheres,** Innovation at Missouri S&T, October, 15th, 2015, Rolla, MO, USA

CO-AUTHORED ORAL PRESENTATIONS (13)

1. Kaysi M Lee, Ming Huang, Klaus Woelk, **^{19}F Nuclear Magnetic Resonance (NMR) Measurements Using 2-Fluoro-3-hydroxymethylpyridine as a pH-sensitive Compound**, 51st Annual Southeastern Undergraduate Research Conference, Feb, 2019, Martin, TN

2. Ming Huang, Matthew Parker, Klaus Woelk, Jie Huang, Rex Gerald II, **Simple Laser System for Hyperpolarized NMR Experiments**, 51st Annual Southeastern Undergraduate Research Conference, Feb, 2019, Martin, TN

3. Lauren M. Kehoe, Ming Huang, Ashish S Zore, Michael Van De Mark, Rex E. Gerald II, Klaus Woelk, **Saturation-transfer Difference Nuclear Magnetic Resonance (NMR) Experiments to Probe into Interactions Between Benzyl Alcohol and Colloidal Unimolecular Polymers**, 51st Annual Southeastern Undergraduate Research Conference, Feb, 2019, Martin, TN

4. Emma L. Wideman, Lauren M. Kehoe, Lingyu Chi, Ming Huang, Brandon Gamelin, Rex E. Gerald II, Klaus Woelk, **T_1 CapPack™ (Capillary tube Package) Devices for Determining the Effects of Spin Lattice Relaxation on Nuclear Magnetic Resonance (NMR) Pulse Sequences**, 51st Annual Southeastern Undergraduate Research Conference, Feb, 2019, Martin, TN

5. Ming Huang, Kaysi M. lee, and Klaus Woelk, **NMR pH Measurements using the ^{19}F Chemical Shift of Fluoro-hydroxymethylpyridines with and without Deuterium Field-frequency Lock**, Missouri Academy of Science Conference, Apr, 2018, Rolla, MO

6. Klaus Woelk, Robert J. Klingler, Rex E. Gerald II, Lingyu Chi, Ming Huang, **From NMR Relaxation Experiments to High-resolution NMR Relaxometry,** Organic Chemistry Seminar Series, October, 26th, 2015, Department of Chemistry, University of Missouri, Columbia, MO

7. Klaus Woelk, Robert J. Klingler, Rex E. Gerald II, Lingyu Chi, Ming Huang, **From Inversion Recovery and CPMG to High-resolution NMR Relaxometry,** 2015 American Chemical Society (ACS) Saint Louis Award Symposium and Banquet, October, 16th, 2015, Washington University, St. Louis, MO, USA

8. Klaus Woelk, Robert J. Klingler, Rex E. Gerald II, Lingyu Chi, Ming Huang, **From Standard NMR Relaxation Experiments to High-resolution Relaxometry,** Departmental Seminar, September, 28th, 2015, Department of Chemistry, Missouri University of Science and Technology, Rolla, Missouri, USA

9. Klaus Woelk, Robert J. Klingler, Rex E. Gerald II, Lingyu Chi, Ming Huang, **A Revised NNLS Approach to High-Resolution NMR Relaxometry,** 56th Experimental NMR Conference (ENC), April, 23rd, 2015, Pacific Grove, CA, USA

10. Lingyu Chi, Eric Anderson, Ming Huang, Rex E. Gerald II and Klaus Woelk, **CapPack Devices**, MISSOURI TECH EXPO 2014, October 16th, 2014, Christopher S. Bond Life Sciences Center, Columbia, Missouri, USA

11. Lingyu Chi, Klaus Woelk, Rex E. Gerald II, Annalise R. Pfaff, Ming Huang, Jie Huang and Emmalou T. Satterfield, **New Quantitative NMR Techniques for Determining the Product Yield of Hydrothermal Biomass to Fuel Reaction**, Chemistry Seminar, December 2nd, 2013, Rm 126, Department of Chemistry, Missouri University of Science and Technology, Rolla, Missouri, USA

12. Rex E. Gerald II, Klaus Woelk, Baojun Bai, Lingyu Chi, Ming Huang, Annalise R. Pfaff, **Subdivision of Zeeman NMR Fields by Static and Dynamic Magnetic Field Distributions and Capillary Tube Compartments: Applications of Quantitative NMR/MRI Employing Cap-Pack Devices**, CM/Bio/ECE Seminars, Oct. 30th, 2013, Rm 233A, Physics Bldg., Department of Physics and Astronomy, University of Missouri – Columbia, Columbia, Missouri, USA

13. Rex E. Gerald II, Klaus Woelk, Baojun Bai, Lingyu Chi, Ming Huang, Annalise R. Pfaff, **Applications of Quantitative NMR/MRI Employing Cap-Pack Devices**, MIT *NewNMRGroup*, October 15th, 2013, Department of Chemistry Instrumentation Facility, Massachusetts Institute of Technology, Cambridge, Massachusetts, USA

POSTER PRESENTATIONS (17)

1. Ming Huang, Kaysi M. Lee, and Klaus Woelk, **NMR pH Measurements Using the ^{19}F Chemical Shift of Fluoro-hydroxymethylpyridines with and without Deuterium Field-Frequency Lock**, 59th EXPEIMENTAL NUCLEAR MAGNETIC RESONANCE CONFERENCE, April 30th – May 5th, 2018, Hyatt Regency Grand Cypress, Orlando, Florida, USA

2. Ming Huang, Sisi Chen, Rex E. Gerald II, Jie Huang, Klaus Woelk, **NMR Studies of Loaded Microspheres**, 59th EXPEIMENTAL NUCLEAR MAGNETIC RESONANCE CONFERENCE, April 30th – May 5th, 2018, Hyatt Regency Grand Cypress, Orlando, Florida, USA
3. Rex E. Gerald II, Jie Huang, Klaus Woelk, William Stocker, Lingyu Chi, Ming Huang, and Sean Cartwright, **Acupuncture-MRI Skin Cancer Probe**, 59th EXPEIMENTAL NUCLEAR MAGNETIC RESONANCE CONFERENCE, April 30th – May 5th, 2018, Hyatt Regency Grand Cypress, Orlando, Florida, USA

4. Lingyu Chi, Ming Huang, Annalise R. Pfaff, Rex E. Gerald II, Jie Huang, and Klaus Woelk, **Optimizing NMR Hardware and Pulse Sequences with CapPack Devices**, 59th EXPEIMENTAL NUCLEAR MAGNETIC RESONANCE CONFERENCE, April 30th – May 5th, 2018, Hyatt Regency Grand Cypress, Orlando, Florida, USA

5. Ming Huang, Sisi Chen, Rex E. Gerald II, and Klaus Woelk, First NMR Studies of Porous Wall Hollow Glass Microspheres, The Suites at Fall Creek Resort, 3rd Branson NMR Meeting, October 16th-17th, 2015, Branson, MO, USA

6. Ming Huang, Sisi Chen, Rex E. Gerald II, and Klaus Woelk, **Probing Reversible and Irreversible Net Magnetization Undergoing Nutation Using TCD and Commercial Probe,** The Suites at Fall Creek Resort, 3rd Branson NMR Meeting, October 16th -17th, 2015, Branson, MO, USA

7. Robert Block, Sierra Herndon, Ming Huang, Rex E. Gerald II and Klaus Woelk. **Advantages of Using Automated Systems for Collection of NMR Data**, Second Annual Branson NMR Meeting, January 16th-17th, 2015. The Suites at Fall Creek Resort, Branson, Missouri, USA *(invited)*

8. Robert Block, Sierra Herndon, Ming Huang, Rex E. Gerald II and Klaus Woelk, **Benefits of Using Automated Systems for Collection of NMR Data**, 2014 Midwest Regional Meeting of the American Chemistry Society, November 12th –15th, 2014. Columbia, Missouri, USA

9. Ming Huang, Kyle Hogan, Robert Block, Tasmia Mustaquim, Rex E. Gerald II, and Klaus Woelk, **Development of In Situ NMR *pH* Meter Based on ^{19}F Chemical Shifts**, 2014 Midwest Regional Meeting of the American Chemical Society, November 12th –15th, 2014, Columbia, Missouri, USA

10. Lingyu Chi, Ming Huang, Rex E. Gerald II and Klaus Woelk, **Calibration CapPack Devices for Magic Angle Spinning (MAS) NMR Experiments,** 2014 Midwest Regional Meeting of the American Chemistry Society, November 12th –15th, 2014, Columbia, Missouri, USA

11. Kathryn Czeschin, Ming Huang, Frederic S. Bush, Christina L. Parrish, Madison N. Rector, Rex E. Gerald II, and Klaus Woelk, **NMR T_1 Analyses of Multiple Sample Tubes Tested Simultaneously,** 2014 Midwest Regional Meeting of the American Chemical Society, November 12th –15th, 2014, Columbia, Missouri, USA

12. Justin Beltz, Ming Huang, Justin Cocke, Olivia Cox, **Refine Fidelity and Accuracy in Low-Filed ^{1}H NMR T_1 Experiments,** 55th EXPEIMENTAL NUCLEAR MAGNETIC RESONANCE CONFERENCE, March 23rd- 28th, 2014, Boston, Massachusetts, USA

13. Ming Huang, Lingyu Chi, Rex E. Gerald II, and Klaus Woelk, **Development of *In* Situ NMR *pH* Meter,** 55th EXPEIMENTAL NUCLEAR MAGNETIC RESONANCE CONFERENCE, March 23rd- 28th, 2014, Boston, Massachusetts, USA

14. Lingyu Chi, Jie Huang, Ming Huang, Rex E. Gerald II and Klaus Woelk, **Two CapPack Devices for Solution and Solid State NMR Applications,** 55th EXPEIMENTAL NUCLEAR MAGNETIC RESONANCE CONFERENCE, March 23rd – 28th, 2014, Boston, Massachusetts, USA

15. Ming Huang , Lingyu Chi , Rex E. Gerald II, and Klaus Woelk**, Phenolphthalein NMR *pH* Detector,** Branson NMR Meeting, February 23rd, 2014, The Suites at Fall Creek Resort, 2nd Branson Meeting, Missouri, USA *(invited)*

16. Ming Huang , Lingyu Chi , Rex E. Gerald II, and Klaus Woelk, **Analysis of Complicated Model T_1 Curves,** 2nd PRACTICAL APPLICATIONS OF NMR IN INDUSTRY CONFERENCE, February 3rd– 5th, 2014, Charlotte, North Carolina, USA

17. Ming Huang, Aligul Buyukaksoy, Klaus Woelk, and Rex Gerald, **Analysis of Simultaneous T_1 Measurements of Non-interacting Samples,** 54th EXPEIMENTAL NUCLEAR MAGNETIC RESONANCE CONFERENCE, April 15th -20th, 2013, Pacific Grove, CA, USA

HONORS & ACTIVITIES

- Chinese Spring Festival, invited host, Missouri University of Science and Technology
  Jan 2013
- Expanding Your Horizons, invited presenter, Missouri University of Science and Technology
  Nov 2013

- Chinese Spring Festival, invited host, Missouri University of Science and Technology
  Jan 2014
- Expanding Your Horizons, invited Lab experiment presenter, Missouri University of Science and Technology
  Nov 2014
- Council of Graduate Students Travel Grant, 59th Experimental NMR Conference
  April/May 2019
- Excellent Graduate Student Service Award
  April 2019

BIBLIOGRAPHY

[1] S. K. Bharti, R. Roy, Quantitative ^{1}H NMR spectroscopy. TrAC Trends in Analytical Chemistry, 2012. **35**: p. 5-26.

[2] Y. Matsui, S. Tokunaga, Internal Reference Compounds Available for the Determination of Binding Constants for Cyclodextrin Complexes by ^{1}H NMR Spectrometr. Bulletin of the Chemical Society of Japan., 1996. **69**(9): p. 2477-2480.

[3] C. J. Jameson, Undertanding NMR Chemical Chemical Shifts. Annual Review of Physical Chemistry, 1996. **47**(1): p. 135-169.

[4] Undergraduate Professional Education in Chemistry, ACS Guidelines and Evaluation Procedures for Bachelor's Degree Programs, Office of Professional Training of the American Chemical Society, https://www.acs.org/content/dam/acsorg/about/governance/committees/training/2015-acs-guidelines-for-bachelors-degree-programs.pdf (last viewed on March 25, 2019)

[5] G. V. D. Tiers, Reliable Proton Nuclear Resonance Shielding Values by "Internal Referencing" with Tetramethyl-silane. The Journal of Physical Chemistry, 1958. **62**(9): p. 1151-1152.

[6] C. R. Morcombe, K. W. Zilm, Chemical shift referencing in MAS solid state NMR. Journal of Magnetic Resonance, 2003. **162**(2): p. 479-486.

[7] G. Orgován, B. Noszál, Electrodeless, accurate pH determination in highly basic media using a new set of 1 H NMR pH indicators. Journal of pharmaceutical and biomedical analysis, 2011. **54**(5): p. 958-964.

[8] L. Chi, M. Huang, A. R. Pfaff, J. Huang, R. E. GeraldII, K. Woelk, Capillary-tube package devices for the quantitative performance evaluation of nuclear magnetic resonance spectrometers and pulse sequences. Review of Scientific Instruments, 2018. **89**(12): p. 123115(1-8).

[9] C. Chen, J. S. Cohen, C. E. Myers, M. Sohn, Paramagnetic metalloporphyrins as potential contrast agents in NMR imaging. FEBS Letters, 1984. **168**(1): p. 70-74.

[10] H. Mo, D. Raftery, Solvent Signal as an NMR Concentration Reference. Analytical Chemistry, 2008. **80**(24): p. 9835-9839.

[11] S. Akoka, L. Barantin, M. Trierweiler, Concentration Measurement by Proton NMR Using the ERETIC Method. Analytical Chemistry, 1999. **71**(13): p. 2554-2557.

[12] P. Giraudeau, I. Tea, G. S. Remaud, S. Akoka, Reference and normalization methods: Essential tools for the intercomparison of NMR spectra. Journal of Pharmaceutical and Biomedical Analysis, 2014. **93**: p. 3–16.

[13] H. E. Gottlieb, V. Kotlyar, A. Nudelman, NMR Chemical shifts of common laboratory solvents as trace impurities. The Journal of Organic Chemistry, 1997. **62**: p. 7512–7515.

[14] T. J. Henderson, Quantitative NMR spectroscopy using coaxial inserts containing a reference standard: Purity determinations for military nerve agents. Analytical Chemistry, 2002. **74**: p. 191–198.

[15] SP Industries, NMR-007: Coaxial inserts in NMR studies, https://www.wilmad-labglass.com/Support/NMR-and-EPR-Technical-Reports/NMR-007–Coaxial-Inserts-in-NMR-Studies/ (viewed March 25, 2019).

[16] Wishart, D.S., et al., ^{1}H, ^{13}C and ^{15}N chemical shift referencing in biomolecular NMR. Journal of Biomolecular NMR, 1995. **6**(2): p. 135-140.

[17] K. Kirk, J. E. Raftos, P. W. Kuchel, Triethyl phosphate as an internal ^{31}P NMR reference in biological samples. Journal of Magnetic Resonance, 1986. **70**(3): p. 484-487.

[18] P. Cleve, V. Robinson, H. S. Duewel, J. F. Honek, Difluoromethionine as a Novel ^{19}F NMR Structural Probe for Internal Amino Acid Packing in Proteins. Journal of the American Chemical Society, 1999. **121**(37): p. 8475-8478.

[19] R. B. Johannesen, F. E. Brinckman, T. D. Coyle, Nuclear magnetic resonance studies of inorganic fluorides. V. Fluorosilanes. The Journal of Physical Chemistry, 1968. **72**(2): p. 660-667.

[20] M. Yoshihisa, T. Shuichi, Internal Reference Compounds Available for the Determination of Binding Constants for Cyclodextrin Complexes by ^{1}H NMR Spectrometry. Bulletin of the Chemical Society of Japan, 1996. **69**(9): p. 2477-2480.

[21] A. N. Stevens, P. G. Morris, R. A. Iles, P. W. Sheldon, 5-fluorouracil metabolism monitored in vivo by ^{19}F NMR. British journal of cancer, 1984. **50**(1): p. 113-117.

[22] C. J. Deutsch, J. S. Taylor, New class of ^{19}F pH indicators: fluoroanilines. Biophysical Journal, 1989. **55**(4): p. 799-804.

[23] P. R. Srinivasan, R. L. Lichter, Nitrogen-15 nuclear magnetic resonance spectroscopy. Evaluation of chemical shift references, Journal of Magnetic Resonance, 1977. **28**(2): p.227-234.

[24] P.Bertani, J. Raya, B. Bechinger, ^{15}N chemical shift referencing in solid state NMR. Solid State Nuclear Magnetic Resonance, 2014. **61**: p. 15-18.

[25] J. A. Tossell, Ab initio calculations of ^{29}Si NMR chemical shifts for some gas phase and solid state silicon fluorides and oxides. The Journal of Chemical Physics, 1986. **84**(1): p. 369-374.

[26] T. Heine, A. Goursot, G. Seifert, J. Webe, Performance of DFT for ^{29}Si NMR Chemical Shifts of Silanes, The Journal of Physical Chemistry, 2001. **105**(3): p. 620-626.

[27] S. P. Szu, L. C. Klein, M. Greenblatt, Effect of precursors on the structure of phosphosilicate gels: ^{29}Si and ^{31}P MAS-NMR study. Journal of Non-crystalline Solids, 1992. **143**: p. 21-30.

[28] H. E. Gottlieb, V. Kotlyar, A. Nudelman, NMR Chemical Shifts of Common Laboratory Solvents as Trace Impurities. The Jouranl of Organic Chemsitry, 1997. **62**: p. 7512-7515.

[29] E. Lima, M. Laspéras, L. Ménorval, D. Tichit,, F. Fajula, Characterization of Basic Catalysts by the use of nitromethane as NMR probe molecule and reactant. Journal of Catalysis, 2004. **223**: p. 28-35

[30] K. Gademann, B. Jaun, D. Seebach, R. Perozzo, L. Scapozza, G. Folkers, Temperature-Dependent NMR and CD Spectra of β-Peptides: On the Thermal Stability of β-Peptide Helices–Is the Folding Process of β-Peptides Non-cooperative? Helvetica Chimica Acta, 1999. **82**(1): p. 1-11.

[31] J. R. Lyerla, C. S. Yannoni, C. A. Fyfe, Chemical applications of variable-temperature CPMAS NMR spectroscopy in solids, Accounts of Chemical Research, 1982. **15**(7): p. 208-216.

[32] D. S. Raiford, C. L. Fisk, E. D. Becker, Calibration of methanol and ethylene glycol nuclear magnetic resonance thermometers. Analytical Chemistry, 1979. **51**(12): p. 2050-2051.

[33] R. D. Farrant, J. C. Lindon, J. K. Nicholson, Internal temperature calibration for ^{1}H NMR spectroscopy studies of blood plasma and other biofluid. NMR in Biomedicine, 1994. **7**(5): p. 243-247.

[34] M. Holz, S. R. Heil, A. Sacco, Temperature-dependent self-diffusion coefficients of water and six selected molecular liquids for calibration in accurate ^{1}H NMR PFG measurements. Physical Chemistry Chemical Physics, 2000. **20**: p. 4740-4742.

[35] D. R. Kinney, I. Chuang, G. E. Maciel, Water and the silica surface as studied by variable-temperature high-resolution proton NMR. Journal of the American Chemical Society, 1993. **115**(15): p. 6786–6794.

[36] M. S. Silver, R. I. Joseph, D. I. Hoult, Highly selective π/2 and π pulse generation. J. Magn. Reson., 1984. **59**: p. 347–351.

[37] E. T. Satterfield, A. R. Pfaff, W. Zhang, L. Chi, R. E. Gerald II, K. Woelk,, EXponentially converging eradication pulse train (EXCEPT) for solvent signal suppression in investigations with variable T_1 times. Journal of magnetic Resonance, 2016. **268**: p. 68-72.

[38] L. O. Morgan, A. W. Nolle, Proton spin relaxation in aqueous solutions of paramagnetic ions. II. Cr^{+++}, Mn^{++}, Ni^{++}, Cu^{++}, and Gd^{+++}. The Journal of Chemical Physics, 1959. **31**: p. 365–368.

[39] A. E. Derome, Modern NMR Techniques for Chemistry Research. The Dyson Perrins Laboratory, University of Oxford, UK, 1987: p. 42-50.

[40] M. Armand, F. Endres, D. R. MacFarlane, H. Ohno, B. Scrosati, Ionic-liquid Materials for the Electrochemical Challenges of the Future. Material for Sustainable Energy, 2010: p. 129-137.

[41] Thomas Welton, Room-Temperature Ionic Liquids. Solvent for Synthesis and Catalysis. Chemical Reviews, 1999. **99**(8): p. 2071-2084.

[42] H. Zhao, J. E. Holladay, H. Brown, Z. C. Zhang, Metal Chlorides in Ionic Liquid Solvents Convert Sugars to 5-Hydroxymethylfurfural. Science, 2007. **316**(5831): p. 1597-1560.

[43] K. R. J. Lovelock, Influence of the ionic liquid/gas surface on ionic liquid chemistry. Physical Chemistry Chemical Physics, 2012. **14**: p. 5071-5089.

[44] H. Weingärtner, Understanding ionic liquids at the molecular level. Facts, problems and controversies. Angewandte Chemie International Edition, 2008. **47**: p. 654-670.

[45] R. Giernoth, D. Bankmann, Magnetic resonance spectroscopy in ionic liquids. Progress in Nuclear Magnetic Resonance Spectroscopy, 2007. **51**: p. 63-90.

[46] R. Giernoth, D. Bankmann, N. Schlörer, High performance NMR in ionic liquids. Green Chemistry, 2005. **7**: p. 279-282.

[47] B. G. Pfrommer, F. Mauri, S. G. Louie, NMR chemical shifts of ice and liquid water: the effects of condensation, Journal of the American Chemical Society, Vol. 122, No. 1, 2000, pp. 123-129. Downloaded by MISSOURI UNIV OF SCIENCE & TECH on March 21, 2019 | http://arc.aiaa.org | DOI: 10.2514/6.2017-4756, American Institute of Aeronautics and Astronautics.

[48] E. Blanco, H. Shen, M. Ferrari, Principles of Nanoparticle Design for Overcoming Biological Barriers to Drug Delivery. Nature Biotechnology, 2015. **33**: p. 941–951.

[49] K. Hamad-Schifferli, Exploiting the Novel Properties of Protein Coronas: Emerging Applications in Nanomedicine. Nanomedicine, 2015. **10**: p. 1663–1674.

[50] J. O'Brien, K. J. Shea, Tuning the Protein Corona of Hydrogel Nanoparticles: The Synthesis of Abiotic Protein and Peptide Affinity Reagents. Account of Chemical Research, 2016. **49**: p. 1200–1210.

[51] J. O'Brien, S. H. Lee, S. Onogi, K. J. Shea, Engineering the Protein Corona of a Synthetic Polymer Nanoparticle for Broad- Spectrum Sequestration and Neutralization of Venomous Biomacromolecules. Journal of the American Chemical Society, 2016. **138**: p. 16604–16607.

[52] J. R. Cynthia, W. Zhao, H. Hu, M. Chen, M. R. Van De Mark, Self-assembly of water insoluble polymers into Colloidal Unimolecular Polymer (CUP) particles of 3-9 nm, Polymer, 2014. **55**: p. 48-57.

[53] A. M. Natu, M. Wiggins, M. R. Van De Mark, Synthesis and characterization of cationic colloidal unimolecular polymer (CUP) particles, Colloid Polymer Science, 2015. **293**:p. 1191–1204.

[54] M. R. Van De Mark, A. M. Natu, S. V. Gade, M. Chen, C. Hancock, C. Riddles, Molecular weight (Mn) and functionality effects on CUP formation and stability, Journal of Coatings Technology and Reserach, 2014. **11**(2): p. 111–122,

[55] S. K. Davidowski, G. P. Holland, Solid-State NMR Characterization of Mixed Phosphonic Acid Ligand Binding and Organization on Silica Nanoparticles. Langmuir, 2016. **32**: p. 3253–3261.

[56] R. L. Johnson, F. A. Perras, T. Kobayashi, T. J. Schwartz, J. A. Dumesic, B.H. Shanks, M. Pruski, Identifying Low-Coverage Surface Species on Supported Noble Metal Nanoparticle Catalysts by DNP-NMR. Chemical Communications, 2016, **52**: p. 1859–1862.

[57] I. Cano, M. A. Huertos, A. M. Chapman, G. Buntkowsky, T. Gutmann, P. B. Groszwicz, P. W. N. M. van Leeuwen. Air-Stable Gold Nanoparticles Ligated by Secondary Phosphine Oxides as Catalyst for the Chemoselective Hydrogenation of Substituted Aldehydes: a Remarkable Ligand Effect. Journal of the American Chemical Society, 2015. **137**: p. 7718–7727.

[58] L. E. Marbella, J. E. Millstone, NMR Techniques for Noble Metal Nanoparticles. Chemistry of Materials, 2015. **27**: p. 2721–2739.

[59] J. R. Sachleben, E. W. Wooten, L. Emsley, A. Pines, V. L. Colvin, A. P. Alivisatos, NMR Studies of the Surface Structure and Dynamics of Semiconductor Nanocrystals. Chemical Physics Letter, 1992. **198**: p. 431–436.

[60] J. R. Sachleben, V. Colvin,v L. Emsley, E. W. Wooten, A. P. Alivisatos, Solution-State NMR Studies of the Surface Structure and Dynamics of Semiconductor Nanocrystals. The Journal of Physical Chemistry B, 1998. **102**: p. 10117–10128.

[61] A. Philippidis, A. Spyros, D. Anglos, A. B. Bourlinos, R. Zboril, E. P. Giannelis, Carbon-Dot Organic Surface Modifier Analysis by Solution-State NMR Spectroscopy. Journal of Nanoparticle Resarch, 2013. **15**: p. 1777.

[62] E. O. Stejskal, J. E. Tanner, Spin Diffusion Measurements: Spin Echoes in the Presence of a Time-Dependent Field Gradient. The Journal of Chemical Physics, 1965. **42**: p. 288–292.

[63] K. F. Morris, C. S. Johnson, Resolution of Discrete and Continuous Molecular-Size Distributions by Means of Diffusion- Ordered 2D NMR Spectroscopy. Journal of the American Chemical Society, 1993, **115**: p. 4291–4299.

[64] A. Kumar, R. R. Ernst, K. Wüthrich. A Two-Dimensional Nuclear Overhauser Enhancement (2D NOE) Experiment for the Elucidation of Complete Proton-Proton Cross-Relaxation Networks in Biological Macromolecules. Biochemical and Biophysical Research Communications, 1980. **95**: p. 1.

[65] R. M. Keller, K. Wüthrich, Assignment of the Heme c Resonances in the 360 MHz H NMR Spectra of Cytochrome c. Biochimica et Biophysica Acta, 1978. **533**: p. 195–208.

[66] B. Meyer, T. Peters, NMR Spectroscopy Techniques for Screening and Identifying Ligand Binding to Protein Receptors. Angewandte Chemie International Edition, 2003. **42**: p. 864–890.

[67] M. Mayer, B. Meyer, Characterization of Ligand Binding by Saturation Transfer Difference NMR Spectroscopy. Angewandte Chemie International Edition, 1999. **38**: p. 1784–1788.

[68] Y. Zhang, H. Xu, A. M. Parsons, L. B. Casabianca, Examining Binding to Nanoparticle Surfaces Using Saturation Transfer Difference (STD)-NMR Spectroscopy, The Journal of Physical Chemistry C, 2017. **121**: p. 24678-24686.

[69] Y. Zhang, H. Xu, L. B. Casabianca, Interaction between cyanine dye IR-783 and polystyrene nanoparticles in solution, Magnetic Resonance in Chemistry, 2018. **56**: p. 1054–1060.

[70] J. Angulo, P. M. Enriquez-Navas, M. N. Pedro, Ligand–Receptor Binding Affinities from Saturation Transfer Difference (STD) NMR Spectroscopy: The Binding Isotherm of STD Initial Growth Rates, Chemistry-A European Journal, 2010. **16**: p. 7803 – 7812.

[71] M. N. Rahaman, D. E. Day, B. S. Bal, Q. Fu, S. B. Jumg, L. F. Bonewald, A. P. Tomsia, Bioactive glass in tissue engineering. Acta Biomaterialia, 2011. **7**(6): p. 2355-2373.

[72] A. W. Wren, Vitreous Materials for Dental Restoration and Reconstruction, in Biocompatible Glasses, 2016. Springer. p. 203-225.

[73] S. Chen, Q. Yang, R. k. Brow, k. Liu, K. A. Brow, Y. Ma, H. Shi, In vitro stimulation of vascular endothelial growth factor by borate-based glass fibers under dynamic flow conditions. Materials Science and Engineering: C, 2017. **73**: p. 447-455.

[74] Q. Yang, S. Chen, H. Shi, H. Xiao, Y. Ma, In vitro study of improved wound-healing effect of bioactive borate-based glass nano-/micro-fibers. Materials Science and Engineering: C, 2015. **55**: p. 105-117.

[75] S. Chen, In vitro study of wound-healing capabilities of bioactive glass fibers under various culture conditions. 2015.

[76] G. Wicks, L. Heung, R. Schumacher, Microspheres and microworlds. American Ceramic Society Bulletin, 2008. **87**(6): p. 23.

[77] H. Liu, Z. Bi, X. Sun, R. R. Unocic, M. P. Paranthaman, S. Dai, G. M. Brown, Mesoporous TiO2–B Microspheres with Superior Rate Performance for Lithium Ion Batteries. Advanced Materials, 2011. **23**(30): p. 3450-3424.

[78] R. K. Brow, M. L. S., A survey of energy and environmental applications of glass. Journal of the European Ceramic Society, 2009. **29**(7): p. 1193-1201.

[79] J. Newell, S. Patankar, D. Edwards, Porous microspheres as additives in lead–acid batteries. Journal of Power Sources, 2009. **188**(1): p. 292-295.

[80] J. Liu, C. Li, Q. Yang, J. Yang, C. Li, Morphological and structural evolution of mesoporous silicas in a mild buffer solution and lysozyme adsorption. Langmuir, 2007. **23**(13): p. 7255-7262.

[81] Z. Wu, K. Yu, S. Zhang, Y. Xie, Hematite hollow spheres with a mesoporous shell: controlled synthesis and applications in gas sensor and lithium ion batteries. The Journal of Physical Chemistry C, 2008. **112**(30): p. 11307-11313.

[82] L. K. Heung, R. F. Schumacher, G. G. Wicks, Hollow porous-wall glass microspheres for hydrogen storage. 2010, US Patents.

[83] F. Thompson, G. Wicks, G. Crawford, Porous-wall Hollow Glass Microspheres for Security Printing Applications. in NIP & Digital Fabrication Conference. 2015. Society for Imaging Science and Technology.

[84] V. R. Sinha, A. Trehan, Biodegradable microspheres for protein delivery. Journal of controlled release, 2003. **90**(3): p. 261-280.

[85] S. Cohen,T. Yoshioka, M. Lucarelli, A. H. hwang, R. Langer, Controlled Delivery Systems for Proteins Based on Poly(Lactic/Glycolic Acid) Microspheres. Pharmaceutical Research, 1991. **8**(6): p. 713-720.

[86] S. Li, L. Nguyen, H. Xiong, M. Wang, T. C. C. Hu, J. She, S. M. Serkiz, G. G. Wicks, W. S. Dynan, Porous-wall hollow glass microspheres as novel potential nanocarriers for biomedical applications. Nanomedicine: Nanotechnology, Biology and Medicine, 2010. **6**(1): p. 127-136.

[87] W. Wei, G. Ma, G. Hu, D. Yu, T. mcleishm Z. Su, Z. Shen, Preparation of hierarchical hollow CaCO3 particles and the application as anticancer drug carrier. Journal of the American Chemical Society, 2008. **130**(47): p. 15808-15810.

[88] S. S. Moosavi, P. Alizadeh, Effect of acid leaching time on pore diameter and volume of porous hollow glass microspheres. Materials Letters, 2016. **167**: p. 98-101.

[89] Y. Zhu, J. Shi, W. Shen, H. Chen, X. Dong, M. Ruan, Preparation of novel hollow mesoporous silica spheres and their sustained-release property. Nanotechnology, 2005. **16**(11): p. 2633.

[90] Y. Cai, Y. Chen, X. Hong, Z. Liu, W. Yuan, Porous microsphere and its applications. International journal of nanomedicine, 2013. **8**: p. 1111.

[91] C. A. Lepre, J. M. Moore, J. W. Peng, Theory and applications of NMR-based screening in pharmaceutical research. Chemical Reviews, 2004. **104**(8): p. 3641-3676.

[92] M. Malet-Martino, U. Holzgrabe, NMR techniques in biomedical and pharmaceutical analysis. Journal of Pharmaceutical and Biomedical Analysis, 2011. **55**(1): p. 1-15.

[93] H. Günther, NMR spectroscopy: basic principles, concepts and applications in chemistry. John Wiley & Sons, 2013.

[94] T. J. Williams, A. D. Kershaw, V. Li, X. Wu, An Inversion Recovery NMR Kinetics Experiment. Journal of Chemical Education, 2011. **88**(5): p. 665.

[95] A. D. Gossert, W. Jahnke, NMR in drug discovery: A practical guide to identification and validation of ligands interacting with biological macromolecules. Progress in Nuclear Magnetic Resonance Spectroscopy, 2016. **97**: p. 82-125.

[96] M. J. O'Neil, A. Smith, P. E. Heckelman, S. Budavari, The Merck Index: An Encyclopedia of Chemicals, Drugs, and Biologicals, 13 e édition. Whitehouse Station (NJ): Merck & Co. 2001, Inc.

[97] M. J. O'Neil, The Merck index: an encyclopedia of chemicals, drugs, and biologicals. Royal Society of Chemistry, 2013.

[98] M. Cavcar, The international standard atmosphere (isa). Anadolu University, Turkey, 2000. **30**: p. 9.

[99] D. Mackay, A. Bobra, W. Y. Shiu, S. H. Yalkowskym Relationships between aqueous solubility and octanol-water partition coefficients. Chemosphere, 1980. **9**(11): p. 701-711.

[100] D. Shaw, IUPAC Solubility Data Series: Hydrocarbons with Water and Seawater, Part II: Hydrocarbons C8 to C36. 1989, Pergamon, Oxford.

[101] S. Sen, Temperature induced structural changes and transport mechanisms in borate, borosilicate and boroaluminate liquids: high-resolution and high-temperature NMR results. Journal of Non-Crystalline Solids, 1999. **253**(1-3): p. 84-94.

[102] X. Zhang, J. Golding, I. Burgar, Thermal decomposition chemistry of starch studied by ^{13}C high-resolution solid-state NMR spectroscopy. Polymer, 2002. **43**(22): P. 5791-5796

[103] H. Günther, NMR spectroscopy: basic principles, concepts and applications in chemistry, 2013. University Siegen, publisher: Wiley-VCH.

[104] G. N. La Mar, W. D. Horrocks, R. H. Holm, NMR of paramagnetic molecules: principles and applications, Academic Press New York and London, Publisher: A Subsidiary of Harcourt Brace Jovanovich. 1973

[105] S. Garrod, E. Humpfer, M. Spraul, S. C. Connor, S. Polley, J. Connelly, J. C. Lindon, J. K. Nicholson, E. Holmes, High-resolution magic angle spinning ^{1}H NMR spectroscopic studies on intact rat renal cortex and medulla. Magnetic Resonance in Medicine, 1999. **41**(6): p. 1108-1118.

[106] M. E. Bollard, S. Garrod, E. Holmes, J. C. Lindon, E. Humpfer, M. Spraul, J. K. Nicholson, High-resolution ^{1}H and ^{1}H-^{13}C magic angle spinning NMR spectroscopy of rat liver. Magnetic Resonance in Medicine, 2000. **44**(2): p. 201-207.

[107] S. Byrn, R. Pfeiffer, M. Ganey, C. Hoiberg, G. Poochikian, Pharmaceutical Solids: A Strategic Approach to Regulatory Considerations, Pharmaceutical Research, 1995. **12**(7): p. 945-954.

[108] S. Ando, I. Ando, A. Shoji, Y. Ozaki, Intermolecular Hydrogen-Bonding Effect on ^{13}C NMR Chemical Shift of Glycine Residue Carbonyl Carbons of Peptides in the Solid State. Journal of the American Chemical Society, 1998. **110**: p. 3380-3386.

[109] S. Cavadini, S. Antonijevic, A. Lupulescu, G. Bodenhausen, Indirect Detection of Nitrogen-14 in Solid-state NMR Spectroscopy. ChemPhysChem, 2007. **8**: p. 1363-1374.

[110] H. D. Morris, P. D. Ellis, 27Al Cross Polarization of Aluminas. The NMR Spectroscopy of Surface Aluminum Atoms. American Chemical Society, 1989. **111**: p. 6045-6049.

VITA

Ming Huang was born in Tianjin, China. In June 2012, she obtained a bachelor's degree in Department of Environment Science and Engineering, Nankai University of Binhai College, Tianjin, R.P. China.

In August 2012, she enrolled at Missouri University of Science and Technology to pursue a Ph.D degree. In July 2017, she received her master's degree in chemistry firstly under the guidance of Dr. Klaus Woelk at Missouri University of Science and Technology. Her research interest is *In situ* pH Determination Based on the NMR Analysis of ^{1}H Signal Intensities and ^{19}F Chemical Shifts, quantitative NMR. In July 2019, she received her PhD degree in chemistry from Missouri University of Science and Technology under the guidance of Dr. Klaus Woelk. Her research interest is *In situ* pH Determination Based on the NMR Analysis of ^{1}H Signal Intensities and ^{19}F Chemical Shifts, quantitative NMR. Her research interest is The Benefit of Precise Chemical Shift and Concentration Referencing in NMR Applications and quantitative NMR.